THE UNIVERSITY OF CHICAGO

EXISTING ACTIN FILAMENTS ORIENT NEW FILAMENT GROWTH TO PROVIDE STRUCTURAL MEMORY OF FILAMENT ALIGNMENT DURING CYTOKINESIS

A DISSERTATION SUBMITTED TO
THE FACULTY OF THE DIVISION OF THE BIOLOGICAL SCIENCES
AND THE PRITZKER SCHOOL OF MEDICINE
IN CANDIDACY FOR THE DEGREE OF
DOCTOR OF PHILOSOPHY

COMMITTEE ON DEVELOPMENT, REGENERATION AND STEM CELL BIOLOGY

BY
YOUNAN LI

CHICAGO, ILLINOIS
MARCH 2021

TABLE OF CONTENTS

LIST OF FIGURES

ACKNOWLEDGMENTS

To my parents, my brother and my sister-in-law, and my friends for all of their support.

ABSTRACT

Cells use actin-based cytoskeletal arrays to accomplish a variety of tasks, including cell division, cell migration, intracellular trafficking, and multicellular tissue morphogenesis. The architectures and assembly dynamics of different actin arrays are closely associated with their different functions. Thus, a key challenge in cell biology is to understand how cells assemble actin arrays with specific architectures at particular places and times. Through decades of effort, cell biologists have identified and characterized the structural components of actin arrays, accessory factors that govern filament assembly, disassembly, crosslink dynamics and motor activity, and upstream signaling pathways that cells use to locally recruit and activate subsets of network elements to initiate the assembly of specific actin arrays. However, the mechanisms by which these components self-organize into specific arrays remain poorly understood.

In this thesis, I study the mechanisms that govern self-organization of the contractile ring in the early *C. elegans* embryo. During cytokinesis, signals from the mitotic apparatus trigger the local assembly of actin filaments and myosin motors at the cell equator, and these then rapidly self-organize into a circumferentially aligned array of actin filaments called the contractile ring that constricts to divide the cell. Previous studies showed that in theory, the reorientation of actin filaments by equatorial contraction could explain the rapid emergence of circumferential alignment. Combining single molecule analysis and modeling, I have shown that equatorial filaments turnover far too fast for equatorial contractions to build the observed alignment, even if favorably oriented filaments are selectively stabilized. By tracking the movements of single formin/CYK-1::GFP speckles to monitor the orientation of filament growth in relation to existing actin filaments, I showed that the orientation of equatorial filament growth is biased to favor circumferential alignment. Using multi-color imaging of formin/CYK-1 and a marker for actin filaments, I identified the mechanism for this bias, which I call filament-guided filament assembly (FGFA), in which existing filaments serve as templates to orient the growth of new filaments. Combining modeling and quantitative analysis of CYK-1 trajectories, I showed that FGFA increases the effective lifetime of filament orientation, providing a structural memory of filament orientation that allows slow equatorial contraction to build and maintain highly aligned filament arrays, despite rapid turnover of individual filaments. Finally, I considered one

possible mechanism for FGFA, in which dynamic crosslinker PLST-1 rapidly zipper elongating filaments onto existing filaments, allowing them to inherit the same orientation. Combining *in vitro* reconstitution experiments and live imaging of embryos expressing endogenously labeled PLST-1, I showed that PLST-1 is capable of driving FGFA *in vitro*, and PLST-1 can decorate growing actin filaments fast enough to drive FGFA *in vivo*. Together, these findings reveal a novel mechanism by which a network of filaments preserves structural information (filament orientation) in the face of rapid turnover of its individual components. This mechanism may underlie the assembly and maintenance of the many other arrays of aligned actin filaments that operate in animal cells.

CHAPTER 1

INTRODUCTION

1.1 Overview

The cytoskeleton is a complex and dynamic subcellular network that provides a structural framework for cell shape, the positions of organelles, and the general organization of cytoplasm (Agarwal and Zaidel-Bar 2019; Levayer and Lecuit 2012; Munjal and Lecuit 2014; Fletcher and Mullins 2010). Assembly and remodeling of the cytoskeleton powers intracellular movements of organelles and dynamic changes in cell shape that are essential for a variety of processes including: cell division, cell migration, cell-cell communication, muscle contraction, and multicellular morphogenesis. In eukaryotic cells, the cytoskeleton is composed of three principle types of protein filaments: actin filaments, intermediate filaments, and microtubules (Fletcher and Mullins 2010). My thesis focuses on the actin cytoskeleton.

The basic unit of actin cytoskeleton is an actin filament - a linear polymer that assembles from subunits of globular actin. G-actin is a 42-kDa protein that was first characterized in 1942 due to its ability to influence the activity of myosin (Banga and Szent-Gyorgyi 1941-42). In cells, four processes underlie the assembly of actin into higher order arrays: dynamic assembly of G-actin into F-actin; dynamic disassembly of F-actin back into G-actin; crosslinking of F-actin into higher order arrays; and reorganization of F-actin by myosin motors (Pollard 2016; Kelber and Klemke 2011; Dos Remedios et al. 2003). Over many decades, biologists have identified a large collection of molecules that bind actin and control the basic four processes mentioned above, which are called actin binding proteins (ABPs).

By differentially controlling these four basic processes, cells can assemble a variety of different arrays that serve different cellular functions (Figure 1.1) (Svitkina 2018a; Blanchoin et al. 2014). For example, just beneath the plasma membrane, actin filaments form a largely isotropic network called the cell cortex to provide mechanical support for different cell shapes (Chugh and Paluch 2018). During cell division, the equatorial cortex self-organizes into a circumferential array of aligned filaments with mixed polarities called the contractile ring that constricts to pinch a cell

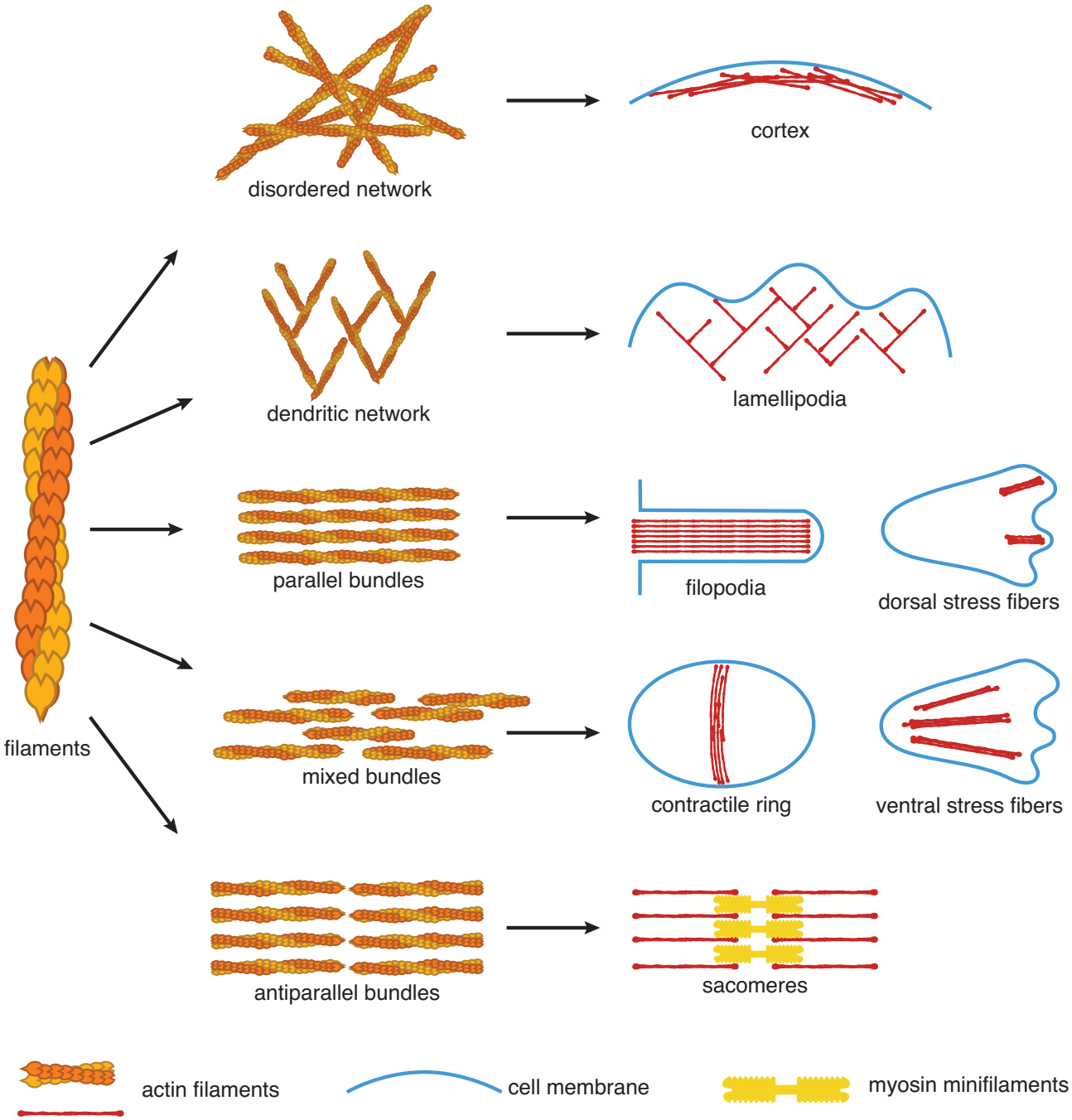

Figure 1.1. Actin filaments are able to assemble into a range of high-order structures.

into two (Leite et al. 2019; Pollard 2010). In muscle cells, actin filaments are organized into highly ordered antiparallel bundles within structures called sarcomeres (Huxley 2004). Dynamic sliding of actin filaments within these sarcomeres provides forces to contract muscle cells. In migrating cells, at the leading edge, actin filaments assemble into polarized dendritic networks called lamellipodia to push the cell forward, and assemble into parallel actin bundles called filopodia, which typically arise from lamellipodia, to generate finger-like protrusions to explore the surrounding regions (Schaks et al. 2019; Rottner and Schaks 2019).

Cells typically assemble many different dynamic actin arrays at the same time, but in different locations. These arrays can work in parallel to perform distinct tasks. For example, in fission yeast, the actin cytoskeleton can simultaneously assemble three different arrays to do three different jobs (Kovar, Sirotkin, et al. 2011; Chang et al. 1996). At the poles, branched actin filaments assemble into actin patches that are important for endocytosis. Along the long axis of the cell, unbranched actin filaments assemble into parallel bundles called actin cables, which are important for vesicle and organelle transport. During cytokinesis, actin filaments assemble into a circumferentially aligned array of actin filaments with mixed polarity called the contractile ring to constrict the cell in two (Kovar, Sirotkin, et al. 2011).

On the other hand, different actin arrays can also work collectively to perform a common task. For example, during cytokinesis, constriction of the contractile ring is coupled with relaxation of the polar cortex, and it is the combination of these two local behaviors that allow a cell to divide into two (Miller 2011). In migrating cells, local assembly of lamellipodia produce forces to push the leading edge forward; crosstalk between lamellipodia and filopodia allow filopodia to steer the direction of migration. Meanwhile, the contractile lamella network behind the leading edge and stress fibers throughout the cell body and at the rear generate contractile forces that move the rear of the cell forward, and translocate organelles during migration (Schaks et al. 2019).

A fundamental challenge for cell biology is to understand how animal cells assemble specific actin arrays at the right places and times, either constitutively, or in response to specific external signals. Central to this challenge is the idea that many of these arrays are assembled through what might best be called "guided self-organization": cells respond to external signals

or generate intracellular signals that specify when and where to assemble an actin array by recruiting specific groups of actin assembly factors and other ABPs to localize and initiate the assembly process. An initial population of actin filaments and ABPs can in turn recruit other factors, and then, spontaneous interactions among all of these components lead to their self-organization into a specific array with a specific architecture, composition and function. Through many decades of effort, cell biologists have identified many of the key components of actin arrays. Their structures, activities and pairwise interactions have been extensively characterized, and many of the signaling pathways that control their activities to control the assembly of specific arrays have been identified and characterized (Pollard 2016; Dos Remedios et al. 2003; Hodge and Ridley 2016; Bishop and Hall 2000). However, we are only beginning to understand some of the basic principles that underlie cytoskeletal self-organization and to uncover the mechanisms by which specific actin arrays form through the process of guided self-organization.

In this introduction, I will first summarize the molecular basis for the four basic processes that underlie the self-organization of the cytoskeleton, including actin assembly, disassembly, crosslinking, and reorganization by myosin motors. Next, I will summarize different mechanisms that cells use to locally recruit/activate/segregate different combinations of assembly factors, disassembly factors, crosslinkers and motors. Then, I will use several well-studied structures, namely lamellipodia, filopodia, contractile arrays, and mitotic spindle, as examples to discuss the key mechanisms that govern self-organization. After that, I turn to the particular topic of my thesis work - the contractile ring. I will summarize our current understanding of how the contractile ring is specified, and how it assembles and constricts, emphasizing the remaining unanswered questions about contractile ring assembly and the advantages of using single molecule imaging and particle tracking to answer such questions.

1.2 All actin arrays are built by an interplay of four basic processes

Over the years, a large collection of ABPs has been identified to control the basic processes, and the core biochemical principles that govern each process have been worked out. In this section, I am going to use a handful of essential ABPs to introduce the core principles behind

each process (reviewed in Pollard 2016; Dos Remedios et al. 2003) (Figure 1.2).

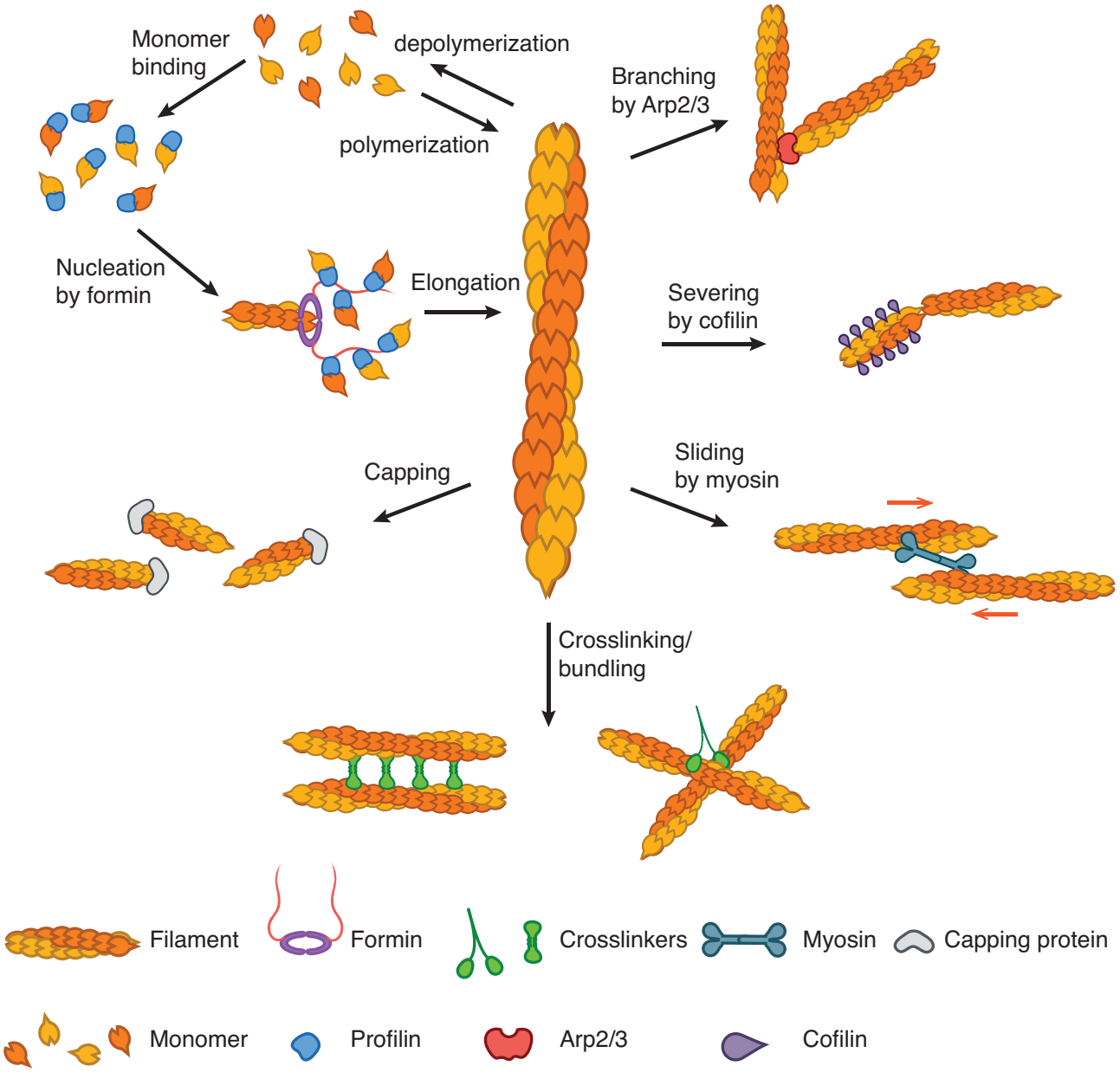

Figure 1.2. A schematic overview of basic processes that govern actin dynamics.

1.2.1 Assembly

In vitro studies have characterized the basic dynamics of actin assembly. Above a critical concentration, in the presence of salts and ATP, G-actin can spontaneously polymerize into F-actin. Spontaneous actin polymerization *in vitro* occurs in three phases: nucleation, elongation and the steady state phase (Cooper et al. 1983). During nucleation, G-actin forms a trimer as a seed for F-actin elongation. Nucleation is the rate limiting step, because both dimers and trimers are highly unstable. During the elongation phase, large actin oligomers rapidly

elongate into filaments, leading to progressive depletion of the pool of available actin monomers. Actin monomers can bind and unbind to both ends of actin filaments. There exists a critical concentration of actin monomers, such that the binding rate of monomers to the barbed/pointed end equals to the unbinding rate from the same end. At this critical concentration, there's no net growth of filament from that end. Once incorporated into filaments, F-actin subunits undergo spontaneous and irreversible ATP-hydrolysis to produce ADP-Pi-actin subunits, which slowly release the γ-phosphate and become ADP-actin. The third phase occurs when F-actin dynamics reaches the steady state, characterized by no net increase of the filament length. This is because the critical concentration of the pointed end is higher than the critical concentration of the barbed end, so there exists an intermediate concentration such that the net growth at the barbed end of the filament is the same as the net loss at the pointed end. At this concentration, there is no net increase of filament's length, and the filament treadmills dynamically (Cooper et al. 1983; Wegner 1976, reviewed in Pollard 2016). In the absence of any regulatory input, the dynamics of filament assembly, including the gap period before the onset of nucleation, the average rate of filament elongation during the elongation phase, and the distribution of filament lengths during the treadmilling phase, are solely controlled by the concentration of the monomer pool.

In a typical cell, the concentration of actin is so high that, without regulation, more than 99% of the actin would polymerize in seconds (Pollard 2016). However, about half of cellular actin remains in the monomeric form (Dominguez and Holmes 2011). This is because cells harness a variety of proteins to inhibit spontaneous nucleation and use additional assembly factors to promote regulated nucleation and elongation in response to internal or external signals.

Two major actin-monomer-binding proteins that prevent spontaneous nucleation in cells are profilin and thymosin-β4. Profilin is expressed in most eukaryotes, while thymosin-β4 is expressed in a more limited subset of cell types (Kinosian, Selden, et al. 2000; Carlier et al. 1993; Yu et al. 1993; Xue et al. 2014). Profilin and thymosin-β4 are sufficiently abundant in cells, and have sufficiently high affinity for G-actin, such that almost all monomeric G-actin bind to either profilin or thymosin-β4 (Pollard 2016). Here I focus on profilin, which has been more intensively studied in recent years. Profilin binds to the barbed end of G-actin, which sterically

inhibits spontaneous nucleation (Pollard and Cooper 1984). Binding of Profilin also inhibits the elongation at pointed, but not at barbed ends. Profilin-bound actin also plays an important role in regulating actin elongation, as I will discuss later in this chapter.

To overcome the effects of factors that suppress spontaneous nucleation, cells use two major nucleation factors: Arp-2/3 complex nucleates side branches on existing actin filaments, and formins nucleate unbranched actin filaments (Rottner, Faix, et al. 2017; Pollard 2016).

Arp-2/3 complex is a seven-protein complex that was first purified due to its affinity for profilin (Machesky et al. 1994). The core subunits Arp-2 and Arp-3 are structurally similar to actin. When activated, Arp-2/3 complex undergoes a conformational change that allows it to bind to the side of a mother actin filament. This binding triggers a secondary conformational change, which brings Arp-2 and Arp-3 closer together to provide a seed (base) for the elongation of daughter filament (Ti et al. 2011). The daughter filament elongates at a 70° angle from the mother filament, leading to the formation of branched actin networks (Goley and Welch 2006). Because Arp2/3 complex has intrinsically low activity, cells use different nucleation-promoting factors (NPFs) to activate the complex (Campellone and Welch 2010). Two major NPFs for ARP2/3 complex are SCAR/WAVEs and WASPs. Both SCAR/WAVEs and WASPs can not only promote binding of Arp2/3 complex to F-actin, but also they recruit additional G-actins as the first two subunits of the daughter actin filament to initiate elongation after nucleation (Ti et al. 2011).

Formins are a second major family of factors that promote both filament nucleation and elongation. Formins, found in nearly all eukaryotic cells, are homodimeric proteins which are defined by a shared, highly conserved formin homology 2 (FH2) domain, which contains the core nucleation and elongation activity (Chesarone et al. 2010). Most formins also contain a proline-rich FH1 domain that recruits profilin-actin and enhances the activity of FH2 (Kitayama and Uyeda 2003; Higgs 2005). Additional N and C terminal domains mediate the regulation of formin activity by Rho family GTPases and other accessory factors (Sit and Manser 2011; Higgs 2005). In the initial phylogenetic classification by Higgs and Peterson, 7 metzaoan groups of formins are defined (Bogdan et al. 2013; Higgs 2005). In this introduction, I am going to focus on the subset of formins that belong to the Diaphanous-related formins (DRFs), which

are structurally similar to *C.elegans* formin CYK-1.

Formins function as homodimers (Goode and Eck 2007; Paul and Pollard 2009). The FH2 domains form head-to-tail dimers with a donut-like structure (Xu et al. 2004). The inner domain of this structure interacts with actin subunits wrapping around the barbed end of an actin filament. *In vitro* studies of yeast formin Bni1 have shown that dimers of isolated FH2 domains can nucleate F-actin by stabilizing an actin dimer, although at a very low efficiency (Pring et al. 2003; Sagot et al. 2002). Other than nucleation, the FH2 domain also impact actin elongation. *In vitro* studies suggest that FH2 dimers bound to barbed ends exist in an equilibrium between two states, an open state which allows G-actin to bind to the barbed end, and a closed state that prevents new subunit addition and stops elongation. Different formins spend different amounts of time in each state. Second, after the addition of a new subunit, the lagging unit of the FH2 dimer steps toward the barbed end, allowing the FH2 dimer to remain associated with the barbed end during filament elongation (Paul and Pollard 2009; Vavylonis, Kovar, et al. 2006). Thus, by itself the FH2 dimer can be treated as a processive barbed end capping factor, which blocks capping proteins and inhibits the elongation of F-actin *in vitro*. The FH1 domain is an unstructured proline-rich domain that can bind to profilin, which plays an essential role in F-actin elongation (Goode and Eck 2007; Paul and Pollard 2009). During elongation, FH1 domain preorients and delivers profilin-actin complexes to the barbed end to accelerate elongation beyond that expected for the diffusion limit for free actin (Vavylonis, Kovar, et al. 2006). For example, *in vitro* experiments show that mammalian formin mDia1 can increase the elongation rate by 5 fold compared to the filament elongation without formin, while the *C.elegans* formin/CYK-1 increases the elongation rate by 7 fold, and fission yeast formin Cdc12p elongates actin filaments at the rate comparable to the elongation without formin at a given actin concentration (Neidt et al. 2008; Kovar, Harris, et al. 2006).

In addition to the FH1/FH2 domains, many DRFs also contain several domains that regulate their activities, including the N-terminal Rho GTPase-binding domain (GBD), Dia-inhibitory domain (DID), and the C-terminal diaphanous autoregulatory domain (DAD) (Breitsprecher and Goode 2013; Goode and Eck 2007). In the default inactive state, DID bind to DAD to auto-inhibit formin's nucleation and elongation activity. An NPF (nuclear-promoting factor)

Rho-GTP can bind to GBD and release the DID-DAD autoinhibition to activate formin. In addition, other factors, such as anillin, can act as cofactors to promote the activation of formin (Watanabe, Okawa, et al. 2010).

Members of the Ena/VASP family of elongation factors do not appear to nucleate actin filaments (Pollard 2016). They can bind to the barbed ends of either branched or unbranched actin filaments (Winkelman, Bilancia, et al. 2014; Havrylenko et al. 2015). Ena/VASP functions as tetramers. Each subunit contains both proline-rich regions and WH2 domains, which allow them to recruit profilin-actin and monomeric G-actin, respectively, to the barbed end (Pollard 2016). Like formins, Ena/VASP tetramers are processive elongation factors that can remain bound to the barbed end of the filament through thousands of rounds of monomer addition. For example, *in vitro*, once attached to the barbed end, VASP tetramers can surf along an actin filament for $\sim$1166 monomers in the presence of 1μM actin before dissociating (Hansen and Mullins 2010).

Finally, in the presence of processive elongation factors, another group of actin binding proteins, capping proteins, are used to regulate the length of actin filaments *in vivo*. Capping proteins can either bind to barbed ends or pointed ends of actin filaments to inhibit subunit exchange, e.g. capping proteins (barbed end, Edwards et al. 2014) and tropomodulins (pointed end, Yamashiro et al. 2012). The most ubiquitous and abundant of this class of proteins, known simply as "Capping Protein (CP)", is found in nearly all eukaryotic organisms (Edwards et al. 2014). It is a 64kDa heterodimer of structurally related $\alpha-$ and $\beta-$subunits. *In vitro*, CP binds to the barbed end of actin filaments in a 1:1 ratio to prevent both the addition and loss of actin subunits. Also, knocking down CP *in vivo* results in excessive elongation of actin filaments and produces a variety of defects, including in muscle structure and cell motility defects (Edwards et al. 2014).

1.2.2 Disassembly

As mentioned above, the different critical concentrations for the barbed and pointed end can lead to treadmilling behavior *in vitro* involving continuous assembly and disassembly of actin

monomers at both ends. However, the spontaneous disassembly rate measured *in vitro* is too slow to account for the rapid turnover of filaments observed *in vivo*, which motivates the discovery of actin disassembly factors (Brieher 2013; Bamburg 1999).

Two major severing proteins in eukaryotes are cofilin and members of the gelsolin super family. Cofilin is a 15-kDa protein that is expressed in all eukaryotic cells (Bernstein and Bamburg 2010). Cofilin binds to the sides of actin filaments in a cooperative manner, with a higher affinity for ADP-actin subunits than ATP-actin subunits. Binding of cofilin has two profound effects on actin filaments. First, weak binding of cofilin to ADP-Pi subunits promotes dissociation of the γ-phosphate, which accelerate ADP-actin producing rate and in turn promotes rapid disassembly (Pollard 2016). Second, cofilin also binds cooperatively to the side of actin filaments. This binding locks actin subunits into a local structural change, making segments of cofilin-bound F-actin more flexible than neighboring naked F-actin segments. This difference in local compliance causes stress to accumulate at the interface between the cofilin decorated segments and naked segments, promoting breaking and severing at the interface (McCullough et al. 2008). In principle, the free barbed ends produced by Cofilin-mediated severing could induce new actin polymerization, if they are not rapidly capped by CP (Ichetovkin et al. 2002).

The gelsolin super family contains large multi-domain proteins (Sun, Yamamoto, et al. 1999). The founding member of this family, gelsolin, was first identified as an actin capping protein, and then subsequently proved to have potent F-actin severing activity. *In vitro*, gelsolin severs actin filaments stoichiometrically and with close to 100% efficiency (Kinosian, Newman, et al. 1998). Like cofilin, gelsolin binds to the side of actin filaments and alters their local conformation to induce rapid disassembly and severing. However, in contrast to cofilin, gelsolin remains associated with the barbed end of newly severed filaments to prevent new assembly (Pollard 2016).

Other than these two major severing factors, more and more proteins have been found to promote actin disassembly. One family is called MICALs (Alto and Terman 2018). MICALs are oxidation-reduction enzymes that directly bind and oxidize actin subunits to disrupt filament stability. Importantly, in contrast to cofilin and gelsolin, MICALs chemically modify actin to promote disassembly, so it doesn't automatically replenish the pool of polymerization-competent

actin monomers, unless other enzymes like SelR/MsrB come in to reverse the modification (Alto and Terman 2018).

1.2.3 Crosslinkers

Cells employ a variety of nucleation factors, elongation factors, capping proteins and severing proteins to assemble filaments at different densities, with different architectures (branched vs unbranched) and lengths. Once assembled, or as they assemble, actin filaments also interact with a variety of crosslinkers and myosin motors, which mediate their organization into different higher order structures.

There are many intensively studied crosslinkers in cells, including fascin, fimbrin, α-actinin, spectrin, and filamin (reviewed in Pollard 2016). Although they vary widely in sequence and structure, all crosslinkers use two actin-binding domains (ABDs) to connect two actin filaments together. Some crosslinkers contain two ABDs within the same polypeptide; others contain single ABDs and operate as dimers (Pollard 2016). Despite this shared feature, crosslinkers differ in several essential ways (Takiguchi et al. 2009): First, variation in the distance between the two ABDs plays a key role in shaping network architecture. Crosslinkers with a small distance between ABDs, such as fascin, fimbrin, and α-actinin, are more likely to bundle actin filaments, while crosslinkers with a large distance between ABDs, such as spectrin and filamin, tend to crosslink actin filaments into networks. Second, some crosslinkers, such as fascin, preferentially crosslink filaments of the same orientation, thus favoring the formation of parallel actin bundles. Finally, as I will discuss further below, different crosslinkers can cooperate or compete with one another for binding to actin filaments.

1.2.4 Myosin

The final group of actin binding proteins that I will discuss are myosin-II motors. Myosin is a diverse superfamily of actin-based molecular motor proteins (Sellers 2000). The founding member of this super family - skeletal muscle myosin-II, powers muscle contractions, but many members of this family operate in non-muscle cells, where they are responsible for a wide variety

of functions, including transport of organelles and other cargoes and generating mechanical forces that drive cell shape change, cell division, cell movements and tissue morphogenesis during embryonic developments. Here, I will focus on non-muscle myosin-II, which is responsible for generating contractile forces in non-muscle cells, including during cell division (reviewed in Sellers 2000; Vicente-Manzanares et al. 2009).

Myosin-II is a hexamer composed of two heavy chains, and two pairs of light chains, called essential light chains and regulatory light chains (MELC and MRLC), respectively (Sellers 2000). Each of the heavy chains contains an N-terminal motor domain, an α-helical neck region, and a long α-helical rod domain. The motor domain is highly conserved among different isoforms of myosin-II, and is responsible for producing the force that propels myosin-II towards the barbed end of actin filaments. The neck domain interacts with both pairs of light chains, and is essential for the regulation of myosin activity. The tail domain is important both for heavy chain dimerization, and the ability of myosin-II to polymerize into bipolar filament. The MELC plays an important role in myosin motor activity and ATPase cycle. The MRLC plays essential roles in the regulation of Myosin activity and polymerization. At the default state, myosin-II is autoinhibited by the interaction between the tail domain and MRLC, which adopts a folded conformation that prevents F-actin binding, ATPases activity, and the formation of minifilaments (Sellers 2000).

Myosin-II generates forces by coupling ATP hydrolysis to conformational changes (De La Cruz and Ostap 2004). The motor domain of the myosin-II heavy chain is an ATPase, which can bind both to ADP and ATP. A myosin motor domain lacking a bound nucleotide binds tightly to an actin filament. Recruitment of ATP reduces the affinity of this interaction and causes the motor domain to detach from the actin filament. This release induces a large conformational change in the motor domain, causing it to swing about 5 nm ahead to a new actin binding site, and hydrolyses ATP into ADP and inorganic phosphate. Weak binding of the motor domain with the actin filament at the new binding site releases the inorganic phosphate, which triggers a force-generating power stroke that slides the actin filament. This cycle restarts when ADP is released and a new ATP is recruited.

One unique feature of myosin-II is its ability to polymerize into bipolar filaments (Moussavi

et al. 1993). A single myosin hexamer is not a processive motor. However, a bipolar myosin mini-filament composed of many myosin-II motors can move processively along actin filaments (Melli et al. 2018; Niederman and Pollard 1975). Both the motor activity of myosin-II and its polymerization ability are regulated by phosphorylation of the MRLC (Moussavi et al. 1993). When unphosphorylated, MRLC binds to the tail domain of the heavy chain, holding myosin-II in a folded conformation to inhibit its motor activity and ability to polymerize. Phosphorylation of MRLC releases the tail domain of heavy chains, which activates myosin-II and allows it to assemble into minifilaments.

1.3 Mechanisms for self-organization

More than 100 different ABPs regulate the four basic processes mentioned above to organize actin filaments into different arrays (Dos Remedios et al. 2003). The current challenge is to understand how dynamic interactions among these ABPs and F-actin allow them to self-organize into different arrays. Building on previous ideas (Michison 2011) (who defines a self-organization as a system spontaneous assemble from soluble precursors, with characteristic size/shape/function, and can rapidly recover from damage), I define a self-organized array as one with the following features: 1). It can spontaneously assemble from a collection of proteins. 2). It has a characteristic shape, size, internal organization and function. 3). The system is dynamic. It consumes energy to maintain its shape/size/organization while undergoing continuous dynamic exchange of components. 4). In addition, self-organized arrays are often stabilized by a dynamical balance of opposing processes. These can be biochemical processes such as binding vs. unbinding of monomers, or mechanical processes such as extension vs. contraction, or active forces acting against passive (e.g.viscoelastic) resistance. The dynamic balance/unbalance of these opposing processes governs the dynamics of the structure. Interestingly, these processes can be regulated both internally or externally. Internally, these opposing processes can be coupled to negative feedback loops, so that the strength of the opposing processes are regulated internally to generate a dynamic steady states that the system can always return to from small perturbations. Also, external signals can act on cells to modulate the strength of these opposing processes to change the dynamics of the systems.

As a simple example, let's consider an idealized scenario in which a single actin filament undergoes treadmilling in a pool of monomers that are unable to nucleate. This actin filament can be viewed as a most basic self-organized array. It has a characteristic shape, which is a rod-shape filament, and adopts a dynamically stable state characterized by treadmilling at constant length, while continuously exchanging actin subunits at both ends. In this simple array, the fundamental opposing processes are monomer binding and unbinding. At each end, a net imbalance of one over the other leads to net polymerization or depolymerization. Internally, since the critical concentration of the pointed end is higher than that of the barbed end, there exists a range of monomer concentrations such that the pointed end depolymerizes while the barbed end polymerizes, leading to treadmilling (for more details, see Introduction:assembly). Importantly, net polymerization reduces the concentration of free monomers and thus reduces polymerization speed, while net depolymerization increases monomers and increases polymerization speed. These feedback loops define a dynamically stable steady state, in which the free monomer concentration approaches a concentration at which the net growth rate of the barbed end equals to the net disassembly rate of the pointed end (for more details, see Introduction: assembly). To maintain this steady state, the actin filament consumes energy from ATP hydrolysis. In addition, various external perturbations and signals can change the dynamics of this actin filament by changing the dynamics of the opposing processes, including small molecules like jasplakinolide and latrunculin A (Yarmola et al. 2000; Bubb et al. 2000), or other actin binding proteins like elongation factors and severing proteins (see previous sections for details).

Of course, a treadmilling actin filament by itself is unable to produce any forces. However, if we place the barbed end of this filament against a piece of cell membrane, and fix the actin filament in space, then binding of new monomers at the barbed end can rectify fluctuations in the membrane and/or the filament barbed end to generate forces to push the membrane outward (Peskin et al. 1993; Mogilner and Oster 1996). This reveals the core concept of assembling actin arrays in cells: although many actin arrays are able to self-organize, they still need external cues to know where and when to assemble. I call this process a guided self-organizing process: firstly, extracellular or intracellular signals defines the time and space an actin array needs to be assembled, and recruit/activate a subset of ABPs locally; then, these ABPs interact with one another and with F-actin to self-organize into specific actin arrays.

About two decades ago, a set of breakthrough experiments showed that a group of small GTPases — the Rho-GTPases — can control the formation of different actin arrays (Nobes and Hall 1994) (Figure 1.3-A). These pioneering experiments showed that cells can use Rho-GTPases to control where and when to build an actin array. More importantly, localized activation of different Rho-GTPases control the assembly of different actin arrays. To do so, Rho-GTPase act through different effectors to recruit/activate specific ABPs/regulators of actin assembly, disassembly, crosslinking and contractility. In addition, synergistic and/or competitive interactions among different network architectures and ABPs lead to further recruitment and/or partitioning of factors to specific networks. It is worth noticing that this is not just a simple linear cascade. It involves a lot of crosstalk and feedback, not only within a specific Rho signal pathway, but also between different Rho signaling pathways to further refine the location of the activated Rho signals, and recruit and/or partition factors to specific arrays (Figure 1.3-C).

In this section, I will first introduce the master regulators, Rho-GTPases, and how cells use them to specify when and where to initiate the formation of various actin arrays. Secondly, I will discuss how different crosstalk and feedback loops among different components within a structure can further segregate specific ABPs to specific arrays. Then, I will use some well-studied examples to further illustrate how different cytoskeletal arrays can form through a process of guided self-organization.

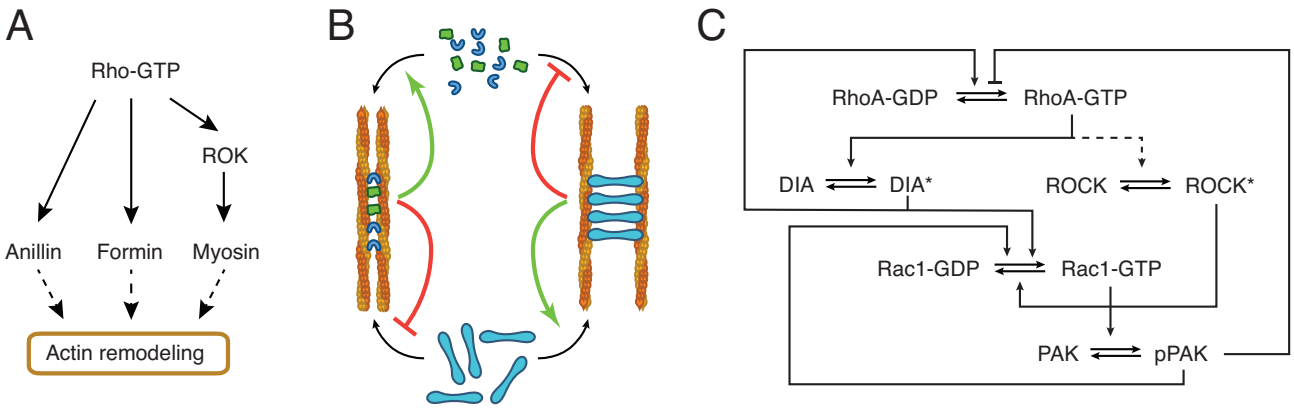

Figure 1.3. Actin arrays use guided-assembly process to segregate specific ABPs to specific arrays. A. An example of upstream signals that activate/recruit downstream effectors that are important for actin arrays assembly (Michaux et al. 2018). B. An example of synergistic/competitive binding among ABPs that sort different ABPs to different structures (Winkelman, Suarez, et al. 2016). C. An example of feedback loops and crosstalk among different Rho-GTPase that further strengthen the sorting of ABPs (Bolado-Carrancio et al. 2020).

1.3.1 Rho-GTPases as master regulators to initiate the formation of self-organized actin arrays

Rho GTPases have emerged as key intracellular mediators of guided self-organization of actin arrays in animal cells (Narumiya and Thumkeo 2018; Sit and Manser 2011; Bishop and Hall 2000). The Rho GTPase family contains eight subfamilies, including RhoA, Rac, and Cdc42. Like other GTPases, Rho proteins cycle between GTP-bound (active) and GDP-bound (inactive) states. This cycle is controlled by three types of proteins: Guanine nucleotide exchange factors (GEFs), GTPase-activating proteins (GAPs), and Guanine nucleotide dissociation inhibitors (GDIs). GEFs accelerate the dissociation of GDP, allowing the nucleotide-free GTPase to quickly rebind to GTP, thus activating GTPase. GAPs accelerate GTP hydrolysis to GDP and thus inactivate GTPase. GDIs sequester the GDP-bound form of GTPase to prevent them from interacting with GEFs, thus inhibiting activation of GTPase.

Seminal studies from Alan Hall's group in the early nineties established key roles for Rac, Rho and CDC-42 in controlling specific actin arrays in fibroblast cells (Nobes and Hall 1994). They found that RhoA stimulates the formation of actin stress fibers, Rac stimulates the formation of lamellipodia, and Cdc42 stimulates the formation of filopodia. These studies raised the fundamental question: How can the activity of a single molecule specify the assembly of such different and complex arrays?

A key part of the answer is that Rac, Cdc42 and Rho act as master regulators by engaging different groups of effector proteins, which in turn promote the local recruitment and/or activation of different sets of ABPs to promote the assembly of different actin arrays. For example, active RhoA engages its downstream effectors ROK and formin. Formins nucleate and elongate unbranched actin filaments while ROCK activates myosin, both of which are essential for stress fiber formation (Tojkander et al. 2012; Alberts and Treisman 1998; Tominaga et al. 2000; Chrzanowska-Wodnicka and Burridge 1996; Honer et al. 1988). In addition, ROCK activates LIM-kinase, which inactivates cofilin to inhibit filament disassembly and maintain the stress fiber integrity (Maekawa et al. 1999). Cdc42 activates a different set of downstream effectors to induce the formation of filopodia (reviewed in Johnson 1999; Olson 2003; Cotteret

and Chernoff 2002). First, Cdc-42 recruits IRSp53, an I-BAR domain containing protein that couples membrane deformation and F-actin polymerization, and activates Ena/VASPs to elongate unbranched actin filaments (Krugmann et al. 2001; Prévost et al. 2015). Second, Cdc-42 recruits IQGAP, which recruits formin mDia to nucleate and elongate unbranched actin filaments, which are then crosslinked into parallel bundles to form filopodia (Bishop and Hall 2000; Brandt and Grosse 2007). Cdc42 can also activate WASP, and thus activates Arp2/3 complex to promote the formation of branched actin networks, which can serve as a basis for filopodia assembly (discussed further below). Finally, Rac can promote the formation of lamellipodia through its downstream effectors WAVE, PI3K, and Pak. Firstly, Rac recruits WAVE, which activates Arp2/3 complex to generate dendritic actin networks necessary for lamellipodia. Secondly, it recruits a protein kinase Pak, which in turn activates LIM-kinase to inhibit cofilin and promote actin polymerization and stability (reviewed in Chernoff 1999; Cotteret and Chernoff 2002; Bishop and Hall 2000).

1.3.2 Synergistic/competitive binding help to recruit more ABPs

Once a subset of ABPs are recruited, they can facilitate the recruitment of addtional factors. Selective recruitment/participation of additional factors can occur in multiple ways. First, different types of actin filaments can recruit different ABPs (e.g. ATP-actin vs ADP actin, curved actin filaments vs straight actin filaments, branched actin filaments vs unbranched actin filaments). Secondly, two ABPs can have directional interactions, in which binding of one ABP to actin filaments promotes binding of the other, either directly or indirectly. For example, as we mentioned above, the scaffold protein anillin can recruit myosin to actin filaments. Thirdly, two ABPs can bind synergistically/competitively to actin filaments.

An excellent example of an ABP showing different affinities for different types of actin filaments comes from studies of the severing factor cofilin (Cao et al. 2006; Hayakawa et al. 2011). As previously mentioned, cofilin has a higher affinity for ADP-actin subunits, so it is more likely to bind to regions of filaments populated with ADP-actin. Interestingly, cofilin also prefers to associate with the curved actin filaments, and tension prevents cofilin from binding to actin filaments (Hayakawa et al. 2011). Thus, myosin can have opposite effects on cofilin recruitment

to an actin filament, depending on whether it induces tension or compression along the filament. In addition, cofilin is also a good example for synergistic ABP binding, because cofilin binds to actin filaments in a cooperative manner. Cooperative cofilin binding arises because binding of one cofilin molecule alters actin structure locally, making it more flexible and inducing twisting of the neighboring region to promote binding of additional cofilins (De La Cruz 2005; Cao et al. 2006; McCullough et al. 2008).

Many examples of synergistic/competitive binding of multiple ABPs come from studies in fission yeast (Christensen, Hocky, et al. 2017; Christensen, Homa, et al. 2019; Winkelman, Suarez, et al. 2016). As mentioned previously, fission yeast has three distinct actin structures – actin cables, actin patches, and the contractile ring (Kovar, Sirotkin, et al. 2011). Different sets of ABPs are activated/segregated to these different networks: Arp2/3 complex, fimbrin, and myosin I are localized to actin patches; the formin/Cdc12, IQGAP, anillin, and myosin II are localized to the contractile ring; and the formin/For3 and myosin V are localized to actin cables (reviewed in Kovar, Sirotkin, et al. 2011). Many of these ABPs are sorted through synergistic/competitive binding. For example, fimbrin and cofilin exclude tropomyosin from actin patches, while tropomyosin and α-actinin prevent fimbrin from associating with actin filaments in the contractile ring (Christensen, Hocky, et al. 2017; Christensen, Homa, et al. 2019). The basis for this mutual exclusion lies in both synergistic and competitive interactions among these proteins. First, binding of tropomyosin/cofilin promotes binding of the same proteins and inhibits binding of the other proteins. Second, the strength of inhibition depends on the environment. With low cofilin concentration, binding of tropomyosin inhibits cofilin binding to actin filaments. However, at higher concentrations of cofilin, or as filaments age and the majority of actin filament subunits become ADP-actin, cofilin can start to bind to actin filaments cooperatively and displace tropomyosin from actin filaments. Third, the strength of inhibition can be affected by other crosslinkers too. For example, fimbrin also inhibit tropomyosin from binding to actin filaments. Working together, cofilin and fimbrin can exclude tropomyosin from the actin patches in fission yeast. Moreover, fimbrin also competes with α-actinin for actin binding sites (Christensen, Homa, et al. 2019). Since fimbrin has higher affinity than α-actinin for actin filaments, it displaces α-actinin when they are the only two crosslinkers present. In contrast, tropomyosin enhances the bundling activity of α-actinin by enhancing the binding of

α-actinin to F-actin. Thus, working together, tropomyosin and α-actinin can displace fimbrin from actin cables.

In addition, synergistic/competitive binding can also involve dynamic changes in local network architecture. For example, fascin- and α-actinin-bundled networks contain intrinsic structural features that can drive protein sorting (Winkelman, Suarez, et al. 2016) (Figure 1.3-B). This is because fascin and α-actinin have large differences in the distance between their two actin binding domains (ABDs), they both prefer, and favor the formation of, bundles with different interfilament spacings. Fascin generates bundles that are more densely packed, promoting its own association and the association of other crosslinkers with comparable distances between their two ABDs, like fimbrin or espin, and inhibiting the association of other crosslinkers like α-actinin. On the other hand, bundles formed by α-actinin have larger interfilament spacing, promoting further binding of α-actinin, and inhibiting the binding of fascin, fimbrin and espin.

1.3.3 Feedback within the same Rho family GTPase signal pathway and crosstalk to other GTPases

As I mentioned above, the Rho pathways are not simple linear cascades. There exist many feedback and crosstalk to further refine the location of the activated Rho signals, and recruit and/or partition factors to specific arrays (Figure 1.3-C).

Firstly, many downstream effectors can feedback to Rho-GTPase signal itself to promote or inhibit its activation. For example, during pulsed actomyosin contraction, activation of RhoA can promote its own activation, although the biochemical natural of this autocatalysis is currently unknown (Michaux et al. 2018). On the other hand, during focal pulses, RhoA activates formins to assemble unbranched actin filaments, which in return recruit a GAP RGA-3/4 to inhibit RhoA activation (Michaux et al. 2018). Like RhoA, active Cdc42 and Rac can also either promote or inhibit their own activity (Gulli et al. 2000; Woods and Lew 2019; Weiner, Neilsen, et al. 2002; Costa et al. 2007; Wu, Wu, et al. 2013; Weiner, Marganski, et al. 2007).

Secondly, there is also a lot of crosstalk among the different Rho GTPase signaling pathways (Guilluy et al. 2011). For example, there is crosstalk through the regulation of GTPase activity.

In migrating cells, at the rear, active RhoA promotes myosin II contractility through ROCK, which in return suppresses the Rac GEF β-Pix to suppress Rac activation and confine Rac activation to the leading edge of the cell. At the leading edge, active Rac recruits a RhoA specific GAP, p190RhoGAP, to inhibit RhoA activation and exclude active RhoA from the leading edge (reviewed in Lawson and Burridge 2014). Secondly, the crosstalk can happen through regulation of protein expression and stability, which is well studied in Rho GTPases' interaction with RhoGDIs. RhoGDIs are Rho guanine nucleotide dissociation inhibitors, which hold Rho proteins passively in an inactive state within cytoplasm and protect them from degradation. Since RhoGDIs level are limiting, different Rho proteins compete for binding to RhoGDIs, and an over expression of one Rho family member can displace other Rho proteins from RhoGDIs, leading to their degradation (Boulter et al. 2010). Thirdly, the crosstalk can also happen through the regulation of downstream signaling pathways. As we mentioned above, many downstream effectors are shared among different Rho signal pathways, allowing different Rho GTPases to act synergistically to regulate one particular cellular processes. For example, in neuronal growth cones, Both Rac and Cdc42 can regulate neurite outgrowth through inhibiting cofilin activity (Kuhn et al. 2000).

1.3.4 Examples of self-organizing actin structures

The lamellipodium as a cell front pushing machine

The lamellipodium is a broad and flat veil that extends outward at the leading edge of many migrating cells. It is composed of a so-called dendritic network of actin filaments, which are polarized with their growing barbed ends pointing towards the leading edge (Schaks et al. 2019). Polymerization of these barbed ends produces forces that push the leading edge forward (Peskin et al. 1993; Mogilner and Oster 1996; Dickinson, Caro, et al. 2004; Kovar and Pollard 2004; Bieling et al. 2016). During migration, the entire structure undergoes continuous treadmilling, with growth localized to the leading edge, and disassembly at the rear, so that it can continuously generate forces to push the cell front forward (Pollard, Blanchoin, et al. 2000).

The dynamic basis for lamellipodium treadmilling *in vivo* is a dynamic interplay among localized

Arp2/3 complex activity, capping, actin filament aging, and disassembly (Mullins et al. 1998; Pollard, Blanchoin, et al. 2000). In lamellipodia, Arp2/3 complex is activated at the front to continuously nucleate branched actin filaments, which are quickly capped by capping proteins. As actin filaments are pushed by leading edge assembly towards the rear of the lamellipodium, they "age" into ADP-bound actin filaments, which attract cofilin to promote disassembly. The disassembled actin monomers then enrich the cytoplasmic monomer pool to support further actin assembly at the front of the structure (Krause and Gautreau 2014; Pollard and Borisy 2003; Mullins et al. 1998; Blanchoin et al. 2014). Similar to the example of single actin filament dynamics mentioned above, this continuous dynamic balance of "assembly at the front" and "disassembly at the rear", driven by the continuous consumption of ATP, allows a lamellipodium to continuously treadmill while maintaining a characteristic size and shape (Figure 1.4).

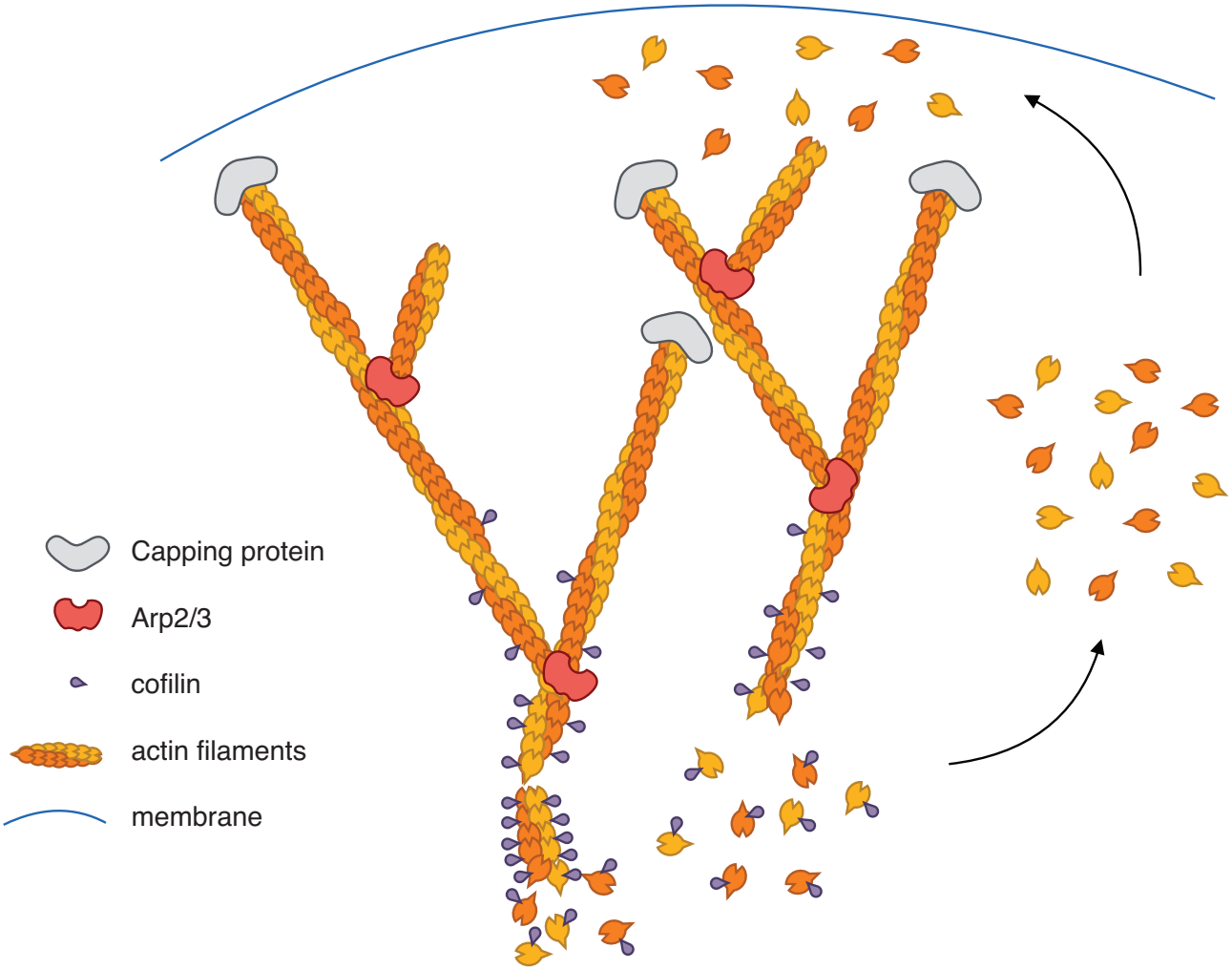

Figure 1.4. A schematic overview of the treadmilling dynamics of lamellipodia. Filaments are nucleated by Arp2/3 close to the plasma membrane, and quickly capped by capping proteins. Filaments age by ATP hydrolysis, and recruit cofilin to facilitate disassembly at the rear. Disassembled actin monomers refill the monomer pool to drive additional nucleation and elongation close to the membrane.

The key features of the dendritic treadmilling model for actin-based propulsion were confirmed

by the *in vitro* reconstitution studies (Theriot et al. 1994; Welch, Iwamatsu, et al. 1997; Welch, Rosenblatt, et al. 1998). These studies were motivated by the seminal observation that certain bacterial pathogens, such as *Listeria monocytogenes*, can propel themselves through the cytoplasm of a host cell by harnessing the host cell's actin assembly machinery (Dabiri et al. 1990). To do so, they express a protein called ActA on their surfaces, which locally activate Arp2/3 complex to promote the polarized assembly of dendritic actin filaments, which trail comet-like behind the moving bacterium. Building on these observations, Loisel et al. were able to reconstitute the actin based propulsion of polystyrene beads coated with ActA in a solution containing only Arp2/3 complex, capping proteins, actin, ATP, and cofilin (Loisel et al. 1999; Cameron et al. 1999). Others later reproduced similar results using *E.coli* expressing the *Shigella* IcsA (which can activate WASP), beads coated with WASP, or micro-printing rectangular patterns coated with WASP (Bernheim-Groswasser et al. 2002; Manhart et al. 2019; Egile et al. 1999). In these experiments, the only external input is the spatial information that locally activates Arp2/3 complex. After Arp2/3 complex is locally activated, the rest of the structure can automatically self-organize from a mixture of the soluble components mentioned above, providing strong evidence that this is a self-organization process. It's worth noticing that in these *in vitro* experiments, the entire beads are coated with the target prteins like ActA. After Arp2/3 complex are activated, symmetry breaking occurs through a Elastic Gel model to allow Arp2/3 complex to form "comet tails" to push beads around (Dayel et al. 2009).

The mechanisms by which migrating cells locally activate Arp2/3 complex at the leading edge *in vivo* are still incompletely understood, but they appear to involve local enrichment of the phospholipid PIP3 at the leading edge, in response to internal cues such as membrane curvature, or in response to external signals such as EGF (Krause and Gautreau 2014; Gallop et al. 2013). PIP3 in turn recruits phosphoindositide-binding proteins to the membrane, leading to local activation of RAC (Krause and Gautreau 2014). Once activated, RAC interacts with WAVE to recruit/activate Arp2/3 complex. In addition to this dominant pathway, other factors such as lamellipodin and clathrin can also directly recruit WAVE complex to the leading edge (reviewed in Krause and Gautreau 2014).

As with other self-organized arrays, many feedback loops are involved in regulating the structure

and dynamics of lamellipodia. For example, a positive feedback loop allows lamellipodia to be mechanosensitive, and produce more pushing force against high load. In the face of high load, more filaments in lamellipodia bend away from the leading edge, causing Arp2/3 complex to generate more filament branches with an average angle of 70° instead of 35°, leading to a dendritic network with a higher density of actin filaments and a more compact architecture. As a result, the network is stiffer, can bear more opposing forces, and has higher barbed ends density, which can generate more pushing force to push the membrane (Bieling et al. 2016; Svitkina 2018b; De La Cruz and Gardel 2015; Lieleg et al. 2010).

Filopodia, the dynamic finger-like protrusions that explore surrounding regions

Filopodia are dynamic finger-like protrusions, 1-100 μm in length, that extend and retract from the surfaces of many different kinds of cells (Jacinto and Wolpert 2001; Rottner, Faix, et al. 2017). The primary function of filopodia is to sense cues within or transmit information to the surrounding environment. For example, filopodia can extend from the leading edge of motile cells to explore adhesive surfaces and sense soluble cues that influence the direction of cell migration.

Filopodia are composed of parallel bundles of actin filaments with their barbed ends oriented in the direction of protrusion (reviewed in Mattila and Lappalainen 2008; Yang and Svitkina 2011; Rottner, Faix, et al. 2017). Like lamellipodia, filopodia harness the oriented polymerization of actin filaments to push the cell membrane outward (Wang 1985; Mallavarapu and Mitchison 1999). In addition, continuous "assembly at the front" and "disassembly at the rear" allows them to treadmill while maintaining a characteristic structure. However, to do so, they use a set of core components and interactions that are unique to filopodia organization (reviewed in Mattila and Lappalainen 2008; Yang and Svitkina 2011; Rottner, Faix, et al. 2017). First they use elongation factors like Ena/VASP/formin to assemble unbranched instead of branched actin filaments. Second, they use the crosslinker fascin to crosslink filaments into parallel bundles (Jansen et al. 2011). Finally, filopodia also utilize myosin motors to transport proteins to the tip of protrusions. One key filopodia-specific factor is the motor protein Myosin X. Myosin X

moves towards the barbed ends of actin filaments. So, combining with retrograde flow, the tip of filopodia is able to exchange proteins back and forth with lamellipodia, such as Mena/VASP and integrins (Mattila and Lappalainen 2008; Jacquemet et al. 2015).

In vitro reconstitution experiments confirmed that the key to assembling filopodia is to assemble parallel actin bundles, which require unbranched actin filaments and fascin (Lee et al. 2010; Vignjevic et al. 2003; Haviv et al. 2006). Lee et al. 2010 showed that filopodia-like structures can automatically self-organize from a mixture of pre-existing dendritic actin network, fascin, and VASP/formin. Importantly, the pre-existing actin network is only important for filopodia initiation, but it's not required to form and maintain a filopodia-like structure after the self-organization process starts.

In vivo, cells need to locally recruit/activate Ena/VASP/formin and fascin to the leading edge to restrict filopodia formation to the leading edge. To do so, cells utilize two small Rho-GTPases to activate Ena/VASP/formin, which are CDC42 and RIF respectively. CDC-42 activates IRSp53, which serves as a scaffold protein for both WAVE2 and Ena/VASP (Krugmann et al. 2001). RIF can directly activate Dia2 to elongate unbranched actin filaments. In Hela cells, an overexpression of RIF promotes the formation of filopodia (Ellis and Mellor 2000). The mechanisms to recruit fascin is less well understood. Some studies suggest that ECM, Rac and Rab35 might play a role in this process, but more studies need to be done to confirm the mechanism (Adams 1995; Fischer, Tucker, et al. 1997; Clancy et al. 2019; Zhang et al. 2009; Parsons and Adams 2008).

Once activated, Ena/VASP/formin can initiate filopodia formation through two proposed models, the "convergent elongation model" and the "tip nucleation model" (reviewed in Yang and Svitkina 2011). The convergent elongation model proposes that filopodial actin filaments are assembled from pre-existing Arp2/3 complex nucleated filaments. The tip nucleation model proposes that nucleation factors such as formins are directly recruited and activated at the leading edge of the membrane, which in turn nucleate and elongate unbranched actin filaments from scratch. However, more studies need to be done to distinguish these two models (Vignjevic et al. 2003; Rottner, Faix, et al. 2017; Young, Heimsath, et al. 2015).

Many opposing processes regulate the dynamics of filopodia, including the speed of polymer-

ization at the barbed ends vs. the speed of depolymerization at the pointed ends, and the mechanical balance among the pushing force generated by actin polymerization, the friction against membrane and ECM, and the contractile forces from lamella. Like other self-organized arrays, many external signals can regulate these processes to change the dynamics of filopodia. For example, one way to stabilize filopodia is to use Myosin X to transport adhesion molecules like β-1 integrins to initiate the formation of focal adhesions (Fischer, Lam, et al. 2019; Steketee and Tosney 2002). In contrast, in retracting filopodia, cofilin are recruited to the shaft and the tip of filopodia, severing the entire bundle to generate rapid retraction (Breitsprecher, Koestler, et al. 2011). However, the mechanisms to recruit cofilin to the entire filopodium is not fully understood.

The ability to contract can emerge from different actin arrays through different mechanisms

In addition to generating pushing forces and resisting deformation, another fundamental role of many actin arrays is to contract (Svitkina 2018a; Murrell, Oakes, et al. 2015). It is essential for many physiological processes, including muscle contraction, cell division, cell migration, organelle transport, and multicellular tissue morphogenesis (Levayer and Lecuit 2012). Based on their organization, the contractile arrays can be divided into two groups: contractile networks and contractile bundles (Ennomani et al. 2016; Murrell, Oakes, et al. 2015; Reymann, Boujemaa-Paterski, et al. 2012). Examples of contractile networks include the cell cortex and lamella networks behind the leading edge. The contractile actin bundles are bundles of aligned filaments with antiparallel or mixed orientation. Examples include stress fibers of crawling cells, junctional belts in epithelia, the contractile ring, and sarcomeres.

Contractility is a self-organized behavior that emerges from individual interactions among actin filaments, crosslinking proteins and myosin motors. Here, I will discuss two types of mechanisms for self-organized contractility, the myosin independent contractility and myosin dependent contractility (Figure 1.5).

The key ingredient for myosin independent contractility is a dynamic coupling of crosslinking

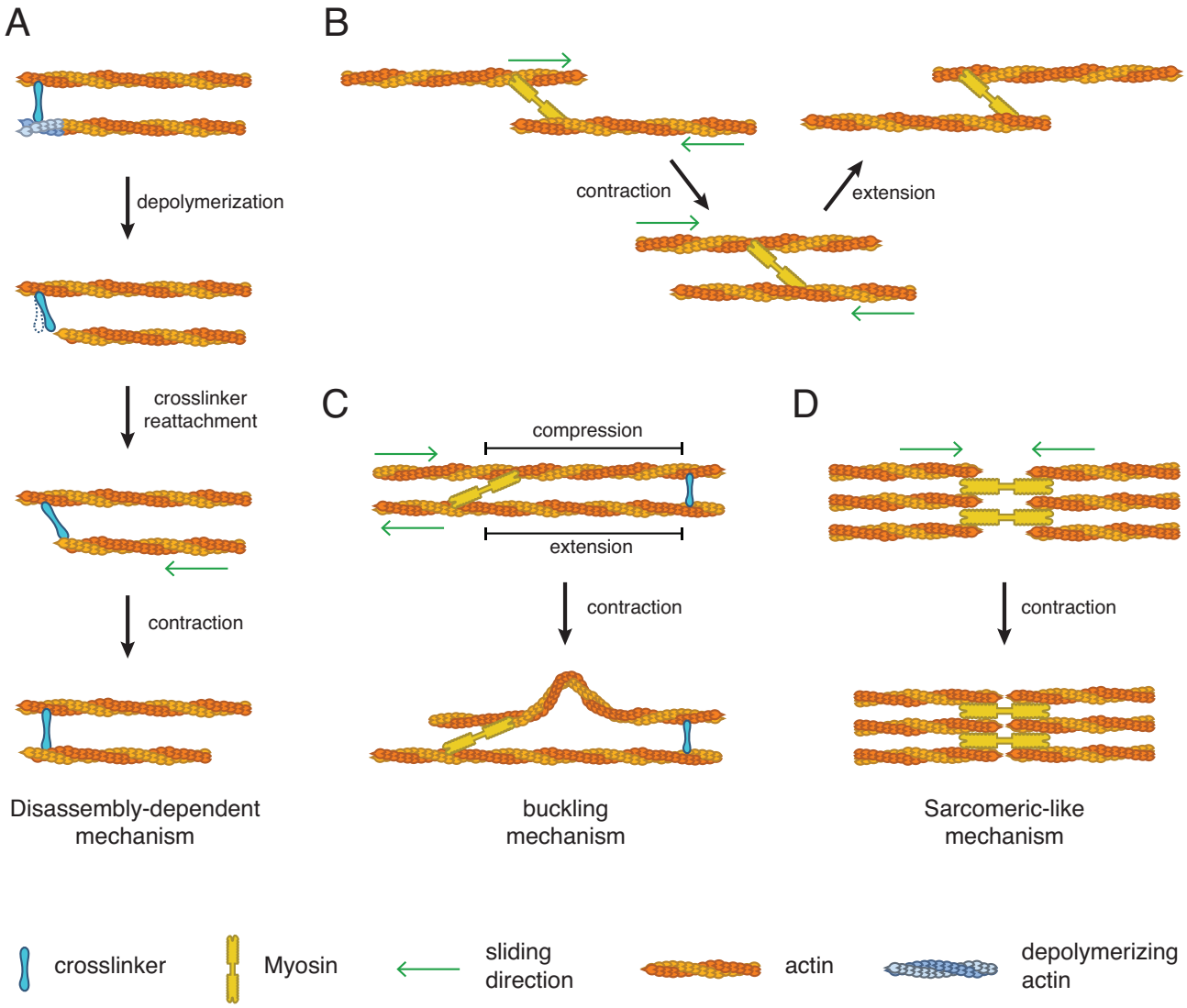

Figure 1.5. A schematic overview of different ways to drive contraction. A. Disassembly dependent mechanism. B. Myosin sliding can lead to either contraction or extension. C. Buckling mechanism. D. Sarcomeric-like mechanism.

and filament disassembly. The possibility of disassembly-dependent contraction was originally explored in a series of theoretical papers (Dickinson, Caro, et al. 2004; Zumdieck et al. 2007; Sun, Walcott, et al. 2010). The basic idea is that end-tracking crosslinkers track the pointed ends of depolymerizing filaments, exploiting thermal fluctuations to bind the depolymerizing filament under strain to drive relative sliding between filaments, leading to a net contractile stress (Figure 1.5-A). In line with this theoretical work, *in vivo* experiments show that in budding yeast, actin depolymerization can drive actomyosin ring contraction (Mendes Pinto et al. 2012).

For myosin-dependent contractility, the microscopic forces that drive contraction are generated by bipolar myosin mini-filaments that pull in opposite directions against pairs of oppositely oriented actin filaments. However, a bipolar motor is just as likely to pull two filaments together as it is to push them apart (Figure 1.5-B). Thus, to generate a net contraction instead of expansion, this fundamental symmetry must be broken (Ennomani et al. 2016; Murrell, Oakes, et al. 2015). The buckling mechanism and the sarcomeric-like mechanism provide two different ways to break this symmetry.

In buckling-based contractions, symmetry-breaking comes from the inherently nonlinear response of single actin filament to compressive vs tensile forces (Figure 1.5-C). In a well-connected network, it's hard for actin filaments to slide freely. Under this condition, when myosin motors exert forces on actin filaments, filaments are more likely to experience compressive forces and tensile forces than sliding (Lenz et al. 2012). Even though in a disorganized network, filaments are equally likely to experience compressive forces and tensile forces, they are more likely to buckle than to expand, because an actin filament can sustain tensile forces up to 200pN with minimal deformation, but it buckles easily in response to compressive forces higher than $\sim$1pN (reviewed in Murrell, Oakes, et al. 2015). Both theoretical and experimental studies show that this basic asymmetry in filament compliance is sufficient to drive macroscopic network contraction (Lenz et al. 2012; Murrell, Oakes, et al. 2015; Li et al. 2017).

The sarcomeric-like contraction mechanism is exemplified by the contraction of sarcomeres in skeletal muscle cells. In sarcomeres, actin filaments are organized into antiparallel bundles with their barbed ends localized at so-called Z-lines, and their pointed ends oriented towards the sarcomere center, where they engage bipolar myosin filaments (Huxley 1957). With

this configuration, myosin minifilaments pull the opposing filament bundles towards each other to generate contraction (Kruse and Jülicher 2000) (Figure 1.5-D). In non-muscle cells, many contractile bundles adopt a sarcomeric-like organization, characterized by alternating accumulations of motors and crosslinking proteins. As in sarcomeres, this organization favors net contraction instead of expansion. However, there does not need to be an obvious sarcomeric-like organization for this mechanism to work. Theoretical and modeling studies show that sarcomeric-like contractions can emerge whenever there is a sufficient bias in the distributions of motors and crosslinkers along filaments, with motors enriched near pointed ends and crosslinks enriched near barbed ends (Belmonte et al. 2017; Oelz et al. 2015; Lenz 2020).

How can actomyosin arrays self-organize into a sarcomeric-like patterns? *In vitro*, actomyosin arrays can self-organize into patterned structures with actin filaments sorted out into periodic arrays linked by myosin clusters (Stachowiak, McCall, et al. 2012). In this system, myosin clusters tend to migrate to locations with zero net actin filament polarity, resulting in myosin cluster separations. In principle, this kind of mechanisms might explain the patterns of motors and crosslinkers observed in stress fibers and adhesion belts. In addition, many theoretical models proposed that processive myosin motors coupled with filament treadmilling can bias myosin clusters to pointed ends and crosslinkers to barbed ends (Oelz et al. 2015). In this model, if a myosin cluster stays sufficiently long on an actin filament, and the filament treadmills faster than sliding, then overtime the elongating barbed end of this actin filament will move away from myosin, while the shortening pointed end moves toward the cluster, biasing myosin to the pointed ends.

Interestingly, different actin arrays can use different mechanisms to contract, and they also contract with different efficiency. For example, actin networks with low connectivity contract mainly through a sarcomeric-like mechanism. When the connectivity goes up, the contribution of buckling mechanism also goes up (Murrell, Oakes, et al. 2015). Secondly, both *in vitro* and *in vivo* studies suggest that aligned actin bundles (with antiparallel or mixed orientation) contract more efficiently than actin networks (Reymann, Boujemaa-Paterski, et al. 2012; Ennomani et al. 2016).

Lastly, like many other self-organized arrays, there exists opposing processes to govern the

dynamics of a contractile array, which in this case are contraction vs. resistance. In a crosslinked actin array, contraction builds up resistance (McFadden et al. 2017; Salbreux, Charras, et al. 2012). Without a way to release the stress, a contractile array either collapse (Alvarado et al. 2013), or buildup the elastic resistance so high that the contraction stalls (Murrell and Gardel 2014). In both cases, the network can no longer contract. In some cases, cells might prefer a contractile array to contract all the way to the end, e.g. the contractile ring. But in many other cases, cells need to build in relaxation to reset the state, so that the array can contract continuously. One mechanism to do so is to incorporate filament turnover into the system. High filament turnover allows the continuous relaxation of elastic resistance, and renews the network so that it can contract continuously (McFadden et al. 2017).

The mitotic spindle: a self-organized microtubule network

The ability to self-organize into higher order structures is not specific to actin. Another intensely-studied example of a self-organized structure is the mitotic spindle, which is organized through interactions among microtubules, crosslinkers, and microtubule-based motors.

Like actin filaments, microtubules are polarized filaments with plus ends (polymerizing ends) and minus ends (depolymerizing ends) that can undergo treadmilling both *in vitro* and *in vivo* (Rodionov and Borisy 1997; Grego et al. 2001). During this process, microtubules hydrolyze GTP instead of ATP. In addition, the dynamic behaviours exhibited by microtubules can come from a rather unique feature termed "dynamic instability". Dynamic instability refers to a behaviour when individual polymers switch stochastically between growth and shortening due to rapid polymerization and depolymerization of the plus ends (reviewed in Goodson and Jonasson 2018).

During cell division, microtubules assemble into mitotic spindles to separate sister chromatids between two daughter cells. Mitotic spindles are bipolar, spindle-like structures that are composed of hundreds of thousands of microtubules and ∼1000 additional proteins (Petry 2016). In this spindle-like structure, microtubules form a bipolar arrangement, such that minus ends are focused at two poles, while plus ends overlap at the midzone, where they are aligned, crosslinked,

and/or attached to the chromosomes. In metaphase, mitotic spindles align chromosomes at the metaphase plate. In anaphase, they pull chromosomes to the opposite poles to separate chromosomes into two daughter cells.

The power of mitotic spindles as a self-organizing system has been elegantly shown by a set of *in vitro* experiments, where mitotic spindles assemble around DNA-coated beads incubated in *Xenopus* egg extracts (Heald et al. 1996). In this experiment, there is no centrosome nor kinetochores for microtubules to attach, nonetheless, a bipolar mitotic spindle can still emerge from interactions among microtubules, crosslinkers, and motors. There are three key points to assemble a mitotic spindle: 1. Nucleate and elongate microtubules, 2. Focus minus ends into bipolar poles, 3. Align and stabilize plus ends at the midzone. There are two well studied mechanisms to assemble mitotic spindles: a centrosome-dependent mechanism, and a centrosome-independent mechanism (Meraldi 2016; Merdes et al. 2000; Heald et al. 1996; Wittmann et al. 2001) (Figure 1.6). I am going to discuss these two mechanisms separately around the three key points I mentioned above, but it is worth noticing that these two mechanisms are not mutually exclusive in cells.

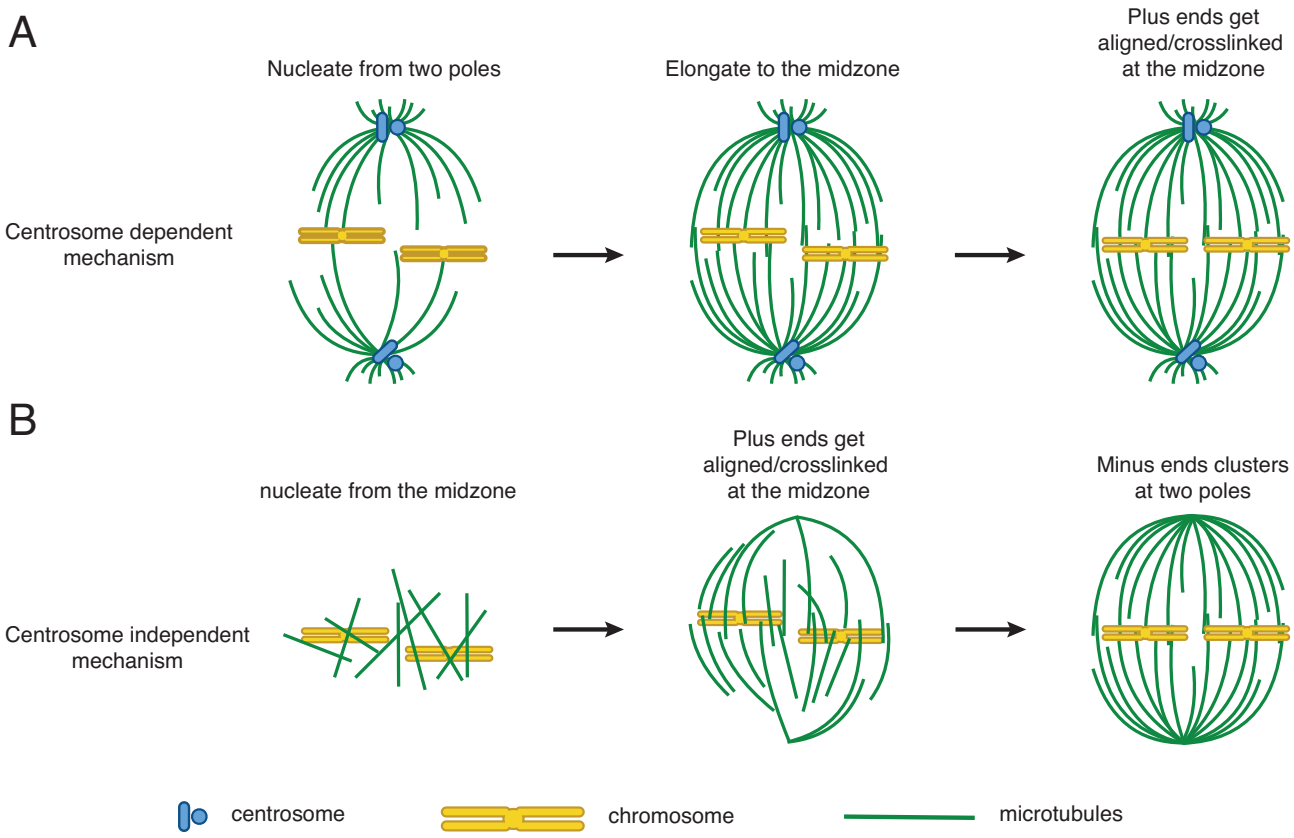

Figure 1.6. A schematic overview of different ways to assembly mitotic spindles. A. Centrosome dependent mechanism. B. Centrosome independent mechanism.

In the centrosome-dependent mechanism, microtubules are nucleated from centrosomes while their minus ends stay associated with the centrosome (Meraldi 2016; Petry 2016). Thus, the position of two centrosomes decide the position of bipolar poles of the mitotic spindle. Cells use several redundant mechanisms to ensure the proper separation of two centrosomes, including interplay among plus end motor kinesins, minus end motor dyneins, actomyosin network, nuclear envelope, etc. (reviewed in Schuldt 2004; Tanenbaum and Medema 2010). After microtubules are nucleated from centrosomes, they elongate to overlap at the midzone, where they are aligned, crosslinked, and/or attached to the chromosomes. Many microtubule binding proteins are involved in this process. First, plus end motors like Eg5 function in two ways: 1), by crosslinking two microtubules with the same orientation and moving toward their plus ends, Eg5 bundles and aligns the microtubules; 2), microtubules growing out from opposite poles will be pushed apart by Eg5, which contributes to pushing the poles apart (Walczak, Vernos, et al. 1998). Secondly, kinesin-4, a chromosomally localized plus-end motor, binds chromosomes to microtubules, which is required both to extend spindle pole away from the chromosomes, and to hold the structure together once it has formed (Walczak, Vernos, et al. 1998). Interestingly, kinesin-4 also bind microtubules into anti-parallel arrays, and determines the overlap length of the midzone (Walczak and Shaw 2010). In addition, crosslinkers like MAP65/Ase1/PRC1 are also recruited to the midzone to cross microtubules into antiparallel bundles, and help to hold the structure together (Goodson and Jonasson 2018; Walczak, Vernos, et al. 1998). The balances between these two opposing processes (pushing forces that push apart two poles and connection that connect microtubules from opposite poles at the midzone) maintain the structure of mitotic spindles and control the size of it.

In the centrosome-independent mechanism, also known as the chromosome-dependent mechanism, chromatin promotes local microtubule nucleation via a GTPase called Ran (Meraldi 2016; Petry 2016). Local activation of Ran near chromosomes, combined with diffusion and rapid inactivation, establishes a sharp gradient of RanGTP around the chromosomes. Thus, within close range to chromosomes, the RanGTP concentration is high enough to bind to importin-β and release a range of spindle assembly factors, including TPX2 and gamma-TuRC, which promote localized microtubule nucleation, stabilization and crosslinking (reviewed in Prosser and Pelletier 2017; Petry 2016). Once they are nucleated, the plus ends of these microtubules are crosslinked into

antiparallel arrays using the same mechanisms as I described above. However, one remaining challenge is to cluster minus ends into two bipolar poles. To do so, cells use oligomeric minus-end motors dynein. *In vitro*, dynein by itself is able organize microtubules into asters (Surrey et al. 2001). *In vivo*, dynein-dynactin-NuMA complexes oligomerize to coalesce dispersed microtubules into a focused pole (Hueschen et al. 2017; Meraldi 2016; Heald et al. 1996).

Although mitotic spindles and actin arrays (such as the contractile ring, which also contains aligned filaments) are two very different structures using different cytoskeletal filaments, they share many underline principles to organize the structure. Firstly, both systems require motor proteins and crosslinkers to align individual filaments (Walczak, Vernos, et al. 1998, see below for actin filament alignment). Secondly, they both maintain a stable structure while individual filaments are very dynamic (Michison 2011, see below for actin dynamics during cytokinesis). Thirdly, they both use filament-guided filament assembly to orient the orientation of newly assembled filament. For mitotic spindles, microtubules assembled from "MT-dependent MT nucleation" preserves the original polarity of the templated MT, which appears to be important for mitotic spindle formation (Petry 2016). In the contractile ring, FGFA plays an important role in filament alignment during contratile ring assembly (see Chapter 2). This suggests that cytoskeletons might use the same underline principles to build different structures.

1.4 The contractile ring is a quintessential example of a self-organized contractile machine

1.4.1 Overview

Cytokinesis is the last step of cell division in which a mother cell cleaves into two daughter cells. In animal and yeast cells, cleavage relies on the assembly of an aligned array of actin filaments called the contractile ring that contracts to pinch the cell into two (Green et al. 2012; Pollard and O'Shaughnessy 2019; Glotzer 2017; Pollard 2010). Over the years, the crucial function of it during cytokinesis and conserved structure across a wide range of organisms have attracted many biologists and physicists, making the contractile ring a quintessential example to study

the self-organization of actin structures.

In animal and yeast cells, cytokinesis can be roughly divided into three phases: cleavage furrow specification, contractile ring assembly, and ring constriction. In animal cells, the cleavage furrow is specified by equatorial activation of the small GTPase RhoA (reviewed in Green et al. 2012; Pollard and O'Shaughnessy 2019; Basant and Glotzer 2018). At anaphase onset, positive signals from the centralspindlin complex and negative signals from astral microtubules promote equatorial activation of the RhoGEF Ect-2 (Glotzer 2017). Activated Ect-2 in turn activates RhoA, which then acts through multiple effectors to promote contractile ring assembly. In particular, RhoA binds and activates formins to promote the local assembly of unbranched actin filaments (Castrillon and Wasserman 1994; Davies, Jordan, et al. 2014; Großhans et al. 2005; Watanabe, Madaule, et al. 1997; Watanabe, Okawa, et al. 2010). It also binds and activates Rho Kinase (ROCK) to promote the local recruitment/activation of myosin II (Matsumura 2005). The accumulation of both unbranched actin filaments and active myosin II, together with other ABPs, provide a molecular basis for contractile ring assembly.

The mechanisms that position the cleavage furrow in yeast cells are less conserved. In fission yeast, both signals from the nucleus and cell poles are used to define the location of the future contractile ring. During interphase, scaffold proteins anillin/Mid1p move from the nucleus to the equator to form precursors of cytokinesis nodes (Paoletti and Chang 2000). Combined with this mechanism, cells also set up a cell level Pom1 (dual-specificity tyrosine-regulated kinase) gradient with the concentration hight at the poles and low at the equator to restrict the spread of Mid1p precursors at the equator (Rincon et al. 2014). During cytokinesis, Mid1p nodes recruit several downstream proteins including the formin Cdc12p and myosin-II Myo2 to set up the molecular basis for contractile ring assembly. Unlike fission yeast, whose cytokinesis takes place at the equator, budding yeast uses the preceding division site to specify the location of the new division site (Chant and Pringle 1995). This regulation process depends on a positive feedback loop that promotes the accumulation of active Cdc42 around the previous division site, which in turn recruits septins to the new division site. Septins then bind to other effectors to activate both formin Bni1 and myosin-II Myo1 to provide the molecular basis for the contractile ring assembly (reviewed in Bi and Park 2012).

In animal cells, the dynamics of contractile ring assembly and constriction varies from cell to cell. First of all, contractile rings vary in size, from (3-4 μm in diameter to as big as 1 mm in diameter). Secondly, the progression of the contractile ring assembly varies. For example, in Hela cell, the contractile ring assembles symmetrically and uniformly (Zhao and Fang 2005). However, in the one-cell *C.elegans* embryo, the contractile ring assembles asymmetrically, with actin filaments and myosin accumulating first at one side of the cell, and then spreading to the entire circumference (Maddox et al. 2007). Thirdly, the degree of contractile ring constriction varies. In most animal cells the contractile ring constricts completely and divides the cell into two during mitosis. However, during the development of certain tissues, ranging from mammals to *C.elegans*, the cytokinesis process is incomplete, so that two daughter cells still share a common pool of cytosol (reviewed in Robinson 1996; Haglund et al. 2011).

Although the assembly and constriction of the contractile ring varies across different organisms, the molecular basis is highly conserved among animal cells, which suggests that common mechanisms underlie these differences.

1.4.2 Models for contractile ring assembly

During the contractile ring assembly phase, actin filaments, together with other ABPs, self-organize from an isotropic array into a contractile ring composed of an aligned array of actin bundles with mixed polarity (Green et al. 2012). Many models have been proposed to explain how actin filaments become aligned during this process. The two dominant models both involve myosin II motor activity. The first proposes that actin filaments are aligned by local motor-filament interactions (also known as the "Search-Capture-Pull-Release" model) (Pollard and Wu 2010; Pollard 2010). The other proposes that filaments are realigned by large scale cortical contraction/flow (White and Borisy 1983) (Figure 1.7).

Realignment by local motor-filament interactions.

One model for contractile ring assembly has emerged from intensive studies in fission yeast (Vavylonis, Wu, et al. 2008; Pollard 2010; Pollard and O'Shaughnessy 2019). In fission yeast, the

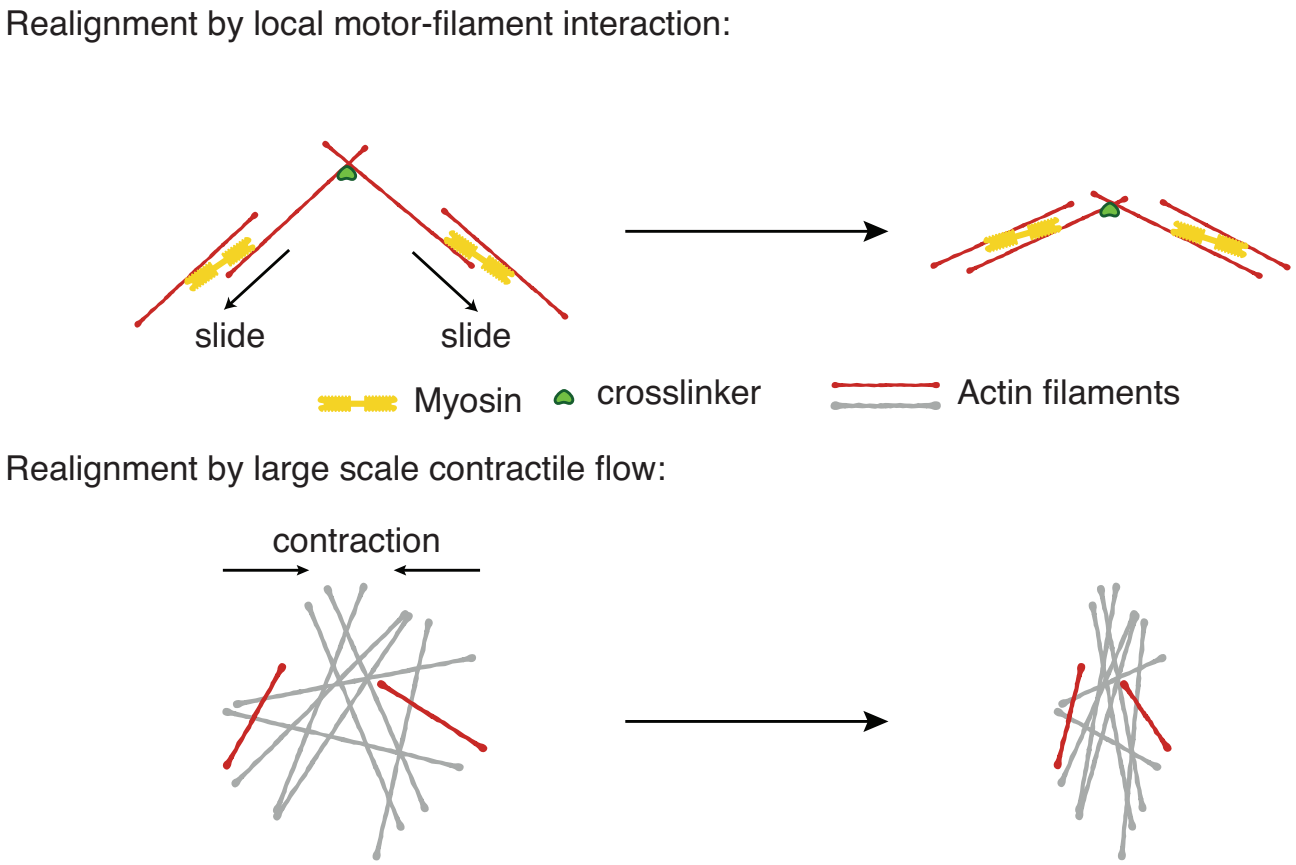

Figure 1.7. Schematic diagram of Actin filaments getting aligned either by local motor-filament interaction, or large scale contractile flow. Top panel: actin filaments get aligned by filament sliding driven by local motor-filament interaction. Bottom panel: actin filaments get aligned by large anisotropic contractile flow.

contractile ring forms through the coalescence of a broad equatorial band of membrane-attached nodes containing the anillin-related protein Mid1p (Wu, Kuhn, et al. 2003; Wu, Sirotkin, et al. 2006). During contractile ring assembly, Mid1p nodes recruit and scaffold formin/Cdc12p and myosin II/Myo2. Super resolution microscopy has revealed that each node contains 2 Cdc-12 dimers and 8 Myo2. Cdc12p promotes the nucleation and elongation of actin filaments with barbed ends anchored to the node and pointed ends extending into the neighboring region. By chance these filaments are captured by Myo2 motors on neighboring nodes, producing forces that pull nodes together, until cofilin-mediated filament disassembly breaks the connection and allows for rapid cycles of this "Search-Capture-Pull-Release" (SCPR) mechanism (Chen and Pollard 2011; Pollard 2010). Empirically constrained computer simulations have shown that SCPR is sufficient to explain the rapid coalescence of nodes from a broad equatorial band into a tight equatorial ring (Vavylonis, Wu, et al. 2008). Interestingly, simulations also show that the connections between the nodes need to break approximately every 20 seconds to avoid clumping of nodes, highlighting the significance of dynamic turnover of actin filaments within

the contractile ring (Vavylonis, Wu, et al. 2008). Indeed, mutating cofilin *in vivo* results in clumps of contractile ring fragments instead of a continuous ring (Chen and Pollard 2011). It is also worth noting that in fission yeast, after assembly, the ring enters 20-min maturation period before the onset of constriction (reviewed in Pollard and O'Shaughnessy 2019). Thus, it's unclear which mechanisms contribute to the maintenance of the filament alignment in the ring during this period.

Realignment by large scale contractile flow

In animal cells, the contractile ring forms within a dense array of filaments and motors, in which discrete nodes that anchor sites of filament assembly and/or myosin activity cannot be detected (Figure 1.8). Back in 1980s, Borisy and White proposed an large scale contractile flow model to explain how a dense aligned array of filaments could form at the equator during cytokinesis (White and Borisy 1983). This model views the cortex as a contractile material, in which local activation of contractility at the equator, and inhibition (relaxation) at the poles, creates a gradient of cortical tension, resulting in a flow of cortical filaments away from the poles and towards the equator. Borisy and White postulated that local realignment of filaments within this flow would lead to buildup of aligned filaments. Compressive flows of cortical material including actin filaments have been documented during cytokinesis in a variety of different cell types (Fishkind et al. 1996; Khaliullin et al. 2018; Murthy and Wadsworth 2005; Reymann, Staniscia, et al. 2016; Zhou and Wang 2008). Mathematical models have shown that the realignment of actin filaments by compressive flows could be sufficient to explain the observed degree of filament alignment during contractile ring assembly in some cells (Reymann, Staniscia, et al. 2016; Salbreux, Prost, et al. 2009; White and Borisy 1983). A key assumption of such models is that individual filaments must be sufficiently stable for the flow to build significant alignment within a population of filaments. However, this assumption has yet to be tested by direct simultaneous measurements of flow and filament turnover in any animal cell. Thus, it remains unclear to what extent the local realignment of filaments by cortical flow can explain the rapid emergence and stable maintenance of filament alignment during cytokinesis, and whether additional mechanisms must be involved.

1.4.3 Models for contractile ring constriction

How does constriction happen?

Once assembled, the contractile ring generates contractile forces to constrict a cell into two. Conventionally, this contraction is thought to be generated through myosin motor activity. In agreement with this idea, many experiments show that knocking down myosin, or mutating myosin motor domains, leads to the failure of cytokinesis in many cell types (Straight et al. 2003; Davies, Jordan, et al. 2014; Reymann, Staniscia, et al. 2016; Descovich et al. 2018; Osório et al. 2019).

As discussed above, contractile forces can be generated either through disassembly and crosslinking activity, a sarcomeric-like mechanism, or a buckling mechanism. Studies in a variety of different cell types reveal that each of these three mechanisms might play a role in contractile ring constriction (reviewed in Leite et al. 2019; Pollard and O'Shaughnessy 2019).

One possibility is that myosin could act as a crosslinker independent of its motor activity, and that contractions are driven by actin disassembly and crosslinking. In budding yeast, the tail domain of Myo1p alone is sufficient to support contractile ring constriction during cytokinesis (Lord et al. 2005; Mendes Pinto et al. 2012). To further evaluate the role of actin depolymerization in the ring constriction, Mendes Pinto et al. 2012 impaired actin depolymerization in budding yeast, either using jasplakinolide (a drug that blocks actin depolymerization) or in a cofilin mutant background. They found that in those embryos, the rate of ring constriction was significantly reduced. The paper also provided a mathematical model showing that actin disassembly coupled with cross linking activity can mimic the contractile ring constriction they observed *in vivo*.

On the other hand, as mentioned above, in many cell types, including one cell *C.elegans* embryos, myosin motor activity is necessary to generate contraction. However, in these myosin-motor dependent contractions, it is unclear whether the contractile force is generated through a sarcomeric-like mechanism or a buckling mechanism. This is because in many of these cells, actin and myosin are highly abundant during cytokinesis at the contractile ring, making it impossible to visualize the sliding/buckling of individual filaments. Evidence supporting the

sarcomeric-like mechanism are based on studies from Hela cells, sea urchin eggs, budding yeast, and fission yeast. In Hela cells, sea urchin eggs, and budding yeast, organized myosin stacks are present in the cleavage furrow, forming a semi-sarcomere structure, suggesting that those contractile rings may constrict using sarcomeric-like mechanism (Henson et al. 2017; Ong et al. 2014; Fenix et al. 2016). In fission yeast, the contractile ring is assembled by connecting many nodes together (Pollard and Wu 2010). Actin filaments within each node are oriented such that barbed ends attach to the node, while pointed ends extend outward and are captured and pulled by myosin to bring nodes closer to each other to constrict a cell into two. This process is a sarcomeric-like mechanism, because myosin are enriched towards pointed ends. However, in many cell types, including one-cell *C.elegans* embryos, there are no obvious myosin distribution bias along actin filaments, suggesting that these cells are more likely to contract through the buckling mechanism (Figure 1.8).

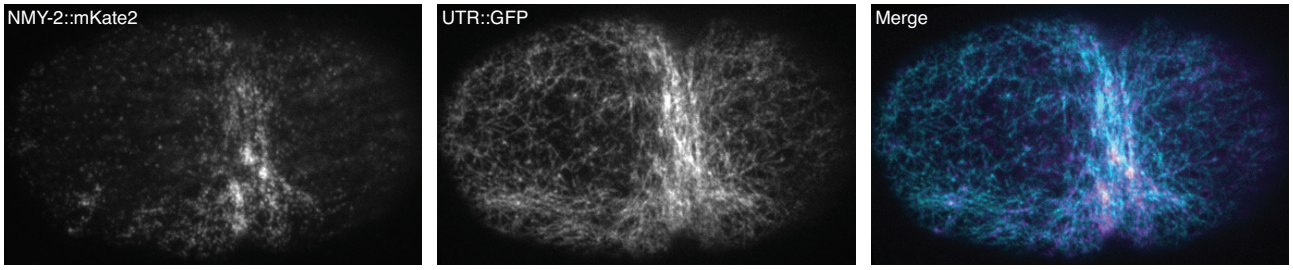

Figure 1.8. Myosin distribution has no obvious pattern during cytokinesis in one-cell *C.elegans* embryos. Surface view of cortical myosin (magenta) and actin (cyan) during cytokinesis.

Last, there are also constriction mechanisms that are not based on contraction of the contractile ring. For example, hTERT-immortalized RPE1 cells are able to divide through an adhesion-dependent mechanism in the absence of a visible contractile ring. In this mechanism, the dividing cell forms polarized lamellipodial extensions at opposing daughter cell poles to migrate two daughter cells in opposite directions. This migration narrows the connection between daughter cells, which eventually leads to severing (Dix et al. 2018).

Importantly, these mechanisms are not mutually exclusive. For example, the ring constriction rate is slightly reduced in the motor-impaired budding yeast cells (Ma et al. 2012; Mendes Pinto et al. 2012), suggesting that the disassembly dependent mechanism cannot account for all the contractions. Thus, additional mechanisms, likely myosin motor dependent mechanisms, are involved in wildtype embryos.

How rapidly do filaments turnover during cytokinesis?

Another general question in cytokinesis is how rapidly filaments turnover during the constriction. There are two different general possibilities, both supported by some observations: One is that filaments are relatively stable and disassemble as the ring constricts; the other is that filaments turnover rapidly as the ring constricts.

Evidence supporting the former possibility comes from studies both *in vivo* and *ex vivo*. In four-cell *C.elegans* embryos, the concentration of contractile ring components stays constant during constriction, and those components don't seem to exchange rapidly with the cytoplasmic pool. Cells treated with latrunculin A (a drug that prevent actin assembly) after the contractile ring is assembled can still constrict (Carvalho et al. 2009). In agreement with this experiment, an *ex vivo* study using fission yeast cell ghosts (fission yeast cells that only retain cortex and plasma membrane, but are devoid of the cell wall and any cytoplasmic structures) shows that retained contractile rings surrounded by permeabilized plasma membrane are able to constrict in a myosin dependent manner, without exchanging actin filaments with the media (Mishra et al. 2013).

On the other hand, there is also evidence supporting the possibility that filament turnover rapidly as the ring constricts. In many different cell types, actin turnover is necessary during the contractile ring constriction, and the addition of latrunculin A leads cytokinesis failure (O'Connell et al. 2001; Chew et al. 2017; Murthy and Wadsworth 2005; Chan et al. 2019). In fission yeast, actin filaments within the contractile ring disassemble around 11 seconds, which enables the contractile ring to quasi-statically shorten during the 20 min of constriction without damaging the organization and compromising ring tension (Pollard and O'Shaughnessy 2019). In 4-cell *C.elegans* embryos, during constriction, the contractile ring can rapidly repair itself from laser cuts in an actin polymerization-dependent manner. Importantly, the gaps generated by laser ablation can be repaired in $\tilde{2}0$ seconds, suggesting that there is rapid filament turnover during the contractile ring constriction (Silva et al. 2016).

More experiments are needed to dispute contradictory evidence (see more discussion on this topic in the Discussion section). It also suggests that redundant mechanisms might be activated during

the constriction, so that the rate of actin turnover is different based on how the contractile ring is perturbed. In my thesis work, I used single molecule analysis to directly measure the mean filament turnover rate during the contractile ring assembly in the wildtype one-cell *C.elegans* embryos, and found out that at that stage, actin filaments turnover rapidly (∼8 seconds).

1.5 About this project

In my thesis work, I focused on the dynamics of contractile ring assembly in the one-cell *C.elegans* embryo (or zygote). In particular, I focused on the question: how does a highly aligned array of filaments form during contractile ring assembly? As mentioned above, a key assumption of the current model is that individual filaments must be sufficiently stable for flow to build significant alignment within a population of filaments. However, this assumption has yet to be tested by direct simultaneous measurements of flow and filament turnover in any animal cell. Thus, it remains unclear to what extent the local realignment of filaments by cortical flow can explain the rapid emergence and stable maintenance of filament alignment during cytokinesis, whether additional mechanisms must be involved.

Here I combine TIRF microscopy with single molecule imaging/particle tracking to directly and simultaneously measure rates of contractile flow and filament disassembly during cytokinesis in one-cell *C. elegans* embryos. I find that filament disassembly is far too fast for the alignment of individual filaments by contractile flow to explain the rapid emergence and stable maintenance of filament alignment within the contractile ring. I identify an additional mechanism, in which new actin filaments use existing filaments as templates to orient their elongation. Combining quantitative image analysis with mathematical modeling, I show that filament-guided filament assembly endows the contractile ring with a structural memory of filament alignment that allows the *C. elegans* embryo to build and maintain a high degree of filament alignment within the contractile ring despite very rapid filament turnover. I propose that similar mechanisms may underlie the assembly and maintenance of aligned filament arrays in many other contexts.

CHAPTER 2

EXISTING ACTIN FILAMENTS ORIENT NEW FILAMENT GROWTH TO PROVIDE STRUCTURAL MEMORY OF FILAMENT ALIGNMENT DURING CYTOKINESIS

Statement of contribution: I carried out all of the experiments ,data analysis, and computational simulations in this project, except that William McFadden helped to solidify the initial theoretical model in Figure 2.2.

2.1 Abstract

During cytokinesis, animal cells rapidly remodel the equatorial cortex to build an aligned array of actin filaments called the contractile ring. Local reorientation of filaments by equatorial contraction is thought to underlie the emergence of filament alignment during ring assembly. Here, combining single molecule analysis and modeling in one-cell *C. elegans* embryos, we show that filaments turnover is far too fast for reorientation of single filaments by equatorial contraction/cortex compression to explain the observed alignment, even if favorably oriented filaments are selectively stabilized. Instead, by tracking single Formin/CYK-1::GFP speckles to monitor local filament assembly, we identify a mechanism that we call filament-guided filament assembly (FGFA), in which existing filaments serve as templates to guide/orient the growth of new filaments. We show that FGFA sharply increases the effective lifetime of filament orientation, providing structural memory that allows slow equatorial contraction to build and maintain highly aligned filament arrays, despite rapid turnover of individual filaments.

2.2 Introduction

Non-muscle cells assemble contractile actomyosin arrays to do a variety of jobs, such as cell polarization, cell division, cell migration, wound healing and multicellular tissue morphogenesis (reviewed in Agarwal and Zaidel-Bar 2019; Levayer and Lecuit 2012; Munjal and Lecuit

2014). Contractile arrays are assembled from actin filaments, crosslinking proteins, and bipolar myosin II minifilaments, together with various accessory factors that regulate filament assembly, disassembly and motor activity. How assembly/disassembly and activity of contractile arrays are tuned in different ways to build and maintain specific functional architectures remains a fundamental question in cell biology.

One quintessential example of a contractile actomyosin array is the contractile ring, a dynamic network of cross-linked actin filaments and myosin motors that assembles at the cell equator and constricts to divide a single cell into two daughters (Fededa and Gerlich 2012; Glotzer 2017; Green et al. 2012; Pollard and O'Shaughnessy 2019). In animal cells, spatial and temporal control of contractile ring assembly is mediated by equatorial activation of the small GTPase RhoA (Bement et al. 2005; Nishimura and Yonemura 2006; Yüce et al. 2005). At anaphase onset, local positive and negative signals from the mitotic apparatus specify an equatorial zone of RhoA activity (Glotzer 2017). RhoA in turn acts through multiple effectors to promote contractile ring assembly. In particular, RhoA binds and activates diaphanous-related formins to promote the local assembly of unbranched actin filaments (Castrillon and Wasserman 1994; Davies, Jordan, et al. 2014; Großhans et al. 2005; Watanabe, Madaule, et al. 1997; Watanabe, Okawa, et al. 2010), and it binds and activates Rho Kinase (ROCK) to promote the local recruitment/activation of myosin II (Matsumura 2005). An initially disorganized network of filaments and motors is then reorganized over time into a more circumferentially aligned array. Although oriented filaments are not required for network contractility, increased filament alignment is associated with increased circumferential tension (Bidone, Tang, et al. 2014; Spira et al. 2017; Stachowiak, Smith, et al. 2014) and thus may be important for timely progression and completion of cytokinesis. But how cells build and maintain filament alignment during contractile ring assembly and constriction remains poorly understood.

One model for contractile ring assembly has emerged from intensive studies in fission yeast (Pollard and Wu 2010). In fission yeast, the contractile ring forms through the coalescence of a broad equatorial band of membrane-attached nodes containing the Anillin-related protein Mid-1 (Wu, Kuhn, et al. 2003; Wu, Sirotkin, et al. 2006). During contractile ring assembly, Mid1p nodes recruit and scaffold the Formin cdc-12 and the Myosin II myp2; cdc-12 promotes the

nucleation and elongation of actin filaments, and chance capture of these filaments by myp2 motors on neighboring nodes produces forces that pull nodes together. Cofilin-mediated filament disassembly allows for rapid cycles of search, capture, pull and release (SCPR) (Chen and Pollard 2011). Empirically constrained computer simulations have shown that SCPR is sufficient to explain the rapid coalescence of nodes from a broad equatorial band into a tight equatorial ring (Vavylonis, Wu, et al. 2008). The same interactions could also contribute to maintaining filament alignment within the ring, if filament turnover is sufficiently slow (Stachowiak, Smith, et al. 2014).

In animal cells, the contractile ring forms within a dense array of filaments and motors, in which discrete nodes that anchor sites of filament assembly and/or myosin activity cannot be detected. Borisy and White proposed an alternative to the SCPR model to explain how a dense aligned array of filaments could form at the equator during cytokinesis (White and Borisy 1983). This model views the cortex as a contractile material, in which local activation of contractility at the equator, and inhibition (relaxation) at the poles, creates a gradient of cortical tension, resulting in a flow of cortical filaments away from the poles and towards the equator. Borisy and White postulated that local realignment of filaments within this flow would lead to buildup of aligned filaments in regions of compressive flow. Compressive flows of cortical material, including actin filaments have been documented during cytokinesis in a variety of different cell types (Fishkind et al. 1996; Khaliullin et al. 2018; Murthy and Wadsworth 2005; Reymann, Staniscia, et al. 2016; Zhou and Wang 2008). Mathematical models have shown that the realignment of actin filaments by compressive flows could be sufficient to explain the observed degree of filament alignment during contractile ring assembly in some cells (Reymann, Staniscia, et al. 2016; Salbreux, Prost, et al. 2009; White and Borisy 1983). A key assumption of such models is that individual filaments must be sufficiently stable for flow to build significant alignment within a population of filaments. However, this assumption has yet to be tested by direct simultaneous measurements of flow and filament turnover in any animal cell. Thus, it remains unclear to what extent the local realignment of filaments by cortical flow can explain the rapid emergence and stable maintenance of filament alignment during cytokinesis, and whether additional mechanisms must be involved.

Here we combine TIRF microscopy with single molecule imaging/particle tracking to directly and simultaneously measure rates of contractile flow and filament disassembly during cytokinesis in one-cell *C. elegans* embryos. We find that filament disassembly is far too fast for the alignment of individual filaments by contractile flow to explain the rapid emergence and stable maintenance of filament alignment within the contractile ring. We identify an additional mechanism, in which actin filaments assembled by the Formin CYK-1 use existing filaments as templates to orient their elongation. Combining quantitative image analysis with mathematical modeling, we show that filament-guided filament assembly endows the contractile ring with a structural memory of filament alignment that allows the *C. elegans* embryo to build and maintain a high degree of filament alignment within the contractile ring despite very rapid filament turnover. We propose that similar mechanisms may underlie the assembly and maintenance of aligned filament arrays in many other contexts.

2.3 Results

2.3.1 Myosin-dependent contractile flow drives the rapid emergence of equatorial filament alignment during contractile ring assembly.

To optimize imaging conditions for quantitative analysis of cortical dynamics, we mounted embryos under coverslips using 16μM diameter beads as fixed-size spacers to achieve a uniform degree of compression. Because mild compression can affect overall cortical dynamics (Singh et al. 2019), we began by characterizing the dynamics of contractile ring assembly and furrow ingression in mildly compressed embryos, using near-TIRF microscopy to image probes for cortical F-actin and Myosin II (GFP::UTR (Tse et al. 2012), and NMY-2::mKate2 (Dickinson, Schwager, et al. 2017), Figure 2.1-A, Movie S1, Experimental Procedures). We set the zero timepoint to be an estimate of anaphase onset inferred from the rapid accumulation of equatorial Myosin II ((Werner et al. 2007), Figure 2.1-B). To quantify furrow initiation and progression, we defined equatorial width to be the width of the region that is in focus at the site of furrow ingression, measured perpendicular to the AP axis (Figure 2.1-B). Using measurements of equatorial width and equatorial densities of F-actin and myosin II, we divided early cytokinesis

into three phases (Figure 2.1-A, B). Phase I (cortical assembly) begins with anaphase onset and is characterized by rapid accumulation of F-actin and Myosin II with minimal equatorial deformation. Phase II (ring formation/furrow initiation) is characterized by the emergence of filament alignment at roughly constant F-actin and Myosin II density, accompanied the gradual formation of a shallow equatorial furrow. Phase III (ring constriction/furrow ingression) is characterized by a rapid decrease in equatorial width.

We used kymography to characterize the pattern and timing of cortical flows that accompany contractile ring assembly in mildly compressed embryos. Axial kymographs revealed a transient posterior to anterior flow that begins with anaphase onset and transitions to a compressive flow, centered on the equator, that persists through phases II and III (Figure 2.1-C; left kymograph). We also observed a transient rapid cortical rotation, perpendicular to the AP axis (Singh et al. 2019) that begins with anaphase onset, and then attenuates during phases II and III (Figure 2.1-C; right kymograph).

To quantify the emergence of equatorial filament alignment during Phases I and II (Figure 2.1-D), we used a standard approach, based on the Sobel operator (Gonzalez and Woods, 2017) to measure the amplitudes and directions of local gradients in the intensity of GFP::UTR, which correspond to individual filaments and/or small bundles (Figure 2.2-A,B, Experimental Procedures). To estimate the distribution of filament orientation, we selected all pixels with gradient amplitudes above a threshold level, and computed a normalized distribution of intensity gradient directions, weighted by gradient amplitude (Figure 2.1-E, Figure 2.2-A,B). Finally, we computed a simple index of filament alignment asymmetry by calculating the ratio of histogram densities within 10° of equatorial (90°) and axial (0°) directions (Figure 2.1-F). Consistent with direct observations, the distribution of equatorial filament orientations was approximately isotropic at anaphase onset, with asymmetry values close to 1.2 (Figure 2.1-E,F). The asymmetry value increased slowly and steadily during Phase I and early Phase II, and then increased more sharply during late Phase II, reaching a mean value of $\sim$2.5 at the onset of furrow ingression (Figure 2.1-E,F). In contrast, the distribution of polar filament orientations remained largely isotropic from anaphase onset through the end of Phase II (Figure 2.2-E). Measurements in fixed, phalloidin-stained embryos suggest that equatorial filaments become even more aligned in

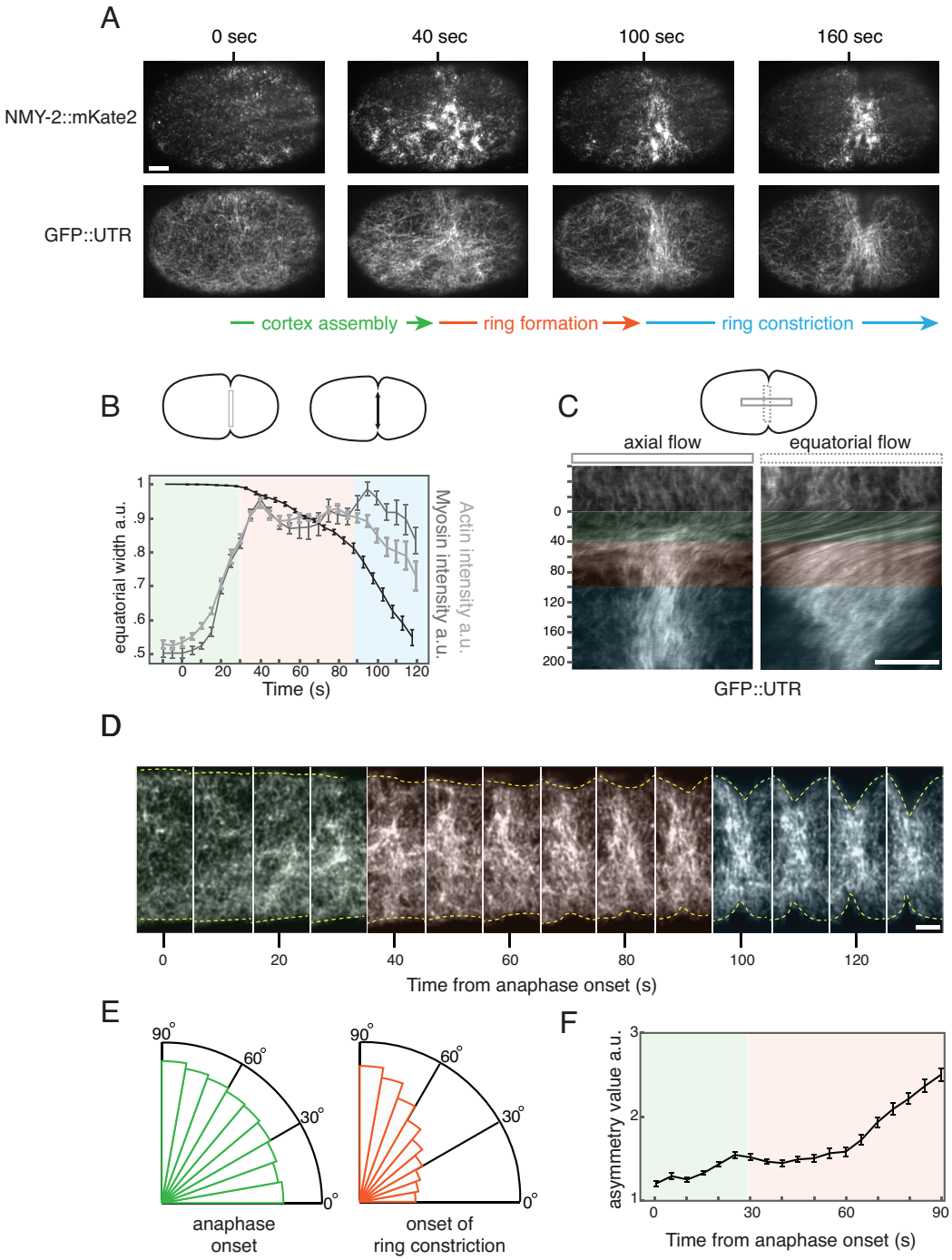

Figure 2.1. Accumulation and alignment of equatorial actin filaments during cytokinesis. (A) Surface views of cortical myosin II (NMY-2::mKate2, top panels) and F-actin (UTR::GFP, bottom panels) at the indicated time points, measured relative to an estimate of anaphase onset (see text for details). Anterior is to the left in this and all subsequent figures. Scale bars = 5μm; (B) Measurements of equatorial width (black), mean intensities of F-actin (UTR::GFP, light grey) and myosin II (NMY-2:mKate2, dark grey) over time during cytokinesis. Color overlays indicate the three phases of cytokinesis defined by these measurements: (I) cortex assembly (green), (II) ring formation/furrow initiation (red), and (III) ring constriction (blue). Error bars indicate SEM (n = 5 embryos). Top schematic indicates the regions used for measurements of probe densities (box), and equatorial width (double headed black arrow). (C) Kymographs showing axial (left) and equatorial (rotational) (right) cortical flows for the embryo in (A). Top schematic indicates the regions used to make axial (solid box) and equatorial (dashed box) kymographs. Color overlays mark the three phases of cytokinesis. Scale bar = 5μm; (D) Magnified views of UTR::GFP on the equatorial cortex, from the embryo in (A), showing the emergence of filament alignment over time. Yellow dashed lines indicate the cell boundary. Color overlays mark the three phases of cytokinesis. Scale bar = 2μm; (E) Radial histograms showing the distribution of local filament orientations at the equator at anaphase onset (left) and at the onset of ring constriction (right) (n = 5 embryos); (F) Plot of mean asymmetry value vs. time measured on the equatorial cortex (6 μm in width) during early cytokinesis. Error bars indicate SEM (n = 5 embryos).

uncompressed embryos (Figure 2.2-C), but here we used the lower values for direct comparison with the single molecule measurements reported below.

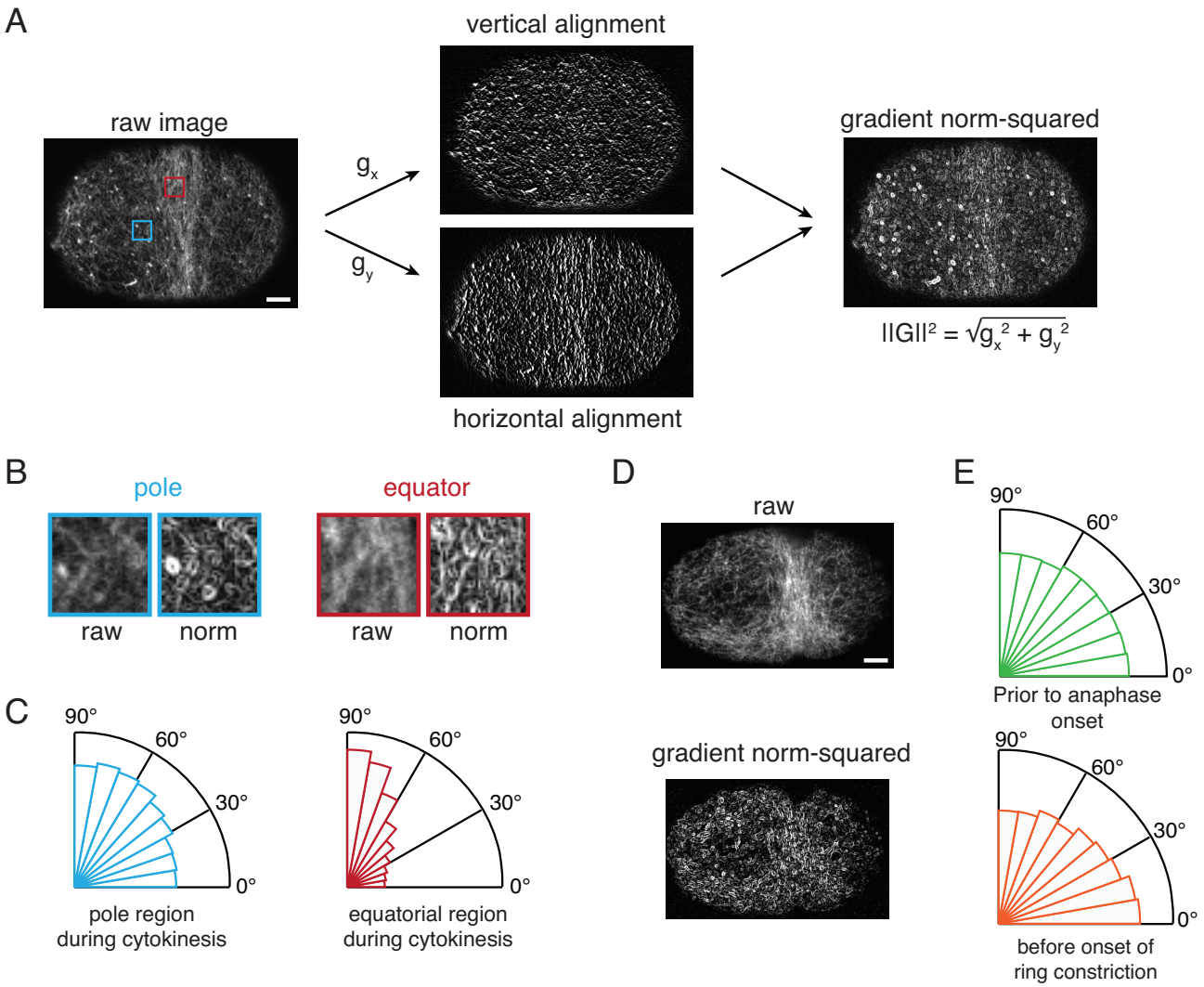

Figure 2.2. Measurement of actin filament alignment. (A) (Left) Raw image of a fixed phalloidin-stained embryo. (Middle top and bottom) The same image subjected to Sobel filters G_x (top) and G_y (bottom) to highlight horizontal and vertical gradients of fluorescence intensity. (Right) Gradient norm-squared image in which pixel intensity is proportional to the squared norm of G = (G_x, G_y). Scale bar = 5 μm. (B) Magnified views of the regions indicated by colored boxes in (A) comparing raw signal and gradient norm squared. size = 4x4 μm. (C) Weighted distribution of polar and equatorial filament orientations averaged over n = 6 fixed phalloidin-stained embryos, that were fixed in cytokinesis, before the onset of rapid furrow ingression. (D) Comparison of raw and gradient norm-squared images for a live embryo expressing GFP::UTR just before the onset of rapid furrow ingression. Scale bars = 5 μm. (E) Weighted distribution of polar filament orientations (anterior pole) in live embryos expressing GFP::UTR just before anaphase onset (left) and just before the onset of rapid furrow ingression (right), averaged over n = 5 embryos.

Importantly, in NMY-2:: mKate2; GFP::UTR embryos strongly depleted of NMY-2 by RNAi, a rapid increase in equatorial actin filaments occurred with similar timing after anaphase onset (Figure 2.3-A,B). However, both axial and equatorial cortical flows were essentially abolished (Figure 2.3-C), and the distribution of equatorial actin filament orientations remained largely isotropic after ~90 seconds, corresponding to the end of Phase II in control embryos (Figure 2.2-D). Thus, in agreement with previous work (Reymann, Staniscia, et al. 2016), myosin-

driven contraction is required for the rapid emergence of filament alignment prior to ring constriction.

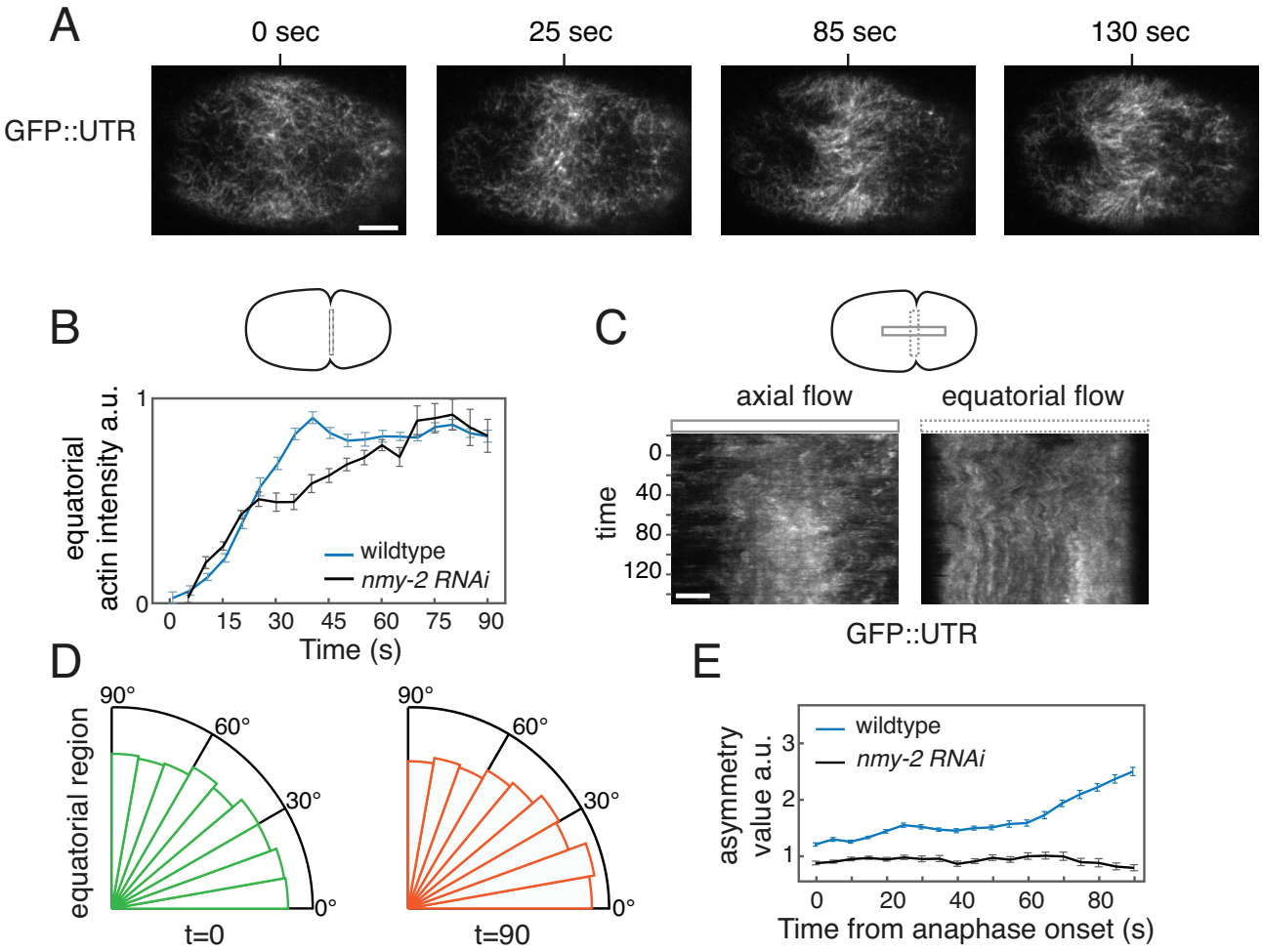

Figure 2.3. Analysis of filament orientation in myosin-depleted embryos. (A) Sequence of near-TIRF images from an embryo expressing GFP::UTR and strongly depleted of myosin II by *nmy-2 (RNAi)*. Times measured relative to anaphase onset. Scale bar = 5 μm. (B) Plot of mean equatorial actin filament intensity vs time in (n = 5) *nmy-2(RNAi)* embryos. Top schematic indicates the regions used for measurements of probe densities (box). Wild type data from Figure 2.1-B is shown for comparison. Error bars indicate SEM. (C) Kymographs showing axial (left) and equatorial (rotational) (right) cortical flows in the embryo shown in (A). Top schematic indicates the regions used to make axial (solid box) and equatorial (dashed box) kymographs. Scale bar = 3 μm. (D) Radial histograms showing the distribution of local filament orientations at the equator at anaphase onset (left, t=0) and 90 seconds later (n=5 embryos). (E) Plot of mean asymmetry value vs time in (n = 5) *nmy-2(RNAi)* embryos. Data for wild type embryos from Figure 2.1-F is shown for comparison. Error bars indicate SEM.

2.3.2 A simple model reveals the dependence of filament alignment on filament turnover and equatorial contraction rate.

The emergence of equatorial filament alignment will depend on three factors: the rate and orientation of local filament assembly; local realignment of existing filaments; and the rate and orientation-dependence of local filament disassembly (Figure 2.4-A). To establish a quantitative

framework for assessing how the emergence of filament alignment is shaped by the interplay of these factors, we modeled a population of filaments within a patch of equatorial cortex that undergoes compression at a constant contraction rate ξ (Figure 2.4-B). We assumed that filaments assemble within the patch at a rate $k_{ass}(\theta)$ and disassemble at a rate $k_{diss}(\theta)(\rho)$, where $\rho(\theta)$ is the density of filaments with orientation θ. The patch boundaries move with local flow, such that there is no net movement of filaments into/out of the patch (Figure 2.4-B). Finally, we assumed that the cortical filament network undergoes locally affine deformation, i.e. the change in a filament's orientation is determined only by the movements of its endpoints, such that the rate of change of a filament's orientation is given by:

$$\frac{d\theta}{dt} = -\xi sin\theta cos\theta$$

With these assumptions (see Modeling Procedures), we can write an equation that governs the time evolution of filament orientations within the contracting equatorial patch:

$$\frac{\delta\rho(\theta)}{\delta t} = k_{ass}\theta - (k_{diss}(\theta) + \xi)\rho(\theta) - \frac{\delta}{\delta\theta}(\xi\rho(\theta)cos(\theta)sin(\theta)) \qquad ((1))$$

We first considered a simple scenario in which assembly and disassembly rates lack orientation bias or dependence ($k_{ass}(\theta) = k_{ass}$; $k_{diss}(\theta) = k_{diss}$). For this scenario, given a constant contraction rate, the total density of filaments will approach a steady state level given by $\rho_{total} = \frac{k_{ass}}{k_{diss}+\xi}$ (see Modeling Procedures). Scaling $\rho(\theta)$ by ρ_{total}, we obtained:

$$\frac{\delta\rho(\theta)}{\delta t} = (k_{diss} + \xi)(\frac{2}{\pi} - \rho(\theta)) - \xi\frac{\delta}{\delta\theta}(\rho(\theta)cos(\theta)sin(\theta)) \qquad (2)$$

The first term in equation 2 represents the continuous evolution of filament orientations towards a flat (isotropic) distribution, at a characteristic rate $k_{diss} + \xi$. The second term represents the continuous reorientation of filaments by flow, driving the distribution of filament orientations away from isotropic. Thus, for this simple scenario in which filament assembly /disassembly rates do not depend on filament orientation, the distribution of filament orientations will depend

only on the disassembly and contraction rates k_{diss} and ξ. To characterize this dependence, we implemented our model as a simple stochastic simulation (see Experimental Procedures), initialized with the distribution of filament orientations observed during Phase I, and ran for 90 secs, corresponding to the total duration of Phases I and II (figure 2.4-C). Plotting the asymmetry value after 90 seconds as a function of k_{diss} and ξ confirms that asymmetry increases with faster contraction and slower disassembly, and reveals the range of values for which simulations reproduce the observed asymmetries (figure 2.4-D).

2.3.3 Filament turnover is too fast for reorientation of actin filaments by cortical flow to explain the emergence of equatorial filament alignment.

To test these predictions, we used single molecule imaging and particle tracking as previously described (Robin et al. 2014) to measure contraction and disassembly rates during cytokinesis *in vivo*. Briefly, we used near-TIRF microscopy to image embryos expressing Actin-GFP at single molecule levels (figure 2.5-A), from anaphase onset through the onset of ring constriction. We performed particle-tracking analysis to obtain a dense sampling of single molecule trajectories throughout the cortex and over time (figure 2.5-B).

To quantify cortical flow, we sampled single molecule displacements over 13.5 second intervals to estimate local actin filament velocities. We then binned these data to produce estimates of mean axial velocity as a function of position and time during Phases I and II (figure 2.5-D, Experimental Procedures). This analysis confirmed the characteristic pattern of axial cortical flow revealed by kymographs (figure 2.1-B, left), with an early posterior-anterior flow giving way to compressive flow from both poles towards the equator, with maximum speeds that increased over time (figure 2.5-D). Notably, we observed only small deviations of single molecule movement from the bulk flow of surrounding molecules, confirming that the cortical network undergoes a locally affine deformation (data not shown). The spatial derivative (the slope) of the axial velocity was approximately constant and negative within an equatorial region about 10 μm wide (gray region in figure 2.5-D), indicating a region of uniform local contraction. Plotting the average equatorial contraction rate as a function of time, using the onset of rapid furrow ingression (Phase III) to align data from multiple embryos, revealed a steady increase in

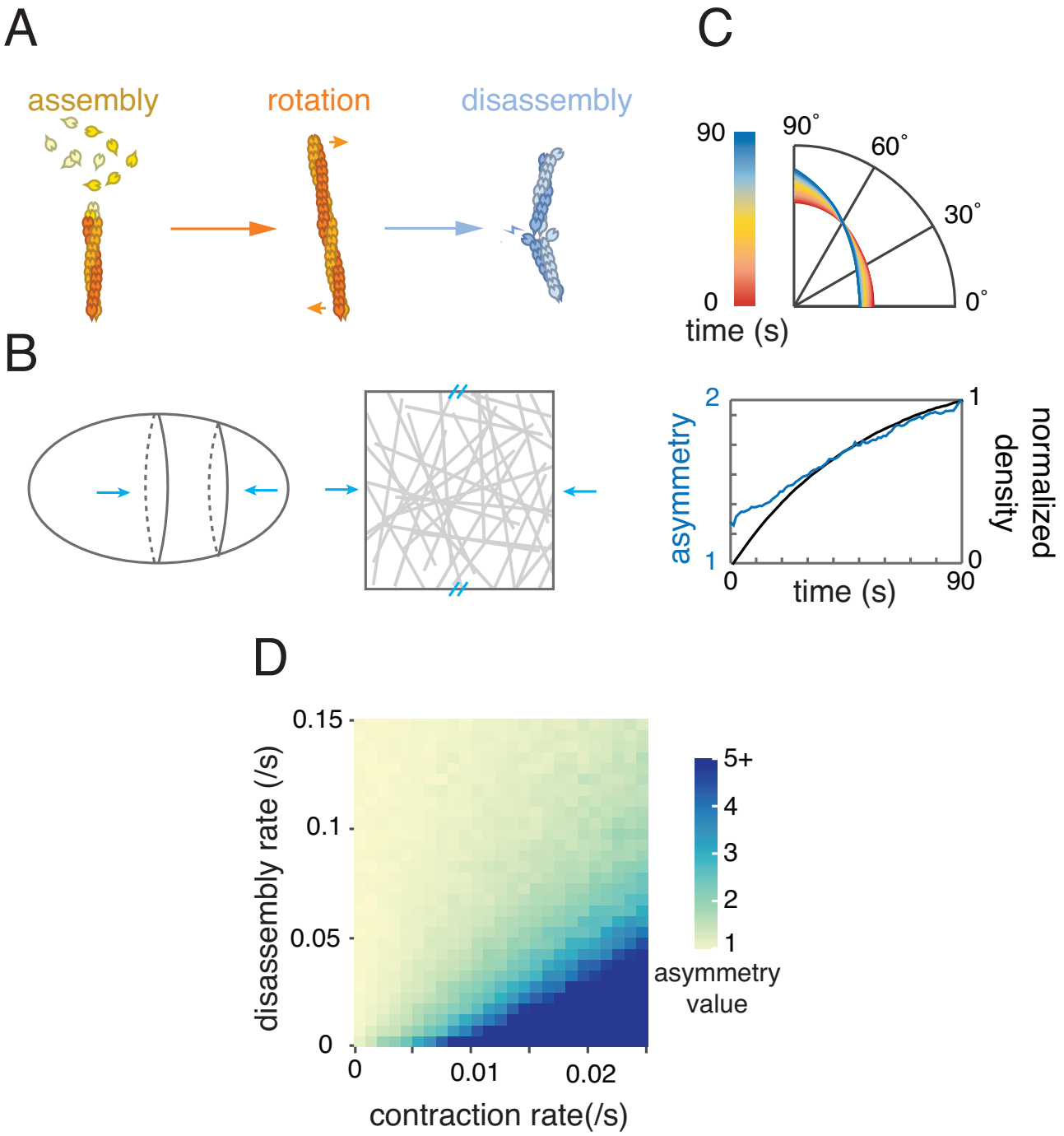

Figure 2.4. A simple model for filament realignment in compressive flow. (A) Schematic overview of the three processes by which filament number and orientation are assumed to change: local assembly, rotation by contractile flow, and local disassembly. (B) Model representation of a patch of equatorial cortex undergoing uniform axial compression. Top and bottom boundaries of the patch are fixed, while left and right boundaries move at the rate of cortical flow, such that there is no flux of filaments across those boundaries. (C) Model output for one choice of model parameters. Top: Time evolution of the filament orientation distribution. Bright red line indicates the initial distribution, as shown in figure 2.1-E. Bright blue line indicates the distribution predicted after 90 seconds. Bottom: Plot of the asymmetry value (blue) and normalized filament density vs. time (black). Parameters: contraction rate = 0.01 /s, disassembly rate = 0.03 /s. (D) Simulation outcomes for different values of disassembly and contraction rates, color coded for the asymmetry value achieved after 90 sec.

contraction rate from anaphase onset through the onset of rapid furrow ingression, approaching a maximum value of 0.011±0.001/sec (n = 5 embryos; figure 2.5-E), in agreement with previous estimates made by other methods (Khaliullin et al. 2018; Reymann, Staniscia, et al. 2016).

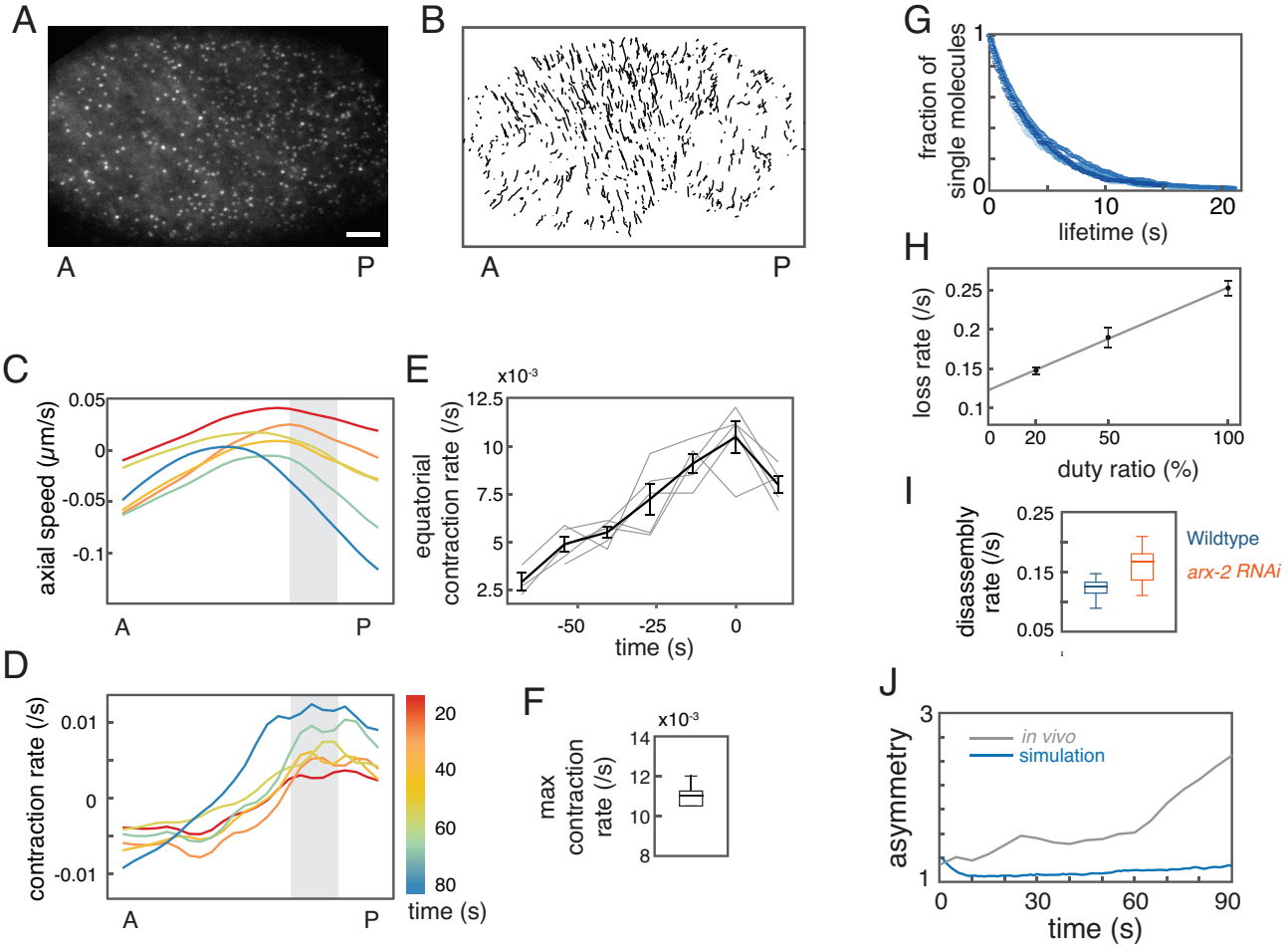

Figure 2.5. Simultaneous single molecule measurements of contraction and disassembly rates *in vivo* (A) Near-TIRF image of an embryo expressing Actin::GFP at single molecule levels, taken under standard conditions for single particle tracking. See also movie S2. Scale bar = 5μm. (B) Trajectories of all single molecules tracked over a 22.5 sec time interval. (C) Mean axial velocity of single molecules measured at different positions along the anterior-posterior axis at different time points during cytokinesis for one sample embryo. A negative value indicates anterior movement. (D) Mean contraction rate measured as the spatial derivative of axial speeds shown in (C). Gray boxes in (C&D) indicate the equatorial region (10μm in width), and the color map indicates the time at which each curve was measured relative to anaphase onset. (E) Mean equatorial contraction rate vs. time measured for five different embryos. Plots are aligned relative to the onset of phase III (furrow constriction). Gray lines show data for individual embryos. Black line and error bars indicate the mean +/- SEM (n=5 embryos). (F) Maximum equatorial contraction rate measured just before constriction in wild-type embryos (n=5). (G) Loss curves plotting the fraction of single molecule trajectories with a given lifetime (n=5). (H) Plots of loss rate vs duty ratio. Data points and error bars indicate mean +/- SEM (20%: n = 5 embryos; 50%: n = 5 embryos; 100%: n = 5 embryos). Solid line indicates fit to loss rate = disassembly rate + photobleach rate * duty ratio. (I) Disassembly rate measured in the equatorial region during late phase II (30 seconds prior to phase III) for wild type (n = 5, blue) and *arx-2 (RNAi)* (n = 6, green) embryos. (J) Model prediction of filament asymmetry over time given measured contraction rate (E) and disassembly rate (I). Gray line shows the mean filament asymmetry measured during cytokinesis in vivo (from figure 2.1-F). Blue line indicates the model-predicted asymmetry value.

To extract local estimates of F-actin disassembly rate from single molecule trajectories, we compiled the trajectories collected within a given time window and region of interest, and then constructed standard decay curves by plotting the number of trajectories with length $> \tau$ sec

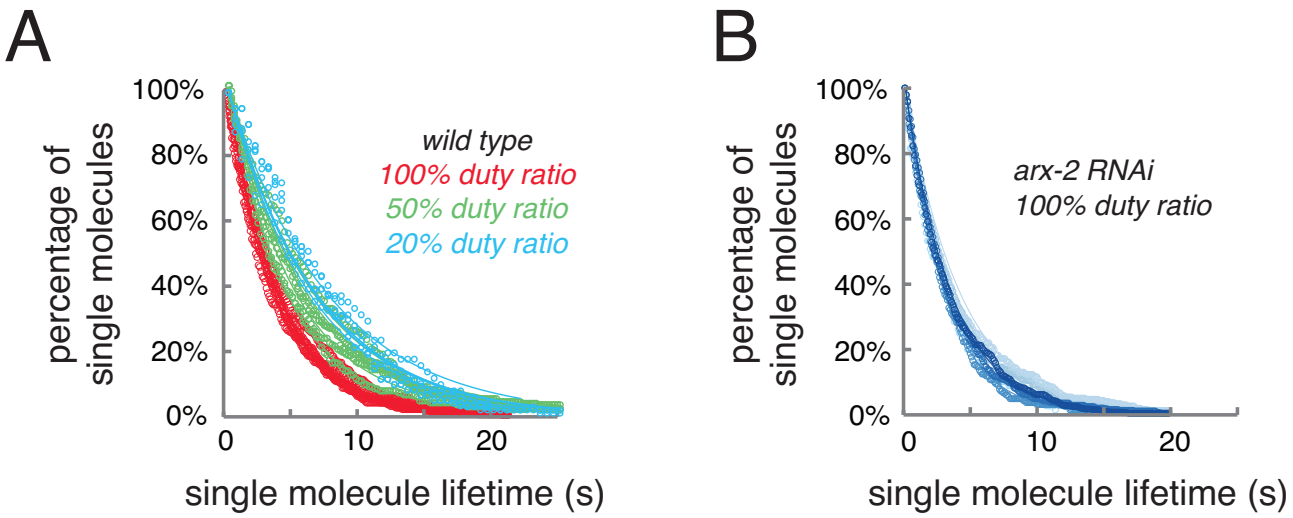

Figure 2.6. Single molecule lifetime measurements at different duty ratios in wild type and *arx-2(RNAi)* embryos. (A) Loss curves plotting the fraction of single molecule trajectories with a given lifetime recorded at the equator during cytokinesis under illumination at three different duty ratios. Loss rates inferred from exponential fits to these data are shown in figure 2.3-H. (B)Loss curves plotting the fraction of single molecule trajectories with a given lifetime recorded at the equator during cytokinesis in *arx-2(RNAi)* embryos using 100% duty ratio.

for different values of τ (figure 2.5-G). These decay curves were well-fit by single exponential, indicating a single loss rate, k_{loss}, which is the sum of an intrinsic filament disassembly rate k_{diss} and a photobleaching rate, k_{pb}, which depends on laser power and duty ratio (i.e. the fraction of time the laser is on). To obtain separate measurements of disassembly and photobleaching rates, we collected a sequence of measurements from different embryos, holding laser power and exposure time constant and varying the duty ratio. These data were well-fit by a function of the form: $k_{loss} = k_{diss} + k_{ph} \cdot dr$ (figure 2.5-H, 3.6-A), yielding an estimate of the actin filament disassembly rate $k_diss = 0.122$/s (figure 2.5-I), which agrees well with the value we previously reported for embryos depleted of Myosin II (Robin et al. 2014).

Because GFP-tagged actin monomers incorporate less efficiently into formin-assembled filaments in other contexts (Chen, Nag, et al. 2012), our measurements could reflect a biased contribution from disassembly of branched actin filaments. To address this concern, we measured filament disassembly rates in embryos strongly depleted of the ARP2/3 complex subunit ARX-2. We again observed mono-exponential decay kinetics, with a slight increase in the estimated disassembly rate to $k_{diss} = 0.167$/s. Thus our approach may slightly underestimate the disassembly rate of formin-assembled filaments within the contractile ring.

Using the measured contraction and disassembly rates, our simple model predicts that filament

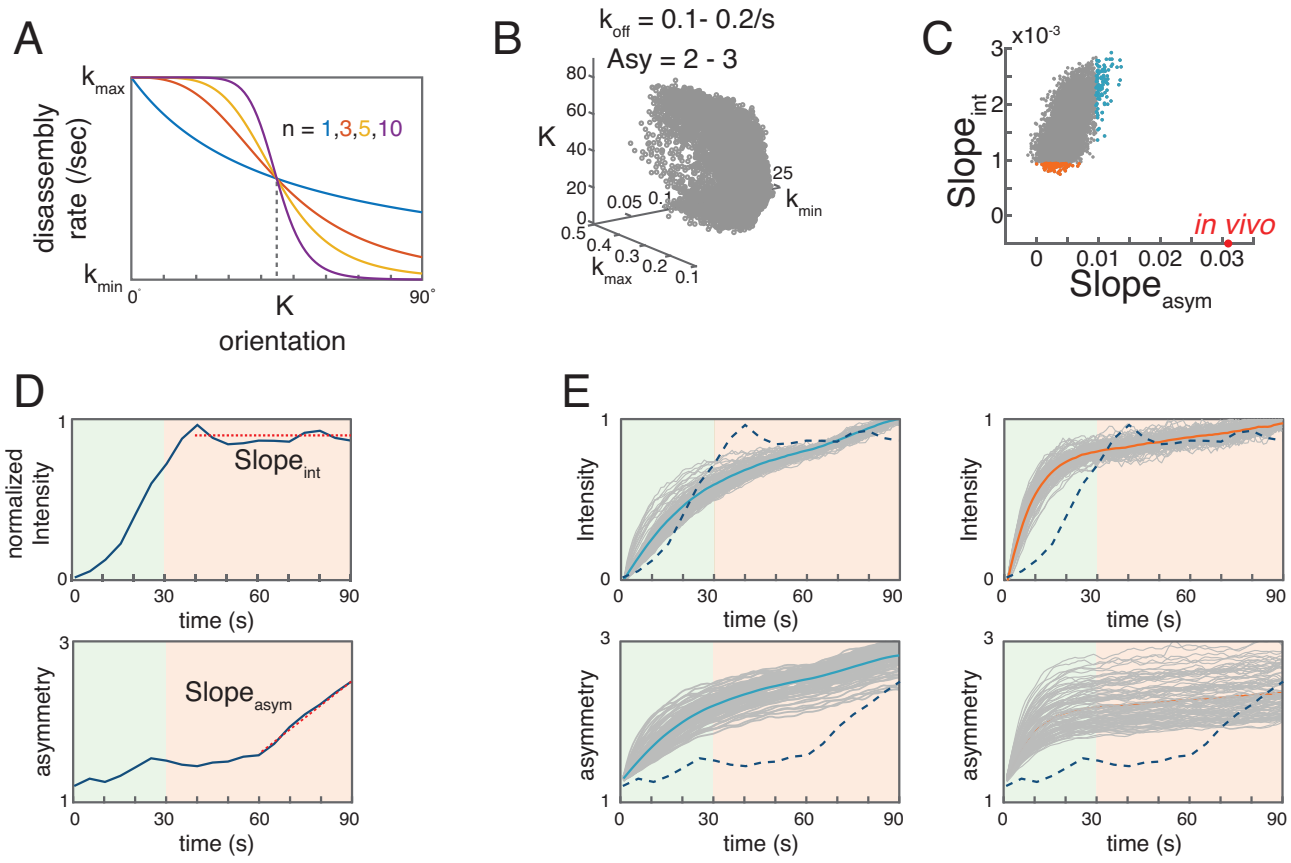

Figure 2.7. Preferential stabilization of oriented filaments cannot explain the emergence of filament alignment. (A) Using a Hill function to represent the dependence of disassembly rate on filament orientation. assembly rate $= H(\theta, k_{min}, k_{max}, K, n) = k_{max} + (k_{min} - k_{max}) \cdot \frac{\theta^n}{K^n + \theta^n}$. 0° is axial, 90° is equatorial. (B) Scatter plot showing the set of values for k_{min}, k_{max}, K, and n for which simulations satisfy two criteria: mean disassembly rate for the last 30 seconds is between 0.1/s – 0.2/s, and the asymmetry value after 90s is between 2 and 3. Parameter values were sampled with the ranges: $k_{max} \in (0, 0.5]$; $k_{min} \in (0, 0.2]$; k $\in$ (0, 90]; n $\in$ [1, 10]. (C) Scatter plot of asymmetry slope vs. intensity slope (defined in (D)) for all sets of parameters from (B). Red circle marks the measured *in vivo* values. Blue circles mark the 100 simulations whose asymmetry slope value best matches *in vivo* asymmetry slope. Orange circles mark the 100 simulations whose intensity slope value best matches *in vivo* intensity slope. (D) Illustration of the method used to measure the intensity slope (top) and asymmetry slope (bottom). Dashed lines indicate the time interval in which the slope was measured by fitting a line to the data. Dark blue curves show the *in vivo* measurements from figure 2.1-B&F. (E) Plots of intensity (top) and asymmetry value (bottom) vs time for the parameter sets indicated by filled circles in (C). Grey curves show the results for individual parameter sets. Colored solid curves show the average of all grey curves. Dark blue dash lines show the *in vivo* measurements from figure 2.1-B&F.

alignment asymmetry will first decrease from an initial value of 1.2, and then slowly increase to reach a value of 1.19 after 90 seconds (figure 2.5-J). We concluded that given constant filament turnover, reorientation of individual filaments by cortical flow cannot explain the rapid emergence of filament alignment during cytokinesis in *C. elegans* zygotes.

2.3.4 Preferential stabilization of correctly oriented filaments cannot explain robust alignment.

One possibility is that correctly oriented filaments are preferentially stabilized during ring assembly. For example, local crosslinking or bundling of co-aligned filaments by factors like Anillin could protect them from disassembly (Tian et al. 2015). To ask whether such an effect could explain the rapid emergence of filament alignment in *C. elegans* zygotes, we introduced into our model a generic form of orientation dependence, in which the disassembly rate is governed by a Hill function of filament orientation (figure 2.7-A):

$$k_{diss}(\theta) = k_{max} + (k_{min} - k_{max})\frac{\theta^n}{K^n + \theta^n}$$

We then performed a series of simulations in which we systematically varied K, n, k_{min} and k_{max}, using our measured values for contraction rate vs time (figure 2.5-E). We identified a subset of parameter values for which simulations predicted mean disassembly rates and asymmetry values (after 90 sec) close to those measured *in vivo* (figure 2.7-B; $2 < asymmetry\ value < 3$; $0.1/s < mean\ k_{diss} < 0.2/s$). Strikingly however, for none of these values could simulations also reproduce the time-dependent changes in filament density and asymmetry measured *in vivo* (figure 2.7-C,D). *In vivo*, a rapid rise in filament density precedes a stable plateau in Phase II, while a slow rise in asymmetry precedes a rapid rise in late Phase II (figure 2.7-D). By contrast, in simulations, rapid rises in filament density and asymmetry were invariably correlated (figure 2.7-E) for a simple reason: if filament stability increases with filament alignment, then a sharp increase in filament asymmetry will inevitably produce a sharp increase in filament density (assuming constant assembly rate). Thus, a rapid increase in filament asymmetry cannot coincide with a stable plateau in filament density, as we observe in late phase II, and thus orientation-dependent filament disassembly cannot alone explain the rapid emergence of filament alignment during contractile ring assembly.

2.3.5 CYK-1-dependent filament elongation is directionally biased at the equator during cytokinesis.

An alternative possibility is that the orientation of actin filament assembly could be biased. To test this possibility, we developed an approach to measure the orientation of filament elongation during cytokinesis in embryos expressing an endogenously-tagged form of the formin CYK-1 (CYK-1::GFP) (Padmanabhan et al. 2017). CYK-1 is required for contractile ring assembly and cytokinesis in early *C. elegans* embryos (Davies, Jordan, et al. 2014; Severson et al. 2002; Swan et al. 1998). Like other diaphanous-related formins, CYK-1 dimers presumably associate with the barbed ends of rapidly elongating actin filaments (figure 2.8-A). Therefore, directional movements of CYK-1 molecules should provide a direct readout of the orientation of filament growth.

Using near-TIRF microscopy, we could detect CYK-1::GFP at the cortex as diffraction-limited speckles (figure 2.8-B). Many of these speckles are stationary, while the remainder undergo rapid directional movement (figure 2.8-C). Fast dual-color imaging of CYK-1::GFP and Life-Act::mCherry revealed the rapid appearance of newly assembled filaments behind a subset of fast-moving CYK-1::GFP speckles moving through regions of low F-actin density (figure 2.8-D), confirming that these speckles mark the barbed ends of actively elongating actin filaments. If immobile CYK-1::GFP speckles are engaged in elongating filaments, those filaments should move rapidly away from stationary CYK-1::GFP speckles as they elongate. However, using particle tracking analysis of single-molecule speckles of Actin::GFP or UTR::GFP, we could not detect a pool of rapidly-moving GFP speckles (figure 2.5-B and data not shown). Thus it is likely that the stationary CYK-1::GFP speckles represent inactive protein, while the fast moving CYK-1::GFP speckles represent CYK-1 dimers associated with the barbed ends of rapidly elongating filaments.

To characterize the orientation of filament growth, we developed methods to detect, track and analyze fast, directionally moving CYK-1 speckles (See Experimental Procedures for details). Briefly, we subtracted a moving minimum intensity projection (∼800 msec window) from the raw data to enhance the signal associated with moving CYK-1 speckles. We performed particle

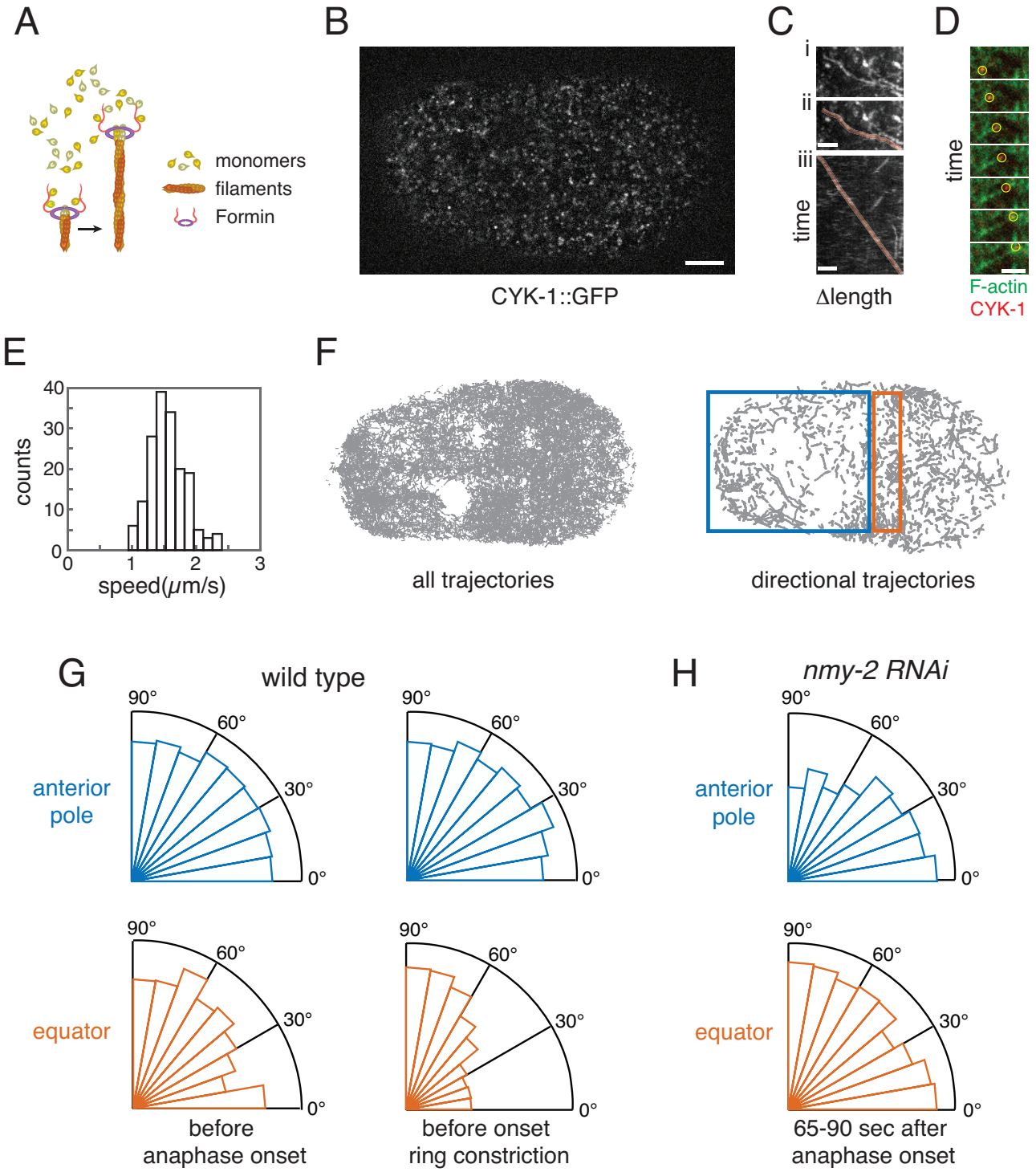

Figure 2.8. Orientation of formin-dependent filament elongation is biased with respect to the equatorial axis during cytokinesis.

Figure 2.8. Orientation of formin-dependent filament elongation is biased with respect to the equatorial axis during cytokinesis. (A) Schematic view of formin-mediated actin filament assembly. Formin dimers remain associated with the barbed ends of elongating filaments. (B) Surface view of a one-cell embryo at anaphase onset expressing CYK-1::GFP, and processed to highlight moving CYK-1::GFP speckles (see Experimental Procedures), Scale bar = 5μm. (C) Focus on a single CYK-1::GFP trajectory during cytokinesis in a wild-type embryo. (i) Maximum intensity projection of a small region of interest over time reveals moving CYK-1 particles. (ii) Trajectory of a single moving CYK-1::GFP particle is highlighted in orange. (iii) Kymograph made by straightening the orange trajectory reveals about constant speed. Scale bar = 2μm. (D) Sequence of images from the polar region of an embryo expressing CYK-1::GFP/LifeAct::mCherry and partially depleted of NMY-2. Yellow circles highlight a CYK-1::GFP particle moving into a region of low F-actin density, leaving a newly assembled actin filament behind it. See also Movie S5. Scale bar = 2μm. (E) Distribution of elongation rates measured for 41 rapidly directionally moving CYK-1::GFP speckle trajectories broken into 170 0.6sec segments (see Experimental Procedures for details). (F) CYK-1 trajectories identified by automated particle tracking analysis. Left panel: all trajectories with lifetime $\geq$ 0.6 seconds. Right panel: The subset of trajectories selected for fast directional movement (see Experimental Procedures for details, and Movie S4). Rectangles indicate polar (blue) and equatorial (orange) regions used for measurements shown in (G) and (H). (G) Distribution of movement orientations for the fast directionally moving cortical CYK-1 particles at the equator (orange) and anterior pole (blue) just before anaphase onset (left) and just before the onset of ring constriction (right). Data pooled from n = 5 embryos. (H) (H) Distribution of movement orientations for the fast directionally moving cortical CYK-1 particles in *nmy-2 (RNAi)* embryos at the equator and anterior pole 65-90 seconds after anaphase onset. Data pooled from n = 5 embryos.

detection and tracking on this filtered data. We first hand-picked and verified 41 fast moving CYK-1 trajectories, subdivided them into shorter (10 frame = 0.6 second) segments, and calculated their average instantaneous speed to be 1.561$\pm$0.286 μm/s (figure 2.8-E), which is similar to the elongation speeds previously measured for the formin mDia2 in XTC fibroblasts (Higashida 2004). Then we subdivided all trajectories into ten-frame segments, and used a statistical filter developed by Jaqaman et al. 2008 to select the subset representing directional motion, whose mean velocities were within the range measured for the hand-picked trajectories in figure 2.8-E (figure 2.8-F). Finally, we fit a straight line to each segment to estimate elongation direction as the angle between the fitted line and the embryo's AP axis.

We then plotted the distribution of elongation directions in equatorial and polar regions during 24-second windows of time just before anaphase onset, and just before the onset of rapid furrow ingression (figure 2.8-G). Before anaphase onset, filament elongation was approximately isotropic in both equatorial and polar regions (figure 2.8-G; asymmetry values = 0.96 at the equator and 0.99 at the poles. equator: n = 1380 trajectory segments; pole: n = 2978 trajectory segments in 5 embryos). Just before the onset of furrow ingression, elongation within the polar region remained isotropic, however, in the equatorial region, elongation was strongly biased perpendicular to the AP axis (figure 2.8-G; asymmetry values = 2.19 at the equator and 1.03 at the poles. Equator: n = 1469 trajectory segments; pole: n = 3029 trajectory segments in 6 embryos). Thus, biased orientation of actin filament assembly underlies the emergence of filament alignment during contractile ring assembly.

2.3.6 Newly assembled filaments use existing filaments to orient their elongation.

These results reveal a correlation between the orientations of existing filaments and the elongation of new filaments: Actin filament orientation and growth are both isotropic on the polar cortex throughout cytokinesis, and at the equator before anaphase onset (figure 2.1-E&2-E, figure 2.8-G). Filament orientation and growth are anisotropic and co-aligned at the equatorial cortex before ring constriction (figure 2.1-E and figure 2.8-G). Importantly, in embryos strongly depleted of NMY-2 by RNAi, equatorial filaments remain isotropic 65-90 seconds after anaphase onset (figure 2.3-A,E), and equatorial filament assembly was also isotropic (figure 2.8-H; asymmetry value = 0.99; n = 2099 trajectory segments in 4 embryos). These results rule out the possibility that some other equatorial signal biases filament elongation independent of existing filament's orientations. Instead, they suggest that aligned equatorial filaments provide a local directional cue to orient new filament assembly.

To examine this further, we analyzed the behavior of CYK-1::GFP speckles in embryos expressing both CYK-1::GFP and LifeAct::mCherry. In polar regions, where the density of filaments is lower, a significant fraction of fast-moving CYK-1 speckles moved along existing actin filaments or small filament bundles. Moreover, in many cases, moving CYK-1 speckles altered direction upon encountering an existing filament/bundle, and then subsequently moved along that filament/bundle (figure 2.9-A). These observations strongly suggest that existing filaments provide cues that act locally and continuously to bias the direction of new filament elongation.

To quantify the strength of this effect at the equator, we analyzed the behavior of 202 CYK-1::GFP speckles from 13 embryos that began outside, and moved into, the equatorial region (figure 2.9-B). We aligned all 202 trajectories with respect to their point of entry into the equatorial region and reflected trajectories about the AP and/or equatorial axis to place them all into the same quadrant (figure 2.9-B). We grouped whole trajectories based on time after anaphase onset (0-30sec, 30-60sec, 60-90sec), and then analyzed changes in individual trajectory orientations based on time after entry into the equatorial region (figure 2.9-C-D). We observed

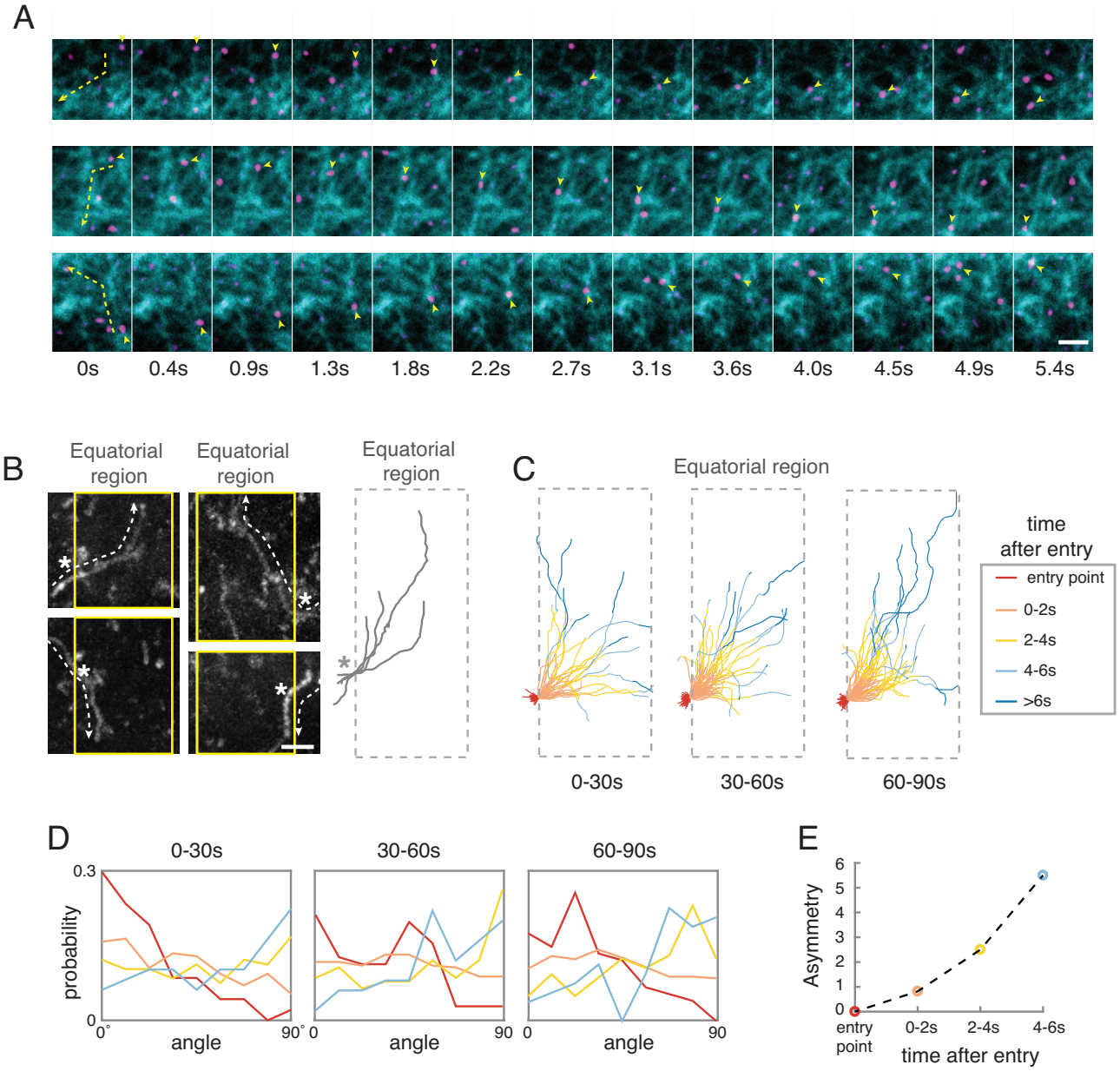

Figure 2.9. Elongating filaments use existing filaments to orient their growth. (A) Image montages highlighting three different filament growth trajectories in a one-cell embryo expressing transgenic CYK-1::GFP/LifeAct::mCherry and partially depleted of NMY-2. Yellow arrow heads mark the position and direction of a rapidly moving CYK-1::GFP speckle; dashed yellow lines and arrows at the left mark actin filament/bundles that the CYK-1 speckle moves along. In all examples CYK-1 speckles move along one actin filament/bundle and then change direction as they encounter a second filament/bundle. Scale bars = 2μm. (B) Left panel: Four example CYK-1 trajectories entering the equatorial region from the left or right and turning either up or down to move along the equatorial axis. Each image is a maximum intensity projection of many frames. Dashed lines and white arrows mark the individual CYK-1 trajectories; white asterisks mark the point of entry into the equatorial region, and vertical yellow lines indicate the boundary of the equatorial region (6μm in width). Right panel: For quantitative analysis in (C) and (D), trajectories were aligned with respect to their equatorial entry point, and flipped vertically and/or horizontally so that all enter from the left and turn upwards. Scale bars = 2μm. (C) Superposition of many CYK-1 trajectories entering the equatorial region (6μm in width) in different time windows, measured relative to anaphase onset. Individual trajectory segments are color-coded based on the time after entry into the equatorial region (see legend at right). (D) Probability histograms showing distributions of CYK-1 movement orientations at different times after entry into the equatorial region, in different time windows during cytokinesis (showing on top of histogram). Individual histograms are color-coded as in (C). (E) Line plot showing the asymmetry value of CYK-1 movement orientations at different times after entry into the equatorial region during the 60-90 second time window (LATE PHASE II).

a shift in trajectory orientations within all three windows of time (figure 2.9-D). However, the most dramatic shift occurred just before onset of ring constriction (60-90sec), when equatorial filaments are highly aligned (figure 2.9-D). In this window, the mean asymmetry of filament growth increased from a value of ∼0 at the time of entry into the equatorial region to ∼6 five seconds later (figure 2.9-E). We conclude that aligned equatorial filaments provide a strong local directional cue to orient the elongation of newly assembling filaments. Hereafter we refer to this biased elongation as filament-guided filament assembly (FGFA).

2.3.7 Filament-guided filament assembly (FGFA) increases the "effective lifetime" of filament orientation, and can explain the observed degree of filament alignment, given measured contraction and disassembly rates.

To further characterize how FGFA shapes the emergence of filament alignment, we modified our original model to incorporate a simple representation of this orientation cue. We assumed that a fraction λ of growing filaments elongate in the direction of an existing filament (i.e. with an orientation chosen at random from the distribution of existing filament orientations), while the remainder (1-λ) elongate with random orientations (figure 2.10-A). With these assumptions, and scaling filament density so that the total filament density approaches a value of 1 (see modeling procedures), we obtain a modified version of equation (2):

$$\frac{\delta\rho}{\delta t} = (k_{diss} + \xi)(1-\lambda)(\frac{2}{\pi} - \rho) - \frac{\delta}{\delta\theta}(\xi\rho cos(\theta)sin(\theta)$$

Comparing Equations (2) and (3), we see that the effect of filament-guided filament assembly is to scale the time for relaxation of filament orientations by a factor 1-λ, yielding an effective relaxation time $\tau_{eff} = \frac{1}{(1-\lambda)}\frac{1}{k_{diss}+\xi}$.

We then returned to simulations to ask how high must λ be to achieve the measured asymmetry of equatorial filaments after 90 seconds, given measured contraction and filament disassembly rates. We found that simulations reproduced the measured asymmetry for λ=0.9 (figure 2.10-B-C). Moreover, compared to simulations based on equatorial contraction with constant turnover,

or equatorial contraction with orientation-dependent disassembly (using best-fit parameters), simulations that combined FGFA (for λ=0.9) with measured rates of equatorial contraction and filament disassembly rate correctly captured the time-dependent changes in filament density and asymmetry observed *in vivo*, with a fast initial rise in density to a stable plateau, and an accelerating rise in asymmetry value (figure 2.10-E). In essence, FGFA allows separate control over the lifetimes of individual filaments and the effective lifetime of filament orientation (figure 2.10-F). This in turn allows for an initially fast rise in filament density governed by the balance of filament assembly/disassembly, followed by later sharp rise in filament asymmetry driven by compressive flow.

Finally, to estimate the value of λ *in vivo*, we used simulations to ask how large would λ have to be, given the measured asymmetry of equatorial filament orientations (figure 2.1-F), so that all trajectories are able to produce the distribution of equatorial CYK-1 movement directions observed *in vivo* (figure 2.8-G). This analysis yielded an estimated value for λ of 0.91, which is comparable to the value required in simulations. We conclude that FGFA could be sufficient to explain the emergence of equatorial filament alignment despite the rapid turnover of individual filaments.

2.4 Discussion

Classical models for cytokinesis propose how compressive cortical flows, driven by equatorial stimulation and/or polar relaxation of cortical contractility, could concentrate and align equatorial filaments during contractile ring assembly (White and Borisy 1983; Salbreux, Prost, et al. 2009; Stachowiak, Smith, et al. 2014; Bidone, Tang, et al. 2014; Reymann, Staniscia, et al. 2016; Spira et al. 2017. For this mechanism to produce a given degree of filament alignment, the rate of equatorial cortex compression must be sufficiently high, and/or the local memory of filament alignment must be sufficiently long. Recent measurements of cortical flow in one-cell *C. elegans* embryos using particle image velocimetry (Reymann, Staniscia, et al. 2016; Khaliullin et al. 2018), confirmed here by our single molecule measurements, have shown that the equatorial contraction rate is sufficiently fast in principle, but only if the memory of filament alignment is greater than 2-3 minutes. Here, we have used single molecule analysis to show that during

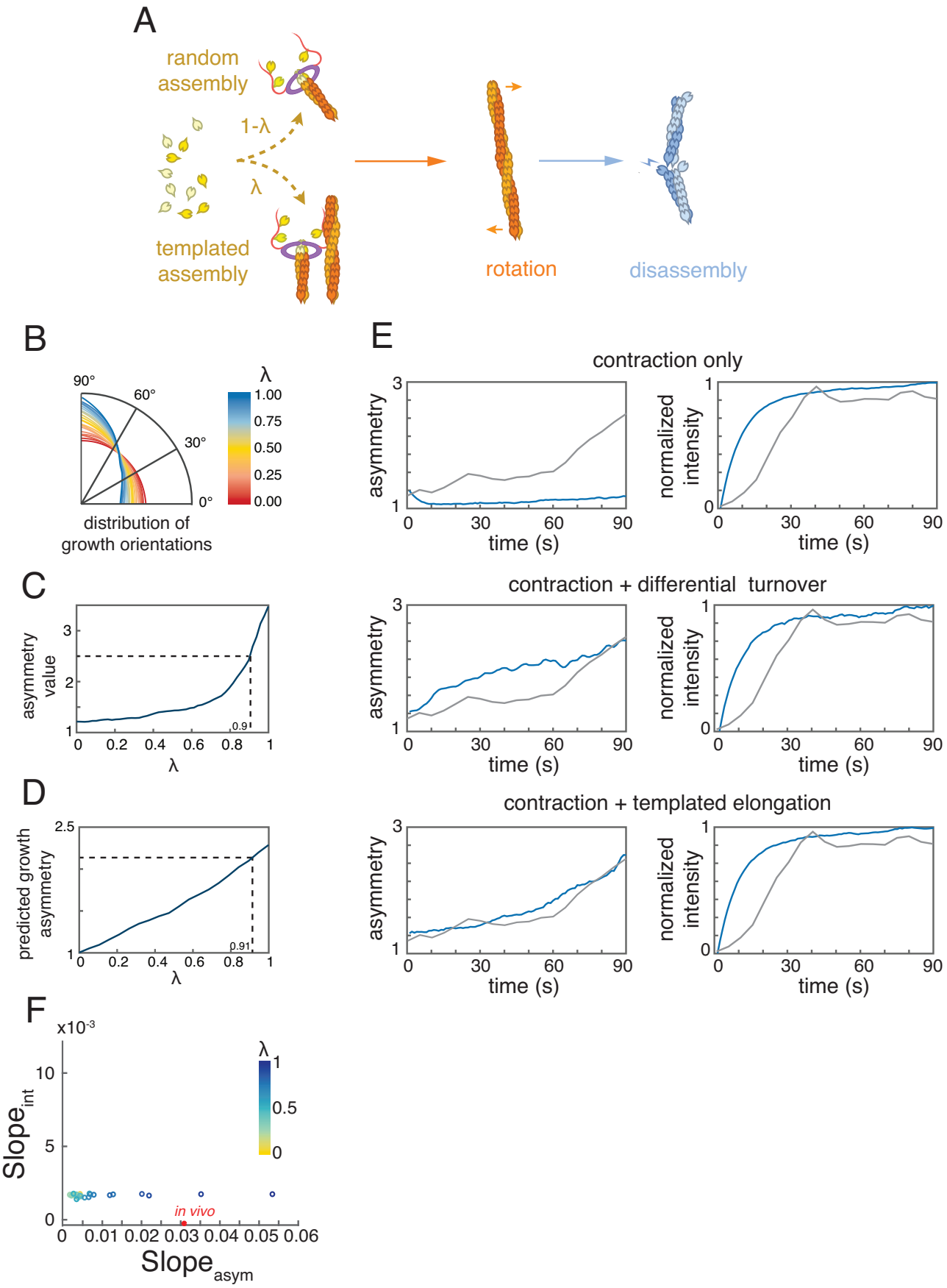

Figure 2.10. Filament-guided filament assembly (FGFA) increases the effective lifetime of filament orientation, and is sufficiently strong to explain the rapid emergence of filament alignment, given measured contraction and disassembly rate.

Figure 2.10. Filament-guided filament assembly (FGFA) increases the effective lifetime of filament orientation, and is sufficiently strong to explain the rapid emergence of filament alignment, given measured contraction and disassembly rate. (A) A simple model for filament-guided filament assembly: a fraction (λ) of growing filaments use existing filaments as guides to orient their growth. (B) The predicted distributions of filament orientations after 90 seconds, for different values of λ, given measured contraction and filament disassembly rate (figure 2.5-E and I respectively). (C) Predicted asymmetry values for the distributions in (B). Dashed line indicates the value of λ required to produce the measured asymmetry value in figure 2.1-E (λ=0.9). (D) Predicted filament growth asymmetry for different values of λ, given the distribution of filament orientations measured in late Phase II (figure 2.1-E). Dashed line indicates the value of λ required to produce the measured asymmetry value in figure 2.8-G (λ=0.91). (E) A comparison of model predictions for three different scenarios. For "contraction only" (top), we assumed constant assembly and disassembly at the measured rate (figure 2.5-I). For "contraction plus orientation-dependent disassembly" (middle), we assumed constant assembly and orientation-dependent disassembly. We selected parameter values (kmin = 0.0301, kmax = 0.1501, K = 80, figure 2.7-A) for which the mean turnover and final asymmetry values matched the measured values, and for which the slope of normalized F-actin density and asymmetry value vs time during Phase II best-matched the measured values (see figure 2.7-C, see Experimental Procedures for details). For "contraction plus filament-guided filament assembly" (bottom), we used the measured disassembly rate and chose λ=0.9 to match the final asymmetry value measured *in vivo*. In each case, model predictions (blue curves) are compared to the measured values (grey curves). For all three scenarios, we used the measured contraction rate (figure 2.5-E). (F) Values of asymmetry slope vs. intensity slope predicted for different values of λ in the filament-guided filament assembly model, given measured contraction and disassembly rates. Red circle indicates the value measured *in vivo*.

contractile ring assembly, polymerized actin has a mean lifetime of ∼8 seconds, which is far too short for individual filaments to encode a stable memory of network alignment. Moreover, comparing the output of simple models to measurements of filament density, alignment and turnover over time, we find that the rapid emergence of filament alignment cannot be explained by preferential stabilization of correctly oriented filaments. Any such mechanism predicts a progressive increase in filament lifetime and density as filaments become more favorably aligned, which we do not observe.

Instead, our direct observations of filament assembly *in vivo* identify a mechanism by which the zygote encodes a long-term memory of filament alignment, in which filaments assembled by formin/CYK-1 use existing filaments as guides to orient their growth. Support for this mechanism comes from three observations: First, we find that filament growth orientations correlate strongly and locally with existing filament orientations in both wild type and myosin-depleted embryos. Second, two-color imaging of filament growth trajectories in relation to existing filaments shows that newly assembling filaments have a strong tendency to elongate along paths defined by existing filaments, and to turn when they encounter existing filaments/bundles. Third, observations of filaments that grow into the equatorial region reveals a very strong tendency for filaments to reorient and align their growth with the equatorial axis, a tendency that increases with increasing alignment of equatorial filaments. Thus, existing filaments act as local templates to continuously influence the alignment of newly elongating filaments, a property that we refer to as filament-guided filament assembly (FGFA).

What is the molecular basis for FGFA? One possible scenario is that one or more factors tether a growing filament's barbed end to the side of an existing filament (Figure 4.1). In principle, this tethering could be mediated by CYK-1 dimers associated with the growing barbed-end, as recently demonstrated for another elongation factor Ena/VASP (Harker et al. 2019). However, Ena/VASP relies on tetramerization to interact processively with multiple filaments. In contrast, formin dimers use both FH2 domains to associate with the barbed-end of an actin filament to maintain rapid processive elongation. Thus additional modes of formin binding to F-actin would be required to tether a processively elongating filament to an existing one.

A second, and perhaps more plausible scenario, is that one or more crosslinking proteins act to rapidly crosslink nascent filaments with existing filaments, allowing the former to inherit the orientation of the latter (Figure 4.1). Two possible candidates in early *C. elegans* embryos are the crosslinkers plastin/PLST-1 (Fimbrin) (Ding et al. 2017) and anillin/ANI-1 (Descovich et al. 2018; Maddox et al. 2007). Both PLST-1 and ANI-1 accumulate in the contractile ring during cytokinesis (Ding et al. 2017; Maddox et al. 2007), and they or their orthologues can bundle F-actin *in vitro* Skau et al. 2011; Ding et al. 2017; Field and Alberts 1995). *plst-1* mutant zygotes display variably penetrant cytokinesis defects, ranging from delayed constriction to a complete failure of cytokinesis (Ding et al. 2017), while strong depletion of ANI-1 abolishes asymmetric furrow ingression and sensitizes embryos to depletion/inhibition of myosin II (Maddox et al. 2007; Descovich et al. 2018). In both cases, these defects are associated with reduced and/or delayed alignment of filaments within the contractile ring Ding et al. 2017; Descovich et al. 2018). However, in both cases, reduced alignment could be also caused by reduced recruitment of myosin II and/or reduced cortical connectivity (Ding et al. 2017; Tse et al. 2012), leading to diminished cortical flows, rather than being caused by changes in the orientation of filament growth. Thus, further experiments are required to test specific roles for these proteins in FGFA.

Regardless of the underlying molecular details, FGFA provides a powerful mechanism for growing filaments to inherit a memory of previous filament's orientations. The strength of this effect will depend on the frequency with which a growing filament encounters existing filaments/bundles and the probability per encounter that a filament reorients its growth. This strength can be

characterized by the average fraction of time λ that new filaments grow with orientations given by existing filaments. Our simple theoretical analysis shows that FGFA increases the effective local lifetime of filament orientation by a factor $1/(1- \lambda)$ over the lifetime of individual filaments. Thus in principle, by increasing the efficiency of FGFA (i.e. by driving $\lambda \rightarrow 1$), it is possible to create an arbitrarily long-lived memory of local filament alignment. Our stochastic simulations, constrained by measured equatorial contraction rates and mean filament lifetimes, predict that λ must be greater than 0.9 to explain the degree of filament alignment observed during contractile ring assembly. By comparing the orientations of equatorial filaments, and equatorial filament growth (figure 2.10-D), we estimate that $\lambda \sim 0.9$. However, this is likely to be an underestimate, because reorientation of filament growth is progressive over the growth trajectories of individual filaments (figure 2.9-E) and particle tracking errors and photobleaching of CYK-1::GFP bias our observations to the beginnings of growth trajectories. Thus, structural memory of filament alignment conferred by FGFA makes a dominant contribution to building filament alignment during contractile ring assembly.

That said, additional forms of structural memory may also contribute to contractile ring assembly. For example, myosin minfilaments turn over more slowly than single actin filaments (Carvalho et al. 2009) and may also be aligned by flow (Singh et al. 2019). anillin/ANI-1 may locally crosslink and/or stabilize F-actin and myosin II to promote their asymmetric accumulation within the contractile ring and asymmetric furrow ingression (Maddox et al. 2007; Tse et al. 2012; Tian et al. 2015). Local curvature induced by ring constriction may also feedback to enhance local filament alignment (Dorn et al. 2016). In principle, any of these mechanisms could synergize with FGFA to enhance filament alignment during cytokinesis.

Why might cells rely on FGFA to build a structural memory of filament alignment, rather than increasing the lifetimes of single filaments? Rapid filament turnover may be important for local network homeostasis – i.e. to maintain uniform filament density and prevent local tearing and/or clumping of contractile ring components (Stachowiak, Laplante, et al. 2014; Chew et al. 2017). At the same time, filament turnover provides an effective way to dissipate local resistance to the rapid remodeling of actin networks that underlies flow and filament realignment (McFadden et al. 2017). Indeed, in a network of cross-linked filaments undergoing axal compression, filaments

cannot realign without some degree of local filament buckling or inter-filament sliding (Murrell, Oakes, et al. 2015; Bidone, Jung, et al. 2017). Thus FGFA provides a way to maintain a selective memory of network deformation, while maintaining filament homeostasis and allowing rapid dissipation of local resistance to network deformation.

Although we have focused here on the initial phase of contractile ring assembly, FGFA is also likely to make an essential contribution to maintaining filament alignment during ring constriction and furrow ingression. For compressive flow to align actin filaments, it must be anisotropic (White and Borisy 1983). The axial compressive flows that accompany ring assembly satisfy this requirement, but during later cytokinesis, the equatorial cortex compresses both axially and circumferentially as it enters the furrow (Khaliullin et al. 2018). Rapid ∼isotropic compression may help to concentrate myosin II to maintain a constant rate of ring constriction through cytokinesis (Carvalho et al. 2009; Khaliullin et al. 2018), but it will no longer contribute to building filament alignment. Therefore, local mechanisms that maintain filament alignment are likely to be even more important during ring constriction. Importantly, if each encounter of a growing filament with an existing filament/bundle carries a fixed probability of realigning filament growth, the strength of FGFA will increase with filament density and degree of alignment and thus it will be strongest during late stages of ring assembly and during ring constriction.

2.5 Experimental Procedures

2.5.1 C.elegans culture and strains.

We cultured *C. elegans* strains under standard conditions (Brenner, 1974). See Supplemental Experimental Procedures for a list of mutations and transgenes used in this study. Unless otherwise specified, strains were provided by the *Caenorhabditis* Genetics Center, which is funded by the National Center for Research Resources.

2.5.2 RNA interference.

We performed RNAi using the feeding method (Lisa et al. 2001). Unless otherwise specified, bacteria targeting specific genes were obtained from the library of (Kamath et al. 2003). L4 larvae were transferred to feeding plates and then cultured at various temperatures for various times before imaging: 24-30 hours at 20 °C for nmy-2(RNAi) for strong NMY-2 depletion (figure 2.4-H&S2), 12-16 hours at 20 °C for nmy-2(RNAi) for mild NMY-2 depletion (figure 2.4-D&5A), 16-24 hours at 24 °C for arx-2(RNAi) (figure 2.3-I&S3B). For experiments involving nmy-2 (RNAi), we verified strong loss of function by complete failure of first cleavage, and mild loss of function by lack of cortical rotation. For experiments involving arx-2(RNAi), we verified strong loss of function by extreme anterior displacement of the pseudocleavage furrow (Shivas and Skop 2012).

2.5.3 Live imaging.

For all live imaging experiments, we mounted embryos in egg salts containing 100 uniformly sized polystyrene beads (15.6 mm diameter; Bangs Laboratories, #NT29N) to achieve mild compression of the embryo surface that is suitable for single molecule imaging and particle-tracking analysis, while maintaining a uniform degree of compression across experiments (Robin et al. 2014).

For two-color imaging of F-actin (GFP::UTR) and myosin (NMY-2::mKate2) or CYK-1 (CYK-1::GFP and F-actin (Lifeact::mCherry), we used a Nikon Ti-E inverted microscope equipped with solid state 50mW 481 and 561 Sapphire lasers (Coherent), a TIRF illuminator, and a Ti-ND6-PFS Perfect Focus unit. A laser merge module (Spectral Applied Research; LMM5) equipped with an acousto-optical tunable filter (AOTF) allowed rapid (1-2 msec) switching between excitation wavelengths. We collected near TIRF images using a CFI Apo 1.45 NA oil immersion TIRF objective, with 1.5X magnification, onto an Andor iXon3 897 EMCCD camera, yielding a pixel size of 107nm. Image acquisition was controlled by Metamorph software.

For single molecule/single particle tracking analysis of GFP::Actin or CYK-1::GFP, we used

an Olympus IX50 inverted microscope equipped with an Olympus OMAC two-color TIRF illumination system, a CRISP autofocus module (Applied Scientific Instrumentation), and a 1.45 NA oil immersion TIRF objective. Laser illumination at 488 nm from a 50-mW solid-state Sapphire laser (Coherent) was delivered by fiber optics to the TIRF illuminator. Images were magnified by 1.6x and collected on an Andor iXon3 897 EMCCD camera, yielding a pixel size of 100 nm. Image acquisition was controlled by Andor IQ software.

For all experiments, we set the laser illumination angle to a standard value that was chosen empirically to approximately maximize signal-to-noise ratio while maintaining approximately even illumination across the field of view.

2.5.4 Single-particle detection and tracking

We performed single-particle detection and localization using a MATLAB implementation (http://people.umass.edu/kilfoil/downloads.html) of the Crocker and Grier method (Crocker and Grier 1996; Pelletier et al. 2009). Briefly, in each image, the method uses a band pass filter to highlight roughly circular regions below a characteristic size (the feature size), in which the pixel intensity exceeds the background. The regions in which the maximum intensity exceeds a user-defined threshold are identified, and their centroids are determined to sub-pixel resolution as the center of mass of pixel intensity within a pixelated circular mask centered on the original maximum. We used a feature size of 3 and chose thresholds subjectively to optimize detection for different types of particles (Actin::GFP and CYK-1::GFP).

We performed particle-tracking analysis using freely available μTrack software (Jaqaman et al. 2008, https://github.com/DanuserLab/u-track). μTrack first links particles frame to frame and then links these short segments into longer sequences. Both linking steps use statistical models for particle motion to compute costs for different possible linkage assignments (particle appearance, disappearance, displacement, fusion, and fission) and then identify the assignments that globally minimize these costs. For all analyses reported here, we used a motion model provided with μTrack that represents a mixture of Brownian and directed motion. We allowed the possibility of "gaps" in trajectories due to transient failure to detect particles in individual

frames. For each embryo, we overlaid the raw movie with tracked particles to verify tracking accuracy, and we chose parameters for particle detection and tracking (thresholds and length of gaps) that minimize tracking errors. We previously verified the accuracy of these for measuring actin filament turnover (Robin et al. 2014). For our analyses of CYK-1 or Actin particle movements, all of our experiments were performed at particle densities for which the major tracking errors are failures to link together real particle trajectories, and these errors will have negligible effects on measurements of particle speed and direction.

2.5.5 Measuring filament density and orientation.

For analysis of filament density and orientation (figure 2.1), we imaged embryos expressing UTR::GFP and NMY-2::mKate2, using stream acquisition mode with 30% laser power, and 100 msec exposure times, for both GFP and RFP channels. At each time point, and for each channel, we collected a stack of 3 focal planes, in 0.1 μm increments, starting from the cortical surface and going inward. Then we used an average intensity projection to obtain a mean intensity for each pixel. To monitor changes in the densities of equatorial F-actin and Myosin II, we measured the total intensity of UTR::GFP and NMY-2::mKate2 signals within the equatorial ROI over time (5 pixels x 122 pixels).

To estimate the distribution of filament orientations within equatorial ROIs (6 μm in width. From hereafter 6 μm equatorial region is used to measure equatorial actin filament disassembly rate, the orientation of the elongation of equatorial filament, and the boundary to decide whether a CYK-1 particle moves into the equatorial region or not.), we used the Sobel operator to identify local gradients of fluorescence intensity, which are sharp in directions orthogonal to individual filaments/bundles. We convolved raw images with the Sobel operator defined by 3x3 kernels $S_x = \begin{bmatrix} 1 & 2 & 1 \\ 0 & 0 & 0 \\ -1 & -2 & -1 \end{bmatrix}$, $S_y = \begin{bmatrix} 1 & 0 & -1 \\ 2 & 0 & -2 \\ 1 & 0 & -1 \end{bmatrix}$ to compute the x and y components G_x and G_y of the local fluorescence intensity gradient (figure 2.2-A). For each pixel, $\phi = tan^{-1}\frac{G_y}{G_x}$ is the gradient's direction, and $G = \sqrt{G_x^2 + G_y^2}$ its magnitude. Therefore, we took the positive angle orthogonal to ϕ, $\theta = tan^{-1}\frac{G_x}{G_y}$, to be a local estimate of filament orientation, with magnitude

G. To estimate the distribution of filament orientations within a given ROI, we assigned each pixel within that ROI to the appropriate orientation bin ($0^\circ \leq \theta \leq 90^\circ$), weighted by the G, to emphasize the sharp local gradients associated with individual filaments/bundles.

2.5.6 Measuring filament asymmetry values.

To estimate a single scalar asymmetry value from distributions of filament orientations, we measured the density of filament orientations between $80^\circ - 90^\circ$ (ρ_{80-90}) and $0^\circ - 10^\circ$ (ρ_{0-10}), and defined the orientation asymmetry to be the ratio of $\rho_{80-90} : \rho_{0-10}$.

2.5.7 Measuring filament disassembly rate and axial contraction rates.

To image single molecules of Actin::GFP for measurements of cortical flow, we collected data in stream acquisition mode using 30% laser power for both wild type embryos and arx-2(RNAi) embryos). For axial contraction rate, we collected data using 450 msec exposure times. For disassembly rate, we collected data using 100 msec exposure times. We performed particle detection and tracking as described above, and then performed all subsequent analyses using custom scripts written in Matlab and R (available upon request).

To measure axial contraction rate, in MatLab we selected the subset of trajectories with lifetimes greater than 5 frames to exclude false positives. We confirmed the reliability of tracking by overlaying the resulting trajectories on the original image data. We applied a linear transformation to map positional coordinates onto X and Y axes aligned with the embryo's AP axis. Finally, we calculated the frame-to-frame displacement for each point of each trajectory and exported these data into R.

In R we took the x-axial component of the frame-to-frame displacements over all trajectories and binned them with respect to time (bin size = 30 frames = 13.5 seconds) and with respect to axial position (bin size = 10 pixels = 1 μm). For each time bin, we performed a Loess fit (https://www.rdocumentation.org/packages/stats/versions/3.6.2/topics/loess) to estimate the mean axial velocity as a function of axial position. We then computed the forward time

difference of mean velocity for each axial position to approximate the derivative of axial velocity (axial strain rate) at each point.

To measure cortical disassembly rates, we first selected all trajectories beginning within a proscribed region (equatorial or polar) and window of time (30 seconds before the onset of ring constriction). We then aligned the beginnings of all single molecule trajectories to construct a standard decay curve plotting the percentage of trajectories that remain after an interval of time τ vs t. These decay curves were well-fit by single exponentials, yielding an estimate of the single molecule disappearance rate, which is the sum of the F-actin disassembly rate and the rate of single molecule photobleaching.

To estimate single molecule photobleaching rates at 30% laser power, we measured decay curves for many individual embryos, holding laser power constant at 30% while varying the duty ratio (fraction of time the laser is on) and then fit the resulting data to $k_{disappearance} = k_{disassembly} + dr * k_{photobleach}$ to estimate $k_{disassembly}$ and $k_{photobleach}$.

2.5.8 Measuring actin filament assembly using CYK-1::GFP.

To monitor Formin-dependent filament assembly during cytokinesis, we imaged embryos expressing GFP-tagged CYK-1 (CYK-1::GFP) expressed form either the endogenous locus (Padmanabhan et al. 2017) or as an integrated transgene. For both strains, and for both wild type and nmy-2(RNAi) embryos, we collected data in stream acquisition mode using 100% laser power and 61 msec exposure. In raw movies, the majority of CYK-1::GFP signal appeared as diffraction-limited speckles, and we could detect two general classes of speckles - stationary and moving. To focus our analysis on the moving speckles, we computed a moving minimum intensity projection of the raw data, with a 13-frame window, to highlight the stationary fraction of CYK-1::GFP speckles. We then subtracted this stationary fraction from the original image data to construct a sequence of images in which the moving particles could be more readily detected and tracked.

We performed particle detection and tracking on these processed data, as described above (see Movie S4, all tracked). We then performed several additional filtering steps to select for

trajectories representing fast directional movement characteristic of formin-mediated filament elongation. First, we manually selected a subset of longer trajectories, which corresponded by eye to rapidly moving CYK-1 particles. For this subset, we divided each trajectory into smaller fragments (10 frames = 0.3 seconds per fragment), and computed a distribution of average mean speeds to serve as a reference for selecting shorter trajectories.

Next, we considered the subset of all trajectories with lengths greater than or equal to 10 frames (see Movie S4, Length $\geq$ 10). We decomposed each of these selected trajectories into shorter 10-frame segments. Then we used a method previously developed by Jaqaman and colleagues (Jaqaman et al. 2008) to select for directional movement. This method assigns an asymmetry parameter (S) to each trajectory based on the eigenvalues λ_1 and λ_2 of its variance-covariance matrix.

$$S = -ln\frac{(\lambda_1 - \lambda_2)^2}{(\lambda_1 + \lambda_2)^2}$$

Based on simulated data, Jaqaman et al. 2008 found that the S value required to achieve > 90% detection accuracy decreases with increasing trajectory length, approaching a plateau at S $\sim$ 1.5 as the trajectory length increases above 10 frames. Therefore, we selected for further analysis the subset of 10-frame trajectory segments with $S > 1.5$ (see Movie S4, Length $\geq$ 10, directional). Finally, we selected the subset of these segments with an average mean speed within the range of the means measured for the subset of manually chosen long trajectories (see Movie S4, Length $\geq$ 10, directional, 0.8 $\geq$ mean speed $\geq$ 2.5). We plotted the selected trajectory segments over the original data to confirm accuracy of particle tracking and trajectory segment selection. Finally, we estimated the movement direction for each selected trajectory segment from the positional difference between the first and last frames of the segment.

2.5.9 Visualizing CYK-1 movements along actin filament bundles.

To visualize movements of CYK-1 speckles along individual filament bindles, we imaged embryos expressing transgenic CYK-1::GFP and Lifeact::mCherry, mildly depleted of myosin II to

abolish acute rapid equatorial cortical rotation during cytokinesis. We used alternating 50 msec exposures for each channel. To enhance visualization of actin filaments, we applied a moving average of 5 frames to the Lifeact::mCherry data. To enhance visualization of moving CYK-1 speckles, we first applied a gaussian blur of 1.3 to the CYK-1::GFP data, then a bandpass filter to suppress pixel noise and spatial variations at wavelengths greater than the characteristic particle size. Then we subtracted a moving minimum average of 3 frames to suppress signals associated with stationary CYK-1 speckles and bleed through from Lifeact::mCherry signal. Finally, we applied a gamma filter of 1.5 to highlight the bright CYK-1::GFP speckles.

2.5.10 Analyzing CYK-1 trajectories moving into the equatorial region.

To capture CYK-1 trajectories moving into the equatorial region, we imaged embryos expressing transgenic CYK-1::GFP (Mi-Mi et al. 2012), which is expressed at lower levels than the endogenous protein. We manually selected 202 CYK-1::GFP particles from 13 embryos that crossed a boundary into the equatorial region, and manually tracked each particle. We aligned all trajectories with respect to their point of entry into the equatorial region and by reflecting trajectories about the AP and/or equatorial axis to place them all into the same quadrant. To calculate the distribution of the movement direction of those trajectories, we divided each trajectory into 5 frame segments, and for each segment, we estimated the movement direction from the positional difference between the first and last frames.

2.6 Modeling Procedures

We constructed a simple model that predicts how the distribution of filament orientations at the equatorial cortex evolves through a combination of local assembly, reorientation by contractile flow, and disassembly. We considered a patch of equatorial cortex, with width W and fixed height H, which contracts at a constant strain rate ξ. We denoted the density of filaments with orientation θ by $\rho(\theta, t)$. We assumed that filaments assemble at a rate $k_{ass}(\theta)$ and disassemble at a rate $k_{diss}(\theta)$. We assumed further that the cortical filament network undergoes a locally affine deformation, such that filaments within this network rotate at a rate $\frac{d\theta}{dt} = r(\theta)$. Finally,

we imposed a moving boundary condition - the left and right boundaries move as the patch deforms to satisfy $\frac{dW}{dt} = \xi W$, such that there is no flux of filaments across the left or right boundaries, and the number of filaments in the domain changes only through assembly and disassembly. Given these assumptions, we wrote an equation that describes how the distribution of filament orientations within the patch evolves over time:

$$\frac{\delta \rho}{\delta t} = k_{ass}(\theta) - (k_{diss}(\theta) + \xi)\rho - \frac{\delta}{\delta \theta}(\rho \cdot \frac{d\theta}{dt}) \tag{1}$$

To derive an expression for $\frac{d\theta}{dt}$, we focused attention on a single filament within the network, with orientation θ, and with axial and circumferential length components L_x and L_y respectively. Affine deformation of the network changes L_x, but leaves L_y unchanged. Orientation θ is related to the axial and circumferential lengths L_x and L_y by $\theta = tan^{-1}(\frac{L_Y}{L_X})$

Taking a time derivative, applying the chain rule, and using $\xi = \frac{1}{L_X}\frac{dL_X}{dt}$ we obtained:

$$\frac{d\theta}{dt} = \frac{-L_Y}{L_X^2 + L_Y^2} \cdot \frac{dL_X}{dt} = -\xi \frac{L_X L_Y}{L_X^2 + L_Y^2} = -\xi cos(\theta) sin(\theta) \tag{2}$$

2.6.1 Orientation-independent filament assembly and disassembly

We initially considered the simplest scenario, in which k_{ass} and k_{diss} are independent of filament orientation. Thus:

$$\frac{\delta \rho}{\delta t} = \frac{2}{\pi} k_{ass} - (k_{diss} + \xi)\rho - \frac{\delta}{\delta \theta}(\xi \rho cos(\theta) sin(\theta)) \tag{3}$$

Where the factor $\frac{2}{\pi}$ has been chosen so that the total filament assembly rate is k_{ass}. Scaling ρ in Equation (3) by $\rho_0 = \frac{k_{ass}}{k_{diss} + \xi}$ yields:

$$\frac{\delta \rho}{\delta t} = (k_{diss} + \xi)(\frac{2}{\pi} - \rho) - \xi \frac{\delta}{\delta \theta}(\rho cos(\theta) sin(\theta) \tag{4}$$

From this it can be seen that the time evolution of the distribution of filament orientations depends only on the value of k_{diss} and ξ. The second term in Equation (4) represents the buildup of alignment due to flow, while the first term represents the relaxation of the filament orientations towards an isotropic distribution with relaxation time $\tau = \frac{1}{k_{diss}+\xi}$.

2.6.2 Orientation-dependent filament assembly

To study how filament guided filament assembly affects the evolution of filament orientation under compressive flow, we considered a scenario in which a fraction of filaments (w) elongate using an existing filament as a guide, while the rest (1-w) assemble with random orientation. Accordingly, we rewrote Equation (3) as follows:

$$\frac{\delta\rho}{\delta t} = (\frac{2}{\pi}(1-w) + \frac{\rho}{\rho_{total}}w)k_{ass} - (k_{diss}+\xi)\rho - \frac{\delta}{\delta\theta}(\xi\rho cos(\theta)sin(\theta)) \tag{5}$$

Where $\frac{2}{\pi}(1-w)k_{ass}$ is the rate of randomly oriented assembly and $\frac{\rho}{\rho_{total}} \cdot w \cdot k_{ass}$ is the rate of filament-guided assembly. Note that we scaled these rates by $\frac{\pi}{2}$ and $\rho_{total}(t) = \int_0^{\pi/2} \rho(\theta, t)d\theta$ so that the total rates of randomly-oriented and filament-guided assembly are $(1-w)k_{ass}$ and $w \cdot k_{ass}$ respectively. The dynamics of $\rho_{total}(t)$ are given by:

$$\frac{d\rho_{total}}{dt} = k_{ass} - (k_{diss}+\xi)\rho_{total} \tag{6}$$

As above, we scaled ρ by $\rho_0 = \frac{k_{ass}}{k_{diss}+\xi}$ to obtain:

$$\frac{\delta\rho}{\delta t} = (k_{diss}+\xi)(\frac{2}{\pi}(1-w) - \rho(1 - \frac{w}{\rho_{total}})) - \frac{\delta}{\delta\theta}(\xi\rho cos(\theta)sin(\theta)) \tag{7a}$$

and

$$\frac{d\rho_{total}}{dt} = (k_{diss}+\xi)(1-\rho_{total}) \tag{7b}$$

Equation (7b) implies that $\rho_{total} \to 1$,for times $t \gg \tau = \frac{1}{k_{diss}+\xi}$, thus at long times, Equation (7a) can be approximated by:

$$\frac{\delta\rho}{\delta t} = (k_{diss} + \xi)(1 - w)(\frac{2}{\pi} - \rho) - \frac{\delta}{\delta\theta}(\xi\rho cos(\theta)sin(\theta)) \tag{8}$$

Comparing Equations (4) and (8), we see that the effect of filament guided filament assembly is to scale the time for relaxation of filament orientations by a factor $1 - w$, yielding an effective relaxation time

$$\tau_{eff} = \frac{1}{1 - w} \cdot \frac{1}{k_{diss} + \xi} \tag{9}$$

In particular, when all filament assembly is guided by existing filaments (w=1), $\tau_{eff} \to \infty$, and the time to build filament alignment is set only by the contraction rate.

CHAPTER 3

THE POTENTIAL ROLE OF PLST-1 IN DRIVING FGFA

Statement of contribution: I carried out all of the experiments and data analysis except for the in vitro experiment in figure 3.2. Alisha Morganthaler trained me to do the in vitro actin assembly assay, and helped me to set up the experiment.

3.1 Introduction

In the previous chapter, I described a new mechanism that cells use to encode a long-term memory of filament alignment during cytokinesis. I showed that the average lifetime of polymerized actin is around 8 seconds, too short for individual filaments to encode a stable memory of network alignment. Instead, I found that filaments assembled by formin/CYK-1 use existing filaments as guides to orient their growth. I used a mathematical model to show that if filament-guided filament assembly (FGFA) is sufficiently strong, then it could explain the emergence of filament alignment during cytokinesis, given measured rates of cortex contraction and filament disassembly. My direct observations of filament turning *in vivo* suggest that FGFA is indeed strong enough to explain the emergence of filament alignment. However, the molecular basis for FGFA remains unknown. In this chapter, I consider two possible (not mutually exclusive) scenarios that could underlie FGFA.

One possibility is that CYK-1 itself could tether elongating filaments to existing ones (figure 3.1). This possibility requires CYK-1 to simultaneously bind one filament while assembling another, so that it moves along the existing actin filament during elongation. A variant of this mechanism has been shown to work for another elongation factor Ena/VASPs. In the context of actin bundle assembly, a subset of Ena tetramer arms can bind to the sides of neighboring F-actin filaments while the rest of the arms bind and elongate trailing barbed ends. This allows the trailing barbed ends to catch up to the leading filaments' barbed ends, resulting in filaments of nearly equal length (Winkelman, Bilancia, et al. 2014; Harker et al. 2019).

In support of the tethering idea, many formins have been shown to crosslink actin filaments,

including mammalian formin FRL1 and Daam1, *arabidopsis* formin AFH1, budding yeast formin Bnr1, and *Drosophila* formin mDia2 (Michelot et al. 2005; Moseley and Goode 2005; Harris et al. 2006; Esue et al. 2008; Machaidze et al. 2010; Jaiswal et al. 2013). Interestingly, *in vitro* actin assembly assay shows that the C-terminus of mammalian formin Daam-1 can drive FGFA by itself (Jaiswal et al. 2013). Importantly, *C.elegans* formin/CYK-1 can also bundle actin filaments *in vitro* (Pawlik 2009). However, little is known about whether the crosslinking activity of formins enables them to elongate actin filaments along existing actin filaments.

Another possibility is that, during elongation, one or more crosslinkers act to quickly "zipper" growing filaments with existing filaments, allowing the former to inherit the orientation of the latter (figure 3.1). In fission yeast, mathematical modeling suggests that a zippering process, in which binding to one myosin cluster rotates the filament within the capture radius of the next, is a key process for actin filament self-organization during the contractile ring constriction in cytokinesis (Stachowiak, Laplante, et al. 2014). In the one-cell *C.elegans* embryo, there are at least two possible candidates that could mediate zippering: the crosslinker plastin/PLST-1 (Ding et al. 2017) and anillin/ANI-1 (Descovich et al. 2018; Maddox et al. 2007). Both PLST-1 and ANI-1 accumulate in the contractile ring during cytokinesis, they decorate actin filaments *in vivo* (Ding et al. 2017; Maddox et al. 2007), and can bundle F-actin *in vitro* (Ding et al. 2017; Tian et al. 2015) (figure 3.1).

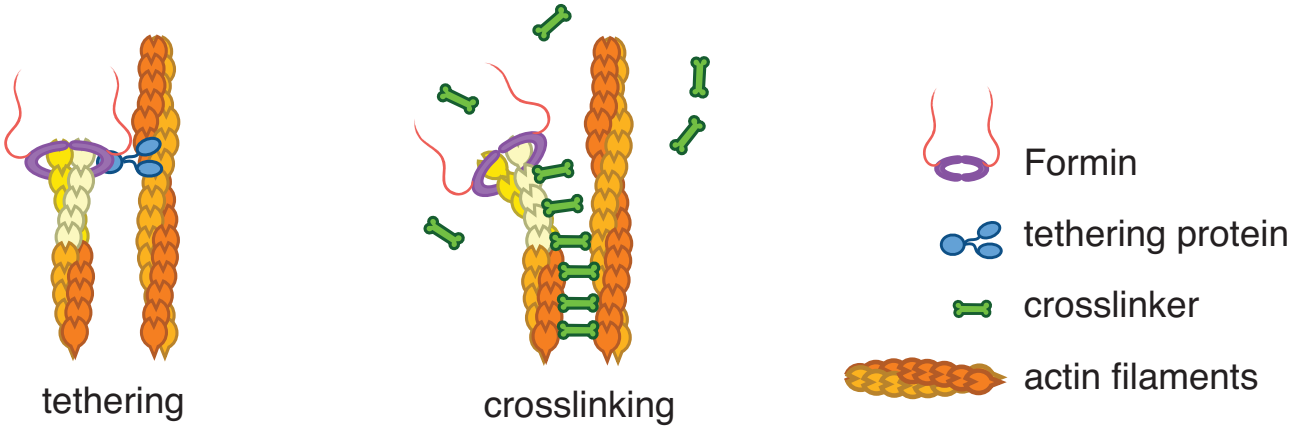

Figure 3.1. Schematic diagram showing two different mechanisms that can drive FGFA in theory. Left: Formin gets tethered to existing filaments through some tethering protein. Right: Elongating actin filaments get rapidly crosslinked to existing actin filaments by crosslinkers.

Here I focus on a potential role for the crosslinker PLST-1 in FGFA. PLST-1 plays an important role in cytokinesis. *plst-1* mutant zygotes display variably penetrate cytokinesis defects, ranging from delayed furrow initiation (85%) to late furrow regression (6%) to complete failure (9%)

(Ding et al. 2017). Confocal imaging of *plst-1* zygotes expressing GFP::Utrophin and NMY-2::mCherry at the cell cortex revealed that *plst-1* zygotes also have reduced actin alignment degree during cytokinesis. However, since PLST-1 is also important for cortical connectivity and the cortical contraction, it is unclear whether PLST-1 plays a role in FGFA, and whether reduced actin alignment degree in the *plst-1* mutant is due to the loss of FGFA, or the change in cortical contraction and connectivity (Ding et al. 2017; Reymann, Staniscia, et al. 2016; Tse et al. 2012).

Here I report on my efforts to test the plausibility of a scenario in which PLST-1 drives FGFA through zippering, using two approaches. First, in collaboration with Rachel Kadzik and Alisha Morganthaler, I used an *in vitro* reconstitution assay to test PLST-1 bundling efficiency. Second, I used TIRF microscopy to ask whether PSLT-1 can bind newly growing filaments fast enough to serve a zippering mechanism *in vivo*. I found that PLST-1 is capable of zippering elongating actin filaments to existing actin filaments *in vitro*. *In vivo*, PLST-1 can decorate actin filament fast enough to allow FGFA.

3.2 Methods

3.2.1 Actin assembly assay:

I added purified PLST-1 protein (made by Alisha Morganthaler) to a polymerization mix containing 10 mM imidazole (pH 7.0), 50 mM KCl, 1 mM $MgCl_2$, 1 mM EGTA, 50 mM DTT, 0.2 mM ATP, 50 μM $CaCl_2$, 15 mM glucose, 20 μg/mL catalase, 100 μg/mL glucose oxidase, and 0.5% (400 centipoise) methylcellulose. I then added this PSLT-1/polymerization mix to Mg-ATP-actin (15% Alexa 488-labeled) to induce F-actin assembly in the presence of PLST-1. I then added this mixture to a flow chamber and Used TIRFM to image at room temperature at 5s intervals. Finally, I varied the concentrations of PLST-1 to study the dependence of crosslinking efficiency of PLST-1 on various concentrations.

I obtained Time-lapse TIRFM movies using an Olympus IX50 inverted microscope equipped with an Olympus OMAC two-color TIRF illumination system, a CRISP autofocus module

(Applied Scientific Instrumentation), and a 1.45 NA oil immersion TIRF objective. Laser illumination at 488 nm from a 50-mW solid-state Sapphire laser (Coherent) was delivered by fiber optics to the TIRF illuminator. Images were magnified by 1.6x and collected on an Andor iXon3 897 EMCCD camera, yielding a pixel size of 100 nm. Image acquisition was controlled by Andor IQ software.

3.2.2 Live imaging of PLST-1:

To image the endogenously tagged GFP::PLST-1 (Ding et al. 2017) in one-cell *C.elegans* embryos, I mounted embryos in egg salts containing ∼100 uniformly sized polystyrene beads (15.6 μm in diameter; Bangs Laboratories, #NT29N) to achieve mild compression of the embryo surface that is suitable for single molecule imaging and particle-tracking analysis, while maintaining a uniform degree of compression across experiments (Robin et al. 2014). I set the laser illumination angle to a standard value that was chosen empirically to approximately maximize signal-to-noise ratio while maintaining approximately even illumination across the field of view.

3.2.3 Measuring PLST-1 filament growing speed:

To measure the growth speed of PLST-1-decorated filaments, I imaged embryos expressing endogenous PLST-1::GFP (Ding et al. 2017). I collected data in stream acquisition mode using 15% laser power and 50 msec exposures. In movies, I handpicked 12 growing PLST-1 streaks, and manually tracked the filament growth trajectory to calculate the mean growth rate overtime.

3.3 Results

3.3.1 PLST-1 is capable of driving FGFA in vitro

To investigate whether PLST-1 can zipper elongating actin filaments together with existing actin filaments to drive FGFA, I first asked whether PLST-1 is a sufficiently good crosslinker to

drive FGFA *in vitro*. To test this, I assembled actin filaments *in vitro* in the presence of different concentrations of PLST-1, ranging from 0 nM to 100 nM, and used TIRF microscopy to monitor actin assembly and crosslinking over time (see Methods). I was able to observe elongating actin filaments growing towards opposite directions on existing actin filaments, suggesting that PLST-1 is capable of crosslinking filaments into both parallel bundles and anti-parallel bundles (figure 3.2-A). At PLST-1 concentration equal to 100nM, the majority of actin filaments that encounter another filament are bundled by PLST-1 (figure 3.2-B). Importantly, I also found that PLST-1 can crosslink actin filaments fast enough to zipper elongating actin filaments onto existing actin filaments (figure 3.2-A). These observations confirm that PLST-1 is capable of driving FGFA *in vitro*, suggesting that zippering by PLST-1 is a possible mechanism for FGFA *in vivo*.

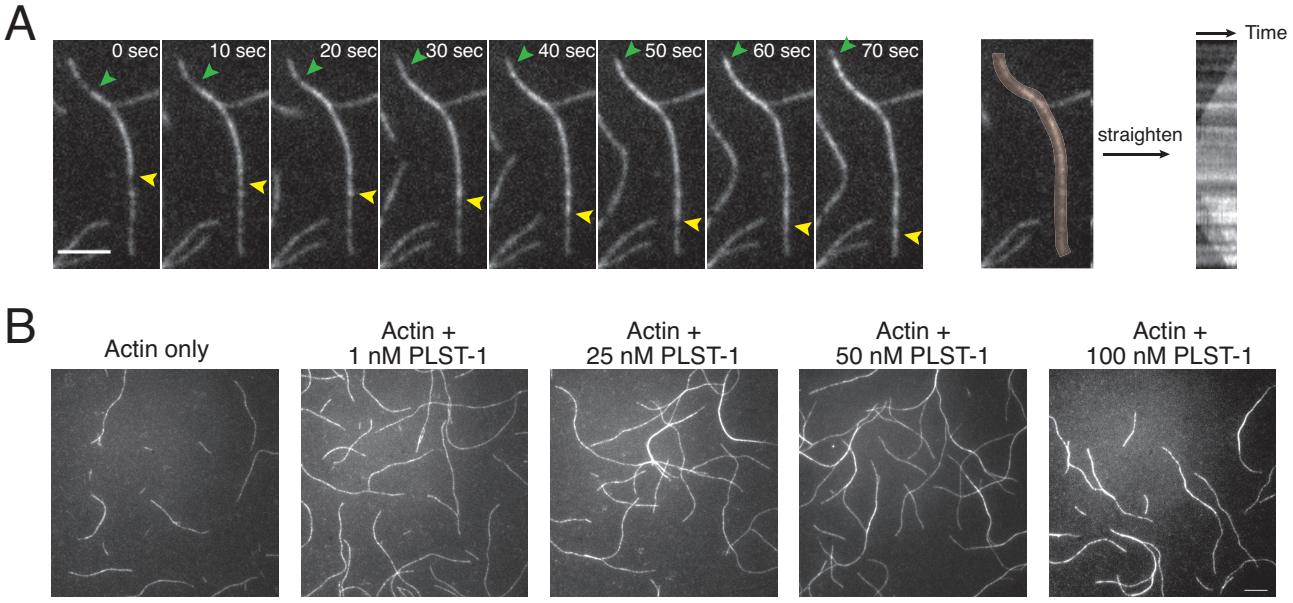

Figure 3.2. PLST-1 is capable of driving FGFA *in vitro*. (A) PLST-1 crosslinks elongating actin filaments to existing actin filaments in *in vitro* actin assembly assay. PLST-1 concentraction: 100nM. Green arrowhead and yellow arrowhead: barbed ends of two actin filaments that are elongating in the opposite directions. Right panel: Kymograph made by straightening the filamentous region highlighted in orange. Scale bar = 3μm. (B) PLST-1 bundling efficiency under different PLST-1 concentrations. Scale bar = 5μm.

3.3.2 PLST-1 can rapidly decorate elongating actin filaments in vivo

Next, I asked whether PLST-1 can bind newly growing filaments fast enough to make it a plausible candidate for a zipper that could mediate FGFA *in vivo*. If PLST-1 mediates FGFA *in vivo*, it should be able to decorate filaments as fast as they grow. To test this, I used high-speed near-TIRF microscopy to study PLST-1 dynamics in embryos expressing endogenous

PLST-1::GFP (Ding et al. 2017). Ding et al. 2017 showed that PLST-1::GFP is highly expressed in early *C.elegans* embryos and it colocalizes with markers (e.g. mCherry::Lifeact) for F-actin. In embryos expressing PLST-1::GFP, I am able to observe PLST-1 streaks that resemble actin filaments (figure 3.3-A). Those PLST-1 streaks are absent in the embryos depleted of actin filaments, which strongly suggests that they are decorating actin filaments (Ding et al. 2017). During cytokinesis, PLST-1 streaks are enriched at the equatorial region. During mitosis, I was able to observe many examples in which linear streaks of PLST-1::GFP appear *de novo* and elongate rapidly at the cortex (figure 3.3-B-C). I manually tracked and measured the growing speed of 12 different PLST-1 streaks, and calculated their average growing speed to be 1.36±0.15 μm/s, which is strikingly close to the average CYK-1 elongation speeds reported above (figure 3.3-D). Interestingly, the kymograph of these streaks reveal that these streaks are growing at a constant speed, which is another feature of elongating actin filaments (figure 3.3-G). Together, my data strongly suggest that growing PLST-1::GFP streaks are likely to represent PLST-1::GFP rapidly decorating newly elongating actin filaments as they assemble.

Interestingly, a growing PLST-1 streak can either represent PLST-1 speckles decorating an elongating actin filament by stationary CYK-1s or by processive moving CYK-1. To distinguish these two possibilities, I imaged PLST-1::GFP embryos under conditions that PLST-1::GFP molecules are sparse speckles, but I was still able to see the formation of PLST-1 streaks (Using photobleaching, figure 3.3-E-F). Kymographs of these streaks show that they grow at a speed comparable to the PLST-1 streaks observed under wildtype conditions, suggesting that they represent the same population (figure 3.3-G-H). If the growing PLST-1 streaks decorate actin filaments elongated by stationary CYK-1s, I expect to see PLST-1 puncta within streaks move together with the growing streak. On the other hand, if they decorate filaments elongated by processive moving CYK-1s, I expect to see PLST-1 punta stay stationary within each streak. I found that PLST-1 puncta stayed stationary, suggesting the latter case (figure 3.3-F). This also supports my finding that the processive moving CYK-1s are the active CYK-1s, and the stationary CYK-1s are the inactive ones.

It is likely that these rapidly-growing PLST-1 streaks represent PLST-1 decorating bundles that appear when a new filament zippers onto an existing filament (or when two filaments grow

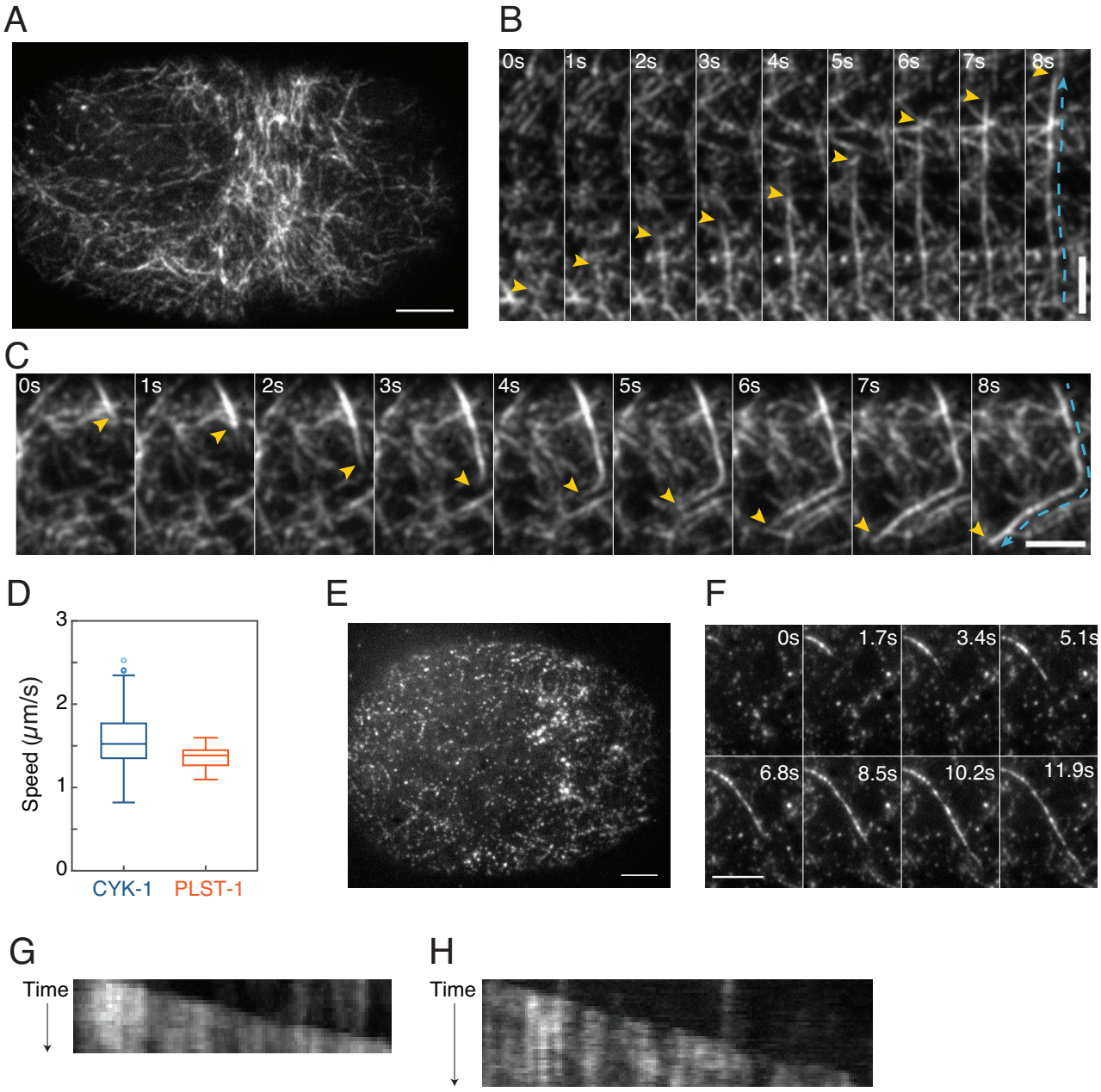

Figure 3.3. PLST-1 can rapidly decorate elongating actin filaments *in vivo*. (A) Surface view of an one-cell embryo expressing endogenous PLST-1::GFP. Scale bar = 5μm. (B-C) Examples of growing PLST-1 streaks. Yellow arrowheads mark the growing end. Blue dash arrows mark the PLST-1 streaks of interest. Scale bar = 3μm. (D) Elongation speed of CYK-1 and PLST-1 streaks. (E) Surface view of an one-cell embryo expressing endogenous PLST-1::GFP at the near-single molecule level. Scale bar = 5μm. (F) One example of growing PLST-1 streaks under near-single molecule level. Scale bar = 5μm. (G) Kymograph made by straightening the PLST-1 streak shown in (C). (H) Kymograph made by straightening the PLST-1 streak shown in (F).

simultaneously), rather than PLST-1 decorating an isolated filament for several reasons: Firstly, linear elements decorated by PLST-1::GFP are sparser than those decorated by UTR::GFP, suggesting that only a subset of filaments are decorated by PLST-1. Secondly, Because PLST-1 is a crosslinker, it is expected to bind single filaments much more weakly than bundles containing two or more filaments, because of simple avidity effects (Courson and Rock 2010). Thirdly, when I reduce PLST-1:GFP expression level to near single molecule level, I am still able to observe bright, rapidly growing streaks against a background of sparse speckles, which confirms that PLST-1::GFP decorates a subset of growing filaments at much higher densities than the rest of the population.

3.4 Discussion

My previous results (Chapter 3) suggested that approximately 90% of newly assembled actin filaments must align with existing filaments to create and maintain a highly aligned array of actin filaments during cytokinesis (figure 2.7). If zippering by PLST-1 is the mechanism for FGFA, then the crosslinking efficiency of PLST-1 *in vivo* must be sufficiently high that 90% of newly assembled actin filaments are crosslinked to existing actin filaments as they elongate. The *in vitro* and *in vivo* results described above suggest that this might be true, because first the *in vitro* actin assembly assay showed that PLST-1 is capable of crosslinking bundles with mixed polarity, and mediating FGFA. Second, *in vivo*, PLST-1 can decorate growing filaments fast enough to (in principle) mediate FGFA. However, a number of additional questions must be addressed to confirm that zippering of growing filaments by PLST-1 plays a central role in FGFA *in vivo*.

3.4.1 Do growing PLST-1 streaks report on elongating actin filaments in vivo?

In embryos expressing PLST-1::GFP, I am able to observe PLST-1 streaks that decorate actin filaments. I am also able to find many examples of fast growing PLST-1 streaks. I reasoned that they represent PLST-1 decorating elongating actin filaments for the following reasons: first, those PLST-1 streaks grow at a constant speed, which is a characteristic behavior of an

elongating actin filament. Second, PLST-1 streaks grow at a speed that is as fast as the actin elongation speed observed *in vivo* (figure 2.8-E).

However, I haven't formally ruled out the possibility that the growing PLST-1 streaks represent zippering of two existing filaments. In order to rule out this hypothesis, it would be useful to make a transgenic *C.elegans* strain expressing both PLST-1::GFP and CYK-1::mCherry. One could use TIRFM to perform dual color imaging analysis of this strain at the one-cell embryo stage. If the growing PLST-1 streaks represent elongating actin filaments, one should be able to see CYK-1 speckles at the moving tip of growing PLST-1 streaks.

3.4.2 Do PLST-1::GFP streaks represent growing filaments zippering into existing ones?

In principle, the rapidly-growing PLST-1 streaks could represent either PLST-1 decorating a single elongating filament, or crosslinking the elongating actin filament to the existing actin filaments. If it's the latter, it is strong circumstantial evidence supporting the hypothesis that zippering by PLST-1 drive FGFA. As I mentioned above, my data strongly suggest that those growing PLST-1 streaks are indeed PLST-1 crosslinking the elongating actin filament to the existing actin filaments. To strengthen our arguments and further distinguish these two possibilities, I propose the following experiments:

Image embryos co-expressing PLST-1::GFP and LifeAct::mKate. In regions with sparse actin filaments (the cortex during interphase or at pole regions during cytokinesis), if the growing PLST-1 streaks represent PLST-1 decorating a single elongating filament, one should be able to see PLST-1 streaks growing into a space absent of the LifeAct::mKate signal. Alternatively, if growing PLST-1 streaks represent PLST-1 cross linking the elongating actin filaments to existing actin filaments, one should be able to see an existing actin filament in the path ahead of the elongating PLST-1 streaks.

Alternatively, one can measure the dissociation rates of PLST-1. Theoretically, PLST-1 with both actin binding domains binding to a pair of nearby filaments should have higher avidity than the ones with only one actin binding domain binding to a single filament. Other crosslinkers

like fascin (and possibly α-actinin) have been shown to dissociate more slowly from bundles than from single filaments (Courson and Rock 2010). Thus, PLST-1 should have two different dissociation rates if some of them crosslink two filaments and the rest decorate single filaments. By comparing the dissociation rate of PLST-1 in growing streaks to the dissociation rates of PLST-1 decorating single filaments and crosslinking two filaments, one should be able to tell whether the PLST-1 streaks represent the ones crosslinking elongating filaments to existing filaments or not.

To do so, firstly we need to know the dissociation rates of PLST-1 decorating single filaments and crosslinking two filaments. I propose to use *plst-1::RNAi* or *gfp::RNAi* to reduce the expression level of PLST-1::GFP to the single molecule level, and use particle tracking to measure the dissociation rate of PLST-1 to analyze whether there are two populations of PLST-1 with different dissociation rates (Robin et al. 2014). If the answer is yes, then the population with the higher dissociation rate should represent the PLST-1 with only one ABD bound to actin filaments, and the population with the lower dissociation rate should represent the PLST-1 with both ABDs bound to actin filaments. Alternatively, one can also measure the different dissociation rates of PLST-1 *in vitro* using the approach developed previously by Courson (Courson and Rock 2010).

To measure the PLST-1 dissociation rate in the growing streaks, one could take advantage of imaging PLST-1::GFP under the near-single molecule condition. In preliminary experiments, imaging PLST-1 close to single molecule level shows that growing PLST-1 streaks can still be detected, which are composed of single molecules (Chapter 3, Fig. 2E-F). In those embryos, one should be able to manually track the PLST-1 single molecules that reside within growing streaks, and measure the dissociation rate of those particles. If this dissociation rate is the same as the dissociation rate of PLST-1 crosslinking two filaments, then the growing streaks represent PLST-1 crosslinking elongating filaments to existing filaments, which would provide strong evidence that zippering by crosslinkers is able to drive FGFA *in vivo*.

3.4.3 Is crosslinking efficiency of PLST-1 measured in vitro sufficient to explain rapid zippering observed in vivo?

As I mentioned in Chapter 3, FGFA should account for around 90% of newly assembled actin filaments to explain the robust filament alignment observed *in vivo*. Even if the growing PLST-1 streaks represent PLST-1 crosslinking elongating actin filaments to existing actin filaments, it doesn't tell us whether PLST-1 crosslinking efficiency is high enough to support FGFA. To test this, one can estimate PLST-1 crosslinking efficiency *in vivo* by measuring crosslinking efficiency of PLST-1 *in vitro* using physiological PLST-1 concentrations and elongation speeds.

To estimate PLST-1 concentration *in vivo*, one can take an approach developed by Wu and Pollard 2005, which used fluorescent intensity to estimate the global and local concentration of endogenously tagged proteins of interest (Wu and Pollard 2005; Lo et al. 2015). To achieve physiological elongation speeds, one can adapt an approach developed by Funk et al. 2019, which reconstitutes actin assembly at physiological profiling-actin concentrations. To measure PLST-1 crosslinking efficiency *in vitro*, one could repeat the actin assembly assay described in figure 3.2 with actin and profilin concentrations that allow actin filaments to elongate at physiological speeds (∼250 subunits/second, around 75 μM profilin-actin, Funk et al. 2019). The PLST-1 concentration should also be at the physiological concentration. One can then count the fraction of filaments that encounter another actin filament and zipper onto it. If the crosslinking efficiency is 90% or above, this strongly suggests that PLST-1 alone is sufficient to account FGFA *in vivo*. If the crosslinking efficiency is below 90%, this suggests that *in vivo* PLST-1 could be assisted by other factors, e.g. anillin.

CHAPTER 4

DISCUSSION

My thesis project used the contractile ring as an example to study the self-organization of actin arrays. The contractile ring is a typical example: it is spontaneously assembled from interplays among myosin, crosslinkers, formin, and actin filaments. It has a characteristic ring-like shape composed of aligned filaments with mixed polarity, which constricts during cytokinesis. During this process, it harnesses energy from ATP hydrolysis to drive myosin motor based contraction. There exists multiple opposing processes within this system: filament elongation vs. filament turnover, and equatorial contraction vs. resistance to control the dynamics of assembly and constriction. It is also a "guided self-organization" process: RhoA activates/recruits downstream targets to the division site, including formin, myosin, and anillin. Then, mechanisms driven by these proteins assemble the cortex into the contractile ring.

Classical theoretical models propose that the mechanism for the contractile ring assembly is alignment through equatorial contraction, where equatorial contractile flows concentrate and align actin filaments at the equator. However, although my data support the idea that equatorial contraction actively aligns actin filaments, it also showed that the contraction is too slow to align actin filaments to the observed level in the face of rapid filament turnover observed *in vivo*. Instead, I identified an additional mechanism - FGFA, which works together with equatorial contractions to align actin filaments. In addition, FGFA elongates actin filaments using existing actin filaments as templates to guide their elongation directions. Although FGFA can't create more alignments, it maintains filament alignment in the face of rapid filament turnover.

4.1 Unanswered questions

4.1.1 The abundance of FGFA

I found that the equatorial contraction and FGFA can build filament alignment *in vivo*, if the strength of FGFA is high enough. To estimate the strength of FGFA, I compared the

asymmetry value of filament alignment degree estimated theoretically to the asymmetry value measured *in vivo*. One caveat for this comparison is that different methods are used to calculate the asymmetry value under different conditions. In my theoretical analysis, the asymmetry value is calculated directly as the ratio of the filaments orientated equatorially verses the filaments orientated anterior-posteriorly. In contrast, the asymmetry value measured *in vivo* is by comparing the sum of the magnitude of all pixels oriented equatorially verses the sum of the magnitude of all pixels oriented anterior-posteriorly. To do so, I assigned each pixel a gradient direction and a weighted magnitude using the Sobel operator (See Methods in Chapter 3). With a perfect image (no noise), the asymmetry values estimated by these two methods should be the same. However, in reality, it is unclear how much the noise interferes with the latter method. Thus, the differences in obtaining the asymmetry values makes it hard to interpret the direct comparison between the asymmetry value obtained theoretically and the asymmetry value obtained experimentally. This doesn't hinder the main conclusion of this project, which is that only with a high value of λ can I observe a high degree of filament alignment observed *in vivo*. However, this does mean that my estimate of λ(to be 0.9) is a crude estimate. To get a more accurate estimate of λ, the ideal experiment would be to use high frequency super resolution microscopy to image embryos expressing CYK-1::GFP/LifeAct::mCherry to directly quantify the percentage of CYK-1s moving along existing actin filaments.

4.1.2 Is FGFA required during contractile ring constriction?

Although in this project I have focused on the initial phase of contractile ring assembly, FGFA is also likely to make an essential contribution to maintaining filament alignment during ring constriction and furrow ingression. One criteria for the compressive flow to align actin filaments is that it must be anisotropic (White and Borisy 1983). The axial compressive flows that accompany ring assembly satisfy this requirement, but during later cytokinesis, the equatorial cortex compresses both axially and circumferentially as it enters the furrow to constrict the cell (Khaliullin et al. 2018). Rapid isotropic compression may help to concentrate Myosin II to maintain a constant rate of ring constriction through cytokinesis (Carvalho et al. 2009; Khaliullin et al. 2018), but it will no longer contribute to building filament alignment. Therefore,

mechanisms that maintain local filament alignment are likely to be even more important during ring constriction. Importantly, if each encounter of a growing filament with an existing filament/bundle carries a fixed probability of realigning filament growth, the strength of FGFA will increase with filament density and degree of alignment and thus it will be strongest during late stages of ring assembly and during ring constriction.

To test whether FGFA still plays a role in the constriction phase, one needs to test whether the movement of CYK-1 molecules are still biased along the equatorial axis during the constriction phase (monitored by CYK-1 particle tracking), whether filament alignment degree still remains high (by imaging UTR::GFP or fixed embryos with Phalloidin staining), and whether the cortical constriction is largely isotropic (monitored by actin::GFP single molecule analysis). Unfortunately, rapid movement of the contractile ring out of the field of view during furrow ingression makes it impossible to track CYK-1 movement or actin single molecule movement during this phase. To bypass the problem created by invagination, previous studies have used confocal microscopy to acquire z stacks through the entire thickness of the embryo, and then reconstructed the contractile ring to monitor the enrichment of target proteins and/or constriction speed during furrow ingression (Descovich et al. 2018; Khaliullin et al. 2018). However, this method cannot provide the spatial or temporal resolution needed for the proposed experiments. Another potential solution is to image the cytokinesis of ABp cells at the four cell stage. At this stage, the plane of division of ABp cells is along the field of view, making it possible to use near TIRF microscopy to monitor movement of CYK-1 and Actin::GFP speckles during the entire contraction phase.

4.1.3 Is the aligned array of actin filaments necessary for cytokinesis?

My thesis focuses on the mechanisms that build an aligned array of actin filaments during cytokinesis, but it doesn't address the question of whether the aligned array of actin filaments is necessary for cytokinesis. Previous studies showed that when myosin level is reduced to ∼45% of wildtype level, F-actin alignment is completely lost at the contractile ring, while the contractile ring still constricts (Descovich et al. 2018). There are several explanations for this result: first, the authors only monitored the change of filament alignment degree up to 80 seconds post

anaphase onset. Both previous studies and my data showed that the contractile ring takes longer time to assemble, and the initiation of constriction is delayed in the embryos depleted of myosin (Descovich et al. 2018; Dorn et al. 2016; Maddox et al. 2007). Thus it's possible that in these mutant embryos, filament alignment degree also takes longer time to build up. If that's the case, one should be able to observe increased filament alignment degree right before constriction, which is about 200 seconds post anaphase onset in the embryos with 45% of myosin (Descovich et al. 2018). Second, it is possible that an aligned array of actin filaments are not necessary for cytokinesis, and are absent from embryos with low level of myosin. Instead, filament alignment facilitates contraction (Dorn et al. 2016).

4.2 Stationary CYK-1 vs processive moving CYK-1

I observe two populations of CYK-1 at the cortex: one population moves processively and the other population is stationary. Individual CYK-1 particles can switch between these two states: I observed that some CYK-1 particles switch from stationary to processive elongation, and vice versa (data not shown).

I used the dual color imaging of CYK-1::GFP/LifeAct::mCherry to show that the processively moving CYK-1s are actively elongating actin filaments. I measured the average CYK-1 elongation speed to be 1.5 μm/s, which is equivalent to $\sim$250 subunits per second. This elongation speed is comparable to the elongation speed of mDia1 in XTC fibroblast cells (2 μm/s; Higashida et al. 2008), but around 5 fold slower than the elongation speed of mDia1 and mDia2 in HT1080 and EL4 cells (Funk et al. 2019). Interestingly, an *in vitro* study showed that CYK-1 elongates actin filaments at 60 subunits per seconds in the presence of *C.elegans* profilin CePFN-1 and 15 μM of ATP-actin. A crude estimate suggests that CYK-1 elongation speed could reach 400 subunits per seconds at physiological actin concentrations, which agrees with the CYK-1 elongation I measured *in vivo* (Neidt et al. 2008).

In theory, both stationary and moving CYK-1 speckles could be actively elongating filaments. In fission yeast, Cdc12p stays attached to the contractile node while elongating actin filaments, allowing the pointed end of actin filaments to extend into neighboring regions (Pollard and Wu

2010). However, I suspect that the stationary CYK-1 dimers I observe in *C.elegans* embryos are inactive for the following reasons: Firstly, if the stationary CYK-1::GFP speckles are engaged in elongating filaments, those filaments should move rapidly away from stationary CYK-1::GFP speckles as they elongate. However, using particle tracking analysis of single-molecule speckles of Actin::GFP or UTR::GFP, I could not detect a pool of rapidly-moving GFP speckles. Secondly, the cortical environment of *C.elegans* is different from the cortical environment of fission yeast, making it much harder to elongate actin filaments from stationary formins. Fission yeast cortex is very simple, with only three structures: actin cables, actin patches, and the contractile ring. During contractile ring assembly, the equatorial region is largely devoid of actin filaments and crosslinkers, which allows the newly assembled filaments to survey the surrounding region freely before they get captured by another node. By comparison, in *C.elegans* embryos, an actin filament elongated by stationary CYK-1 will shoot out into a cortex filled up with other actin filaments and crosslinkers. Thus, it is very likely to be captured and crosslinked to an existing actin filament immediately after its assembled. After that, if the filament keeps elongating, it will lead to filament buckling and disassembly.

However, I can't rule out the possibility that the stationary CYK-1s can elongate actin filaments into the cytoplasmic pool, which can re-attach to the cortex to contribute to filament alignment degree at the cortex. To test this possibility, it will be essential to image embryos expressing single molecule F-actin probes at different z positions under conditions that would allow detection of actin speckles moving rapidly into the cytoplasm.

Interestingly, imaging embryos expressing both CYK-1::GFP and LifeAct::mCherry, I also found that many stationary CYK-1s bind to the side of actin filaments. *In vitro* sedimentation assays have shown that CYK-1 is able to both bind and bundle actin filaments, although it remains unclear whether CYK-1's ability to bind the side of actin filaments competes with its ability to nucleate and elongate filaments (Pawlik 2009). Nonetheless, if/when stationary CYK-1s become activated, they are primed to elongate actin filaments along an existing filament, which should greatly increase the chance of FGFA. Thus, it will be interesting to quantify the percentage of stationary CYK-1s that bind to the side of actin filaments, to measure the frequency with which they are activated, and whether they have a higher percentage of FGFA.

4.3 Additional features that are missing from this simple model

My model suggests that filaments are aligned by the equatorial contraction and FGFA. Although this simple model successfully explain the observed filament alignment degree measured *in vivo* and the dynamic change of actin intensity and filament alignment overtime, previous studies suggest that there are other features to cytokinesis that might be missing from this simple model.

4.3.1 Additional mechanisms to actively align actin filaments

As I mentioned in the introduction, previous theoretical studies have suggested that the cortical contractile flow towards the equator during cytokinesis should be able to build robust filament alignment if the contraction rate is sufficiently high and the filament turnover rate is sufficiently low (White and Borisy 1983; Reymann, Staniscia, et al. 2016). To support this theory, different groups have used PIV to measure the cortical contraction rate independently, and got similar results, suggesting that cortical contraction rate is around 0.01/s (0.012/s for Reymann, Staniscia, et al. 2016, 0.017 for Singh et al. 2019). However, using PIV as a crude method to estimate the contraction rate, both labs fail to capture the temporal evolution of the cortical contraction. Thus, in Reymann, Staniscia, et al. 2016, the authors used 0.012/s as a constant contraction rate for their theoretical model.

Here, using single actin molecule analysis (Robin et al. 2014), I am able to accurately monitor contractile flow over time. I found that the contraction rate is quite low initially, only ∼0.0025/s. For the next 90 seconds, the contraction rate gradually increases, and plateaus at around 0.01/s. Consistent with previous findings, I found that this contraction rate depends on myosin. In embryos strongly depleted of myosin, there is no contractile flow, and thus no actin alignment. It is worth noting that this cortical contraction rate is relatively slow: the theoretical highest degree of alignment (ratio of vertical filaments to horizontal filaments) by this contraction after 90 seconds is around 3.5, which is lower than filament alignment degree in embryos fixed and stained with phalloidin. Thus, additional mechanisms might be involved to align actin

filaments. To verify this hypothesis, one can measure filament alignment degree in embryos partially depleted of NMY-2. Previous studies (Maddox et al. 2007; Descovich et al. 2018; Dorn et al. 2016) have shown that one-cell *C.elegans* embryos that are partially depleted of NMY-2 can complete cytokinesis, although with a longer time span. In theory, in those embryos, the cortical contraction rate is also reduced. Thus, it would be interesting to measure the cortical contraction rate and filament alignment degree in those embryos to test whether a contraction rate with an even lower value is still able to build the alignment I observe *in vivo* in face of fast filament turnover. If not, which are the additional mechanisms that actively align actin filaments.

4.3.2 Turnover rate of contractile ring components during cytokinesis

Multiple studies have proposed that actin filament turnover rate must be low to explain their findings in one-cell *C.elegans* embryos during cytokinesis (Reymann, Staniscia, et al. 2016; Carvalho et al. 2009). However, using single molecule imaging, I am able to accurately estimate the average lifetime of actin filaments during the contractile ring assembly phase, which is around 8 seconds, indicating a rapid filament turnover rate. This measurement is consistent with the average lifetimes previously measured in embryos depleted of NMY-2 (10 seconds, Robin et al. 2014). Importantly, my single molecule decay curves were well-fit by single exponentials (figure 2.5-G), arguing against the possibility that there are two or more abundant populations of actin filaments with different turnover rates. Thus, my data strongly challenge the conclusions of previous studies that assumed much slower filament turnover rates during cytokinesis.

Carvalho et al. 2009 observed that the duration of cytokinesis is independent of cell size in early *C. elegans* embryos. To explain this observation, the authors proposed that the contractile ring is composed of fix-sized contractile units. These contractile units are proposed to be small actomyosin bundles, which are fixed in size, and shorten at a constant rate during constriction. Thus, a bigger contractile ring incorporates proportionally more units. During the constriction, all of the contractile units constrict (shorten) at the same rate, but they don't disassemble from the contractile ring. As a result, the constriction rate is proportional to the number of units, which is proportional to the initial size of the ring. Thus, the duration of the constriction is

independent of ring size.

A key assumption of this model is that actin filaments, together with other ring components (e.g. myosin and anillin), turnover slowly as the contractile ring constricts. Carvalho et al. 2009 relied on two experimental results to support this assumption. Firstly, FRAP analysis of myosin dynamics within the contractile ring showed that the GFP signal in the bleached region recovered slowly and progressively as constriction proceeded. During the recovery phase, the signal gradually expanded from two sides towards the center, instead of recovering uniformly across the entire bleached region. This is consistent with the idea that the recovery of the signal is due to equatorial contraction and constriction of the contractile ring, which brings in unbleached regions to fill the gap, instead of rapid turnover of myosin molecules within the gap itself. Thus, this experiment suggests that myosin is very stable within the contractile ring during constriction. Secondly, in both ABa and ABp cells, an acute treatment with latrunculin A after constriction onset did not stop the ingression of the contractile ring, which suggests that no newly assembled actin filaments are needed during constriction. Instead, actin filaments gradually shorten over time.

My observation that actin filament turnover rate is in fact very high during contractile ring assembly strongly challenges these assumptions and the fixed-unit model for contractile ring constriction. Thus, here I revisit their model with my results in mind. First, it is indeed likely that myosin is relatively stable within the contractile ring during cytokinesis, but stable myosin does not mean that actin filaments are also stable. Consistent with the myosin FRAP experiment, I have also observed that in embryos expressing endogenously labeled NMY-2-GFP, myosin particles have much longer lifetimes at the cortex than single actin molecules. In addition, I observed that in embryos partially depleted of NMY-2, residual NMY-2::GFP speckles can remain associated with the cortex for minutes before disassembly (figure 4.1). In agreement with my observations, other studies have also shown that myosin speckles have a longer lifetime than actin filaments in *C.elegans* during cytokinesis (Singh et al. 2019). However, this does not mean that other ring components also have a long lifetime.

Second, recent studies strongly argue that actin assembly is required during the constriction phase in ABa and App cells (the same cell types that have been shown to constrict without actin

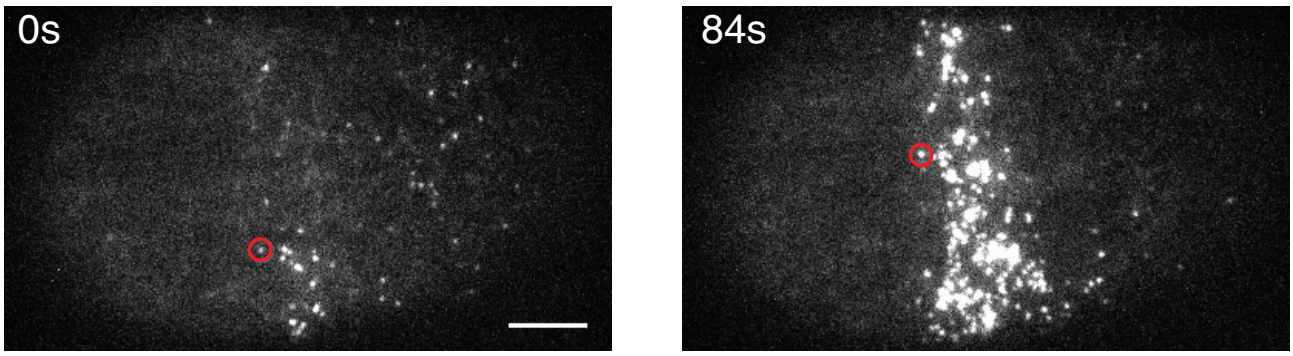

Figure 4.1. NMY-2 clusters remain associated at the cortex for long time in embryos partially depleted of myosin. Surface view of an embryo expressing endogenous NMY-2::GFP, which is partially depleted of myosin using *myosin::rnai*. Red circles label the same cluster that remain associated at the cortex for over a minute.

assembly by Carvalho et al. 2009) (Davies, Kim, et al. 2018; Silva et al. 2016), suggesting that the latrunculin A treatments of Carvalho et al. 2009 might only partially inhibit actin assembly. Using fast-acting temperature-sensitive mutants to analyze the specific requirements for different ring components during different phases of cytokinesis in four-cell *C.elegans* embryos, Davies, Kim, et al. 2018 have found that in both ABa and ABp cells, CYK-1 is required for both contractile ring assembly and constriction. In addition, Silva et al. 2016 have shown that in ABp cells, the contractile ring can repair itself in ∼20 seconds following laser ablation. Both of these results suggest that ABa and/or ABp cells have a continuous requirement for actin filament assembly during constriction, and undermine the conclusion from Carvalho et al. 2009 that stable filaments mediate contraction of the ring in those cells.

Third, besides the fixed-size contractile unit model, other mechanisms have been proposed to explain the phenomenon that the duration of constriction is independent of the contractile ring. Stachowiak, Laplante, et al. 2014 used protoplasts and modeling to study the mechanism of contractile ring construction in fission yeast. In their model, actin filaments are aligned with mixed polarity, filaments turnover rapidly, and the contraction is generated by filament sliding. Interestingly, in this model, the ring constricts at a fixed rate proportional to its initial length, similar to Carvalho et al. 2009 observations in *C.elegans*.

Lastly, it's also important to keep in mind that actin dynamics might be totally different between the contractile ring assembly at the one-cell stage and contractile ring constriction at the four-cell stage. Many data suggest that the requirement for contractile ring components varies during different phases of cytokinesis, and is cell-type specific. For example, in one-cell

C.elegans embryos, formin is required for contractile ring assembly and for the early phase of contractile ring constriction, but not the late phase of the constriction. In contrast, Myosin is required for the entire process of cytokinesis (Davies, Jordan, et al. 2014). In addition, in four-cell *C.elegans* embryos, a portion of EMS and P2 cells can finish cytokinesis even when CYK-1 is inactivated right after anaphase onset, while ABa cells fail to divide 100% of the time with CYK-1 inactivated at anytime during cytokinesis (Davies, Kim, et al. 2018). It's worth noticing that in these experiments, the authors used fast-acting temperature sensitive strains. It's unclear how effective these temperature sensitive mutants are, so it's possible that even at the restrictive temperature, there still exists a small fraction of the target protein that remains functional.

Most of these experiments (Carvalho et al. 2009; Davies, Kim, et al. 2018) depend on how effective the treatment is. Thus, to clarify these seemly contradictory results, it would be interesting to directly measure actin disassembly rate during contractile ring constriction at a four-cell stage using single molecule analysis to test whether the differences in the actin turnover rate between my project and previous studies is due to different actin dynamics in two different phases.

My project focuses on the turnover rate of actin filaments, which turnover fast. Due to the fast turnover rate, the system uses FGFA to preserve the structural memory. However, many other contractile ring components turnover much slower than actin filaments, e.g. myosin (Carvalho et al. 2009, figure 4.1). Thus, it is possible that other long lasting contractile ring components can serve as landmarks to preserve the structure in the face of rapid filament turnover.

4.3.3 Asymmetric furrow ingression

The contractile ring ingresses asymmetrically in one-cell *C.elegans* embryos (Maddox et al. 2007). During cytokinesis, the contractile ring cuts across the division plane unilaterally, instead of with circumferential symmetry. With asymmetric ingression, myosin levels can be reduced by 10 fold, and cells can still finish cytokinesis. In contrast, when asymmetric ingression is disrupted (in the paper it is done by a strong depletion of anillin), cells become more sensitive to myosin

levels, and more than 50% of cells fail to divide in the embryos partially depleted of myosin. However, as a scaffold protein, anillin contributes to many other aspects of the cortex other than asymmetric furrow ingression, thus it is unclear whether the increasing myosin sensitivity is due to the loss of asymmetric ingression. Maddox et al. 2007 proposed that a local positive feedback underlies this phenomenon: during contractile ring initiation phase, crosslinkers like anillin and septins stabilize and amplify an initial stochastic asymmetry in the cortical cytoskeleton by promoting their own recruitment. This positive feedback loop concentrates anillin locally; anillin in turn act as a scaffold to recruit and concentrate other ring components, including actin and myosin. High concentrations of actin and myosin initiate the furrow ingression locally, and then the furrow gradually ingresses to divide the cell into two.

My measurements of ring assembly kinetics ignored the asymmetry of furrow ingression, and instead focused on average values (including actin/myosin fluorescent intensities, filament alignment degree, actin turnover rate, and the orientation distribution of CYK-1 movement), measured over whatever part of the entire equatorial region was in focus for a given embryo. Then I averaged these values over multiple embryos that were presumably oriented differently relative to the axis of asymmetric furrow ingression. However, it would be interesting to repeat those experiments under conditions in which one could score the axis of asymmetric furrow ingression, to see if regions that ingress first and accumulate higher actin/myosin intensities, also achieve a higher filament alignment degree, and a more biased distribution of the orientation of CYK-1 movement. I anticipate that this correlation exists, suggesting that not only the global contractile flow driven by myosin can align actin filaments, but also the local enrichment of myosin levels can also help to align actin filaments.

4.3.4 Membrane induced filament alignment

More recently, a theoretical model proposed that a positive feedback loop between membrane curvature and filament re-alignment could also be important to build robust filament alignment during contractile ring assembly (Dorn et al. 2016). It is energetically favorable for filaments to align circumferentially along the furrow instead of orthogonally. By rectifying thermal fluctuations of actin filaments, this bias drives more filaments to align along the equatorial

axis. Aligned filaments in turn facilitates actomyosin contractility to further drive furrowing. Quantitative analysis showed that this model coupled nicely with the previously proposed asymmetric furrow ingression model (Maddox et al. 2007), in which the initial stochastic asymmetry of anillin and septin concentration promotes their own accumulation and aggregates high concentrations of ring components locally. This local enrichment of ring components creates the initial ingression, which enhance the curvature-dependent filament alignment to further facilitate ring assembly and constriction.

In theory, curvature-dependent filament alignment, myosin driven filament alignment, and FGFA are compatible. However, it is likely that these different mechanisms contribute to different degrees at different stages during contractile ring assembly and constriction. During the contractile ring assembly phase, while furrow ingression is small, the main driving force to align actin filaments is likely to be anisotropic myosin contraction, coupled with FGFA. During the constriction phase, as myosin contraction becomes more isotropic, and the membrane curvature increases significantly, curvature-dependent filament alignment will likely become more important and can work together with FGFA to maintain the filament alignment. It would be interesting to use the simulation approach from Dorn et al. 2016 to test how much the curvature-dependent mechanism contributes to filament alignment, relative to the myosin-dependent mechanism and FGFA, during these different stages.

Interestingly, the curvature-dependent and FGFA models make opposite predictions about the roles of crosslinkers. In the curvature-dependent model, thermal fluctuations allow the membrane curvature to bias filaments to align along the equatorial axis. Thus, decreasing crosslinker concentrations will decrease the friction between the individual filaments and the cortex, allowing the thermal fluctuations to align filaments more easily. However, in the FGFA model, my current hypothesis is that crosslinkers zipper nascent actin filaments with existing actin filaments to achieve FGFA. If so, decreasing crosslinker concentrations will decrease filament alignment degree. To distinguish between these two predictions, one could partially deplete embryos of the crosslinker PLST-1 using *plst-1::RNAi*, and measure the filament alignment degree during furrow ingression to compare it with the filament alignment degree in wild-type embryos with the same furrow ingression level. If the alignment degree is lower in mutant embryos, during

the contractile ring assembly phase, anisotropic myosin contraction coupled with FGFA is the dominant method to drive filament alignment.

4.4 Future direction: the mechanism of FGFA

4.4.1 Is PLST-1 required for FGFA?

I showed some preliminary data suggesting that PLST-1 drive FGFA by rapidly crosslinking elongating actin filaments onto existing actin filaments, allowing the former to inherit the orientation of the latter. I showed that PLST-1 is able to drive FGFA *in vitro*, and that it can decorate elongating actin filaments fast enough to drive FGFA *in vivo*. However, even if PLST-1 can account for FGFA *in vivo*, it is still unclear whether PLST-1 is required for FGFA. To test this idea, it will be necessary to analyze how removing PLST-1 affects FGFA *in vivo*.

One approach would be to use high-speed near-TIRF microscopy to image embryos co-expressing CYK-1::GFP and LifeAct::mCherry in wildtype and *plst-1* null embryos. If PLST-1 drives FGFA by rapidly crosslinking elongating actin filaments to existing actin filaments, then FGFA should be significantly reduced in *plst-1* null embryos. One approach to compare the degree of FGFA in wildtype and *plst-1* null embryos would be to manually score the percentage of CYK-1s that are moving along the existing actin filaments. As a control, one could use the same CYK-1 trajectories, subjected to a small displacement and rotation, then superimpose back to the same movie, and repeat the quantification. If PLST-1 plays a major role in FGFA, one would expect to see a significant reduction of the percentage of CYK-1s that are moving along existing actin filaments in the *plst-1* null embryos.

This approach would require sufficiently high temporal resolution to track fast moving CYK-1s, and sufficiently high spatial resolution to reliably detect individual filament/bundles. However, it's hard to achieve both conditions, because higher temporal resolution leads to lower signal to noise ratio and thus lower spatial resolution. With current imaging conditions, I can only reliably distinguish a difference in the percentage of CYK-1s that are moving along existing actin filaments in regions with a sparse actin distribution (e.g. in polar regions during cytokinesis).

In order to do the proposed experiments, two aspects of the imaging need to be improved: first, the spatial resolution of the actin signal is not high enough. Second, bleed through from the GFP channel to the RFP channel makes the signal to noise ratio even lower.

To acquire movies with higher spatial resolution, one could create a *C.elegans* strain expressing UTR::GFP and CYK-1::HaloTag. UTR::GFP produces higher spatial resolution than mCherry::Lifeact, and by using HaloTag, it is possible to label CYK-1 using a far-red fluorophore, which prevents the bleed through between the two channels. Additional improvements in spatial resolution could come from recent advances in super-resolution imaging (e.g. super-resolution radial fluctuations Gustafsson et al. 2016), and advances in machine learning (e.g. the content-aware image restoration Weigert et al. 2018).

An alternative approach would be to measure F-actin signal just ahead of the paths of processively moving CYK-1 speckles in embryos co-expressing HALO::CYK-1 and an F-actin marker (e.g. GFP::UTR). The basic approach would be to track processively moving CYK-1s as described in Chapter 3, then measure the average F-actin intensities along each trajectory just ahead of CYK-1. Again, one could use the same trajectories rotated and displaced to provide a baseline measurement. If PLST-1 drives FGFA, one would expect to see higher average F-actin intensities just ahead of CYK-1 trajctories in wildtype than in *plst-1* null embryos.

A third (more indirect) approach would be to compare the distributions of CYK-1 movement directions at the equator of wild-type and the *plst-1* null embryos during contractile ring assembly. If PLST-1 drives FGFA, then in the *plst-1* null embryos, one would expect to see no (or a much weaker) bias in CYK-1 movement directions.

However, one caveat for this third experiment is that crosslinkers can also affect the connectivity and the contractility of the actin network (see Introduction), and thus affect equatorial filament alignment during cytokinesis. Indeed, Ding et al. 2017 observed significant differences in the degree of filament alignment during cytokinesis in wildtype and *plst-1* null embryos. Thus, it will be important to perform controlled comparisons that take into account the degree of filament alignment. One approach would be to use *nmy-2(RNAi)* to tune rates of equatorial contraction, so that the average degree of filament alignment observed in wildtype and *plst-1* null embryos are comparable. Alternatively, one could do a pairwise comparison of filament

alignment degree and the distribution of CYK-1 movement directions during contractile ring assembly in wildtype and *plst-1* mutant embryos. If PLST-1 drives FGFA, one would expect to see a significant reduction in the correlation between the filament alignment degree and the bias in the distribution of CYK-1 movement direction in *plst-1* null embryos.

Lastly, one could also test the role of PLST-1 in FGFA indirectly by comparing the temporal correlation of actin structures in wild-type and *plst-1* background. The function of FGFA is to maintain structural memory of the cortex in the face of rapid individual filament turnover. This is because in wild-type embryos, the overall organization of the actin network should be maintained much longer than the average lifetime of individual filament. If FGFA is disrupted, the overall structure of the actin network should change rapidly. Thus, if PLST-1 drives FGFA, in *plst-1* null embryos, a significant decrease in the temporal correlation of the actin organization should be observed.

4.4.2 PLST-1 contribution to FGFA as a non-essential protein

One question raised from my project is that, based on previous studies, PLST-1 is a non-essential protein. 91% of *plst-1* null embryos complete first cytokinesis, while 50% are able to develop into adult worms (Ding et al. 2017). So, how could PLST-1 play a key role in assembling the contractile ring, giving the fact that it is not essential? There are two possibilities: first, as mentioned above, an aligned array of actin filaments might not be essential for constriction. Aligned actin arrays plays a critical role in making constriction more effective, but cells still constrict without them. Consistent with this possibility, among the *plst-1* null embryos that successfully divide, 93% show delayed furrow initiation, and 7% show late furrow regression (Ding et al. 2017).

Secondly, other crosslinkers might work redundantly with PLST-1. One potential candidate is anillin. Strong depletion of ANI-1 in one-cell *C.elegans* embryos abolishes asymmetric furrow ingression, delays furrow ingression overall, reduces the size of myosin patches, renders cytokinesis less robust to inhibition of contractility, and of particular relevance to this study, decreases F-actin alignment degree during cytokinesis (Maddox et al. 2007; Descovich et al. 2018; Tse et al.

2012). Thus, it would be interesting to explore the contribution of Anillin in FGFA, using the same approaches outlined for PLST-1 above, e.g. the *in vitro* actin assembly assay with ANI-1 to test whether ANI-1 is capable of driving FGFA *in vitro*, *in vivo* imaging analysis with embryos expressing ANI:GFP, and imaging analysis with embryos depleted of ANI-1 to test whether ANI-1 plays an essential role in FGFA *in vivo*. Importantly, since these two crosslinkers might work redundantly, it will be essential to inhibit both proteins individually and in combination to test their roles in FGFA.

4.4.3 Can F-actin tethering by CYK-1 mediate FGFA in vitro?

As I mentioned above, elongation factors like Ena/VASPs can elongate actin filaments along the existing actin filaments. Along with this idea, Daam-1 is able to drive FGFA by itself (Jaiswal et al. 2013). In addition, CYK-1 can also bind and bundle actin filaments *in vitro* (Pawlik 2009), raising the possibility that CYK-1 itself could act simultaneously as a tether and as an elongation factor to mediate FGFA.

A key test of this hypothesis would be to perform the actin assembly assay *in vitro* in the presence of CYK-1. To do so, one could repeat the actin assembly assay described in Chapter 4, but using CYK-1 instead of PLST-1. If CYK-1 is able to mediate FGFA through tethering, one should be able to observe FGFA. It is possible that CYK-1 can drive FGFA as a crosslinker, which is different from a tethering mechanism. To eliminate this possibility, one could perform the actin assembly assay at low CYK-1 concentrations, where bundling activity is negligible.

If CYK-1 is able to drive FGFA through a tethering mechanism, the next step would be to analyze the functional motifs that are important for this tethering. Different formins seem to use different domains to bind to the sides of actin filaments (Michelot et al. 2005; Harris et al. 2006; Moseley and Goode 2005; Jaiswal et al. 2013), and a variety of models are proposed for this interaction. In principle, the FH2 domain could use the same interface to bind the sides and barbed ends of filaments. Alternatively, residues on the outside surface of the FH2 donut, or on the FH1 domain, could mediate binding to filament sides (figure 4.2).

To explore the molecular basis for CYK-1's crosslinking ability, one could systematically synthesis

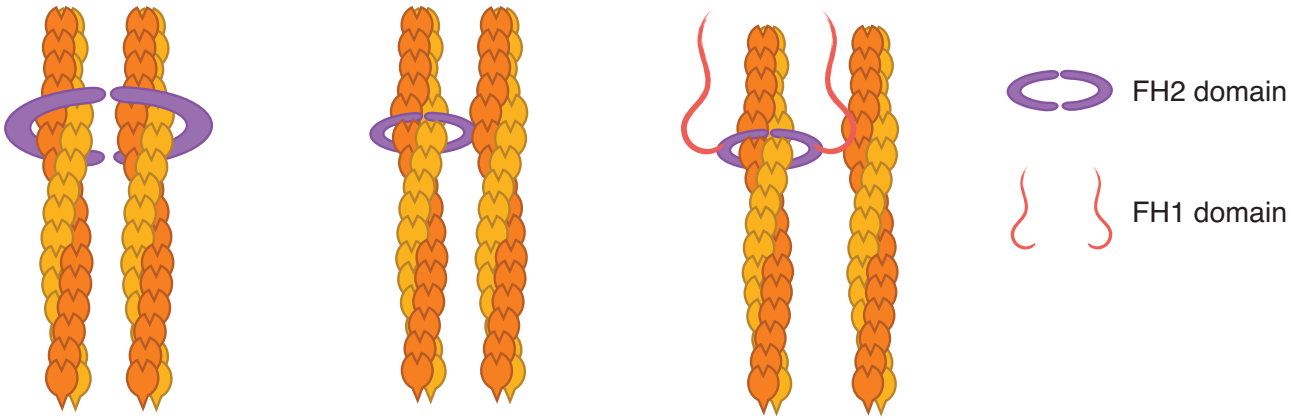

Figure 4.2. Different theoretical models for formin crosslinking activity. Left: two FH2 domains wrap aroung two filaments (Harris et al. 2006). Middle: the outside surface of the FH2 donut crosslinks to another filament. Right: the FH1 domain crosslinks to another filament.

various truncated versions of CYK-1 to test their ability to bundle actin filaments *in vitro*. Ultimately, it would be interesting to make mutated versions of CYK-1 *in vivo*, which are able to elongate actin filaments but unable to crosslink actin filaments, to test whether CYK-1 tethering property is necessary for FGFA.

4.5 Future direction: FGFA can be used to maintain actin organization in other structures

The key contribution of FGFA is to maintain actin filament alignment in the face of rapid turnover of individual components, such that the alignment can persist much longer than the lifetime of individual components. Neither of the two mechanisms proposed for FGFA require components specific to cytokinesis. In fact, I also observe FGFA during interphase in P0 and P1 cells, and at the pole regions during the cytokinesis of P0 cells, suggesting that FGFA can contribute to maintaining actin structures outside of cytokinesis. Thus, it would be interesting to explore other actin structures to see whether FGFA plays a role in building and/or maintaining aligned arrays of filaments in other contexts.

For example, during later development in *C. elegans*, epidermal cells extend along the anterior-posterior axis of the embryo and constrict along its circumference (Chisholm and Hardin, 2005). Within these cells, actin filaments are aligned circumferentially to contribute to cell elongation (Priess and Hirsh 1986; Vuong-Brender et al. 2017; Lardennois et al. 2019). Many experiments

have been done to understand the anisotropic contraction force that drives cell elongation. However, little is known about the assembly and the maintenance of the aligned actin filaments during this process. Interestingly, the embryo elongation lasts for hours, during which period actin filaments orientation are maintained (Diogon et al. 2007).

Another candidate structure is stress fibers. To maintain mechanical homeostasis, actin stress fibers undergo local, acute, force-induced tearing and repairing. During stress fiber repairing events, the tearing site exhibits spontaneous restoration of actin integrity, while the actin intensity of surrounding regions remain largely unchanged (Smith et al. 2010). This suggests that the repairing events are due to assembly of newly aligned actin filaments, instead of recruiting filaments from surrounding regions. Interestingly, formins are also involved in stress fiber formation (Young and Copeland 2010).

In fact, aligned arrays of actin filaments are used in many other cellular processes, including: different types of stress fibers, actin arcs formed by centripetal flows in migrating cells, or during synapse formation in T cells, cortical arrays that underlie cellular constrictions equatorial region of *Ciona robusta* notochord cells, and transient arrays that form during wound healing (Murugesan et al. 2016; Spira et al. 2017; Burnette et al. 2011; Sehring et al. 2014; Hotulainen and Lappalainen 2006; Mandato and Bement 2001). In future work, it will be interesting to examine formin dynamics and additional roles of crosslinkers in the structures mentioned above. The fact that many of those structures are contractile suggests that they also need to have high filament turnover rate to dissipate local stress caused by contraction and at the same time maintain their structure, suggesting that FGFA might also play a role in maintaining filament alignment in these structures. In addition, FGFA is not restricted to maintain the organization of actin bundles. In any long lived actin arrays, FGFA could contribute to maintaining the structures by allowing new filaments to inherit the filament orientation of the existing pattern. Thus, FGFA provides the answer to a more fundamental question: in a biological organism, how to preserve structural information, giving that the individual components are turning over rapidly and constantly.

REFERENCES

Adams, J. C. (1995). "Formation of stable microspikes containing actin and the 55 kDa actin bundling protein, fascin, is a consequence of cell adhesion to thrombospondin-1: Implications for the anti-adhesive activities of thrombospondin-1". In: *Journal of Cell Science* 108.5, pp. 1977–1990. ISSN: 00219533.

Agarwal, Priti and Ronen Zaidel-Bar (2019). "Principles of Actomyosin Regulation In Vivo". In: *Trends in Cell Biology* 29.2, pp. 150–163. ISSN: 18793088. DOI: 10.1016/j.tcb.2018.09.006. URL: https://doi.org/10.1016/j.tcb.2018.09.006.

Alberts, Arthur S. and Richard Treisman (1998). "Activation of RhoA and SAPK/JNK signalling pathways by the RhoA-specific exchange factor mNET1". In: *EMBO Journal* 17.14, pp. 4075–4085. ISSN: 02614189. DOI: 10.1093/emboj/17.14.4075.

Alto, Laura Taylor and Jonathan R. Terman (2018). "MICALs". In: *Current Biology* 28.9, R538–R541. ISSN: 09609822. DOI: 10.1016/j.cub.2018.01.025.

Alvarado, José et al. (2013). "Molecular motors robustly drive active gels to a critically connected state". In: *Nature Physics* 9.9, pp. 591–597. ISSN: 17452481. DOI: 10.1038/nphys2715.

Bamburg, James R (1999). "Proteins of the ADF/Cofilin Family: Essential Regulators of Actin Dynamics". In: *Annual Review of Cell and Developmental Biology* 15.1, pp. 185–230. ISSN: 1081-0706. DOI: 10.1146/annurev.cellbio.15.1.185. URL: http://www.annualreviews.org/doi/10.1146/annurev.cellbio.15.1.185.

Banga, I and A Szent-Gyorgyi (1941-42). "Preparation and properties of myosin A and B". In: *The institute of medical chemistry University Szeged* I.

Basant, Angika and Michael Glotzer (2018). "Spatiotemporal Regulation of RhoA during Cytokinesis". In: *Current Biology* 28.9, R570–R580. ISSN: 09609822. DOI: 10.1016/j.cub.2018.03.045. URL: https://doi.org/10.1016/j.cub.2018.03.045.

Belmonte, Julio M, Maria Leptin, and François Nédélec (2017). "A theory that predicts behaviors of disordered cytoskeletal networks". In: *Molecular Systems Biology* 13.9, p. 941. ISSN: 1744-4292. DOI: 10.15252/msb.20177796.

Bement, William M., Hélène A. Benink, and George Von Dassow (2005). "A microtubule-dependent zone of active RhoA during cleavage plane specification". In: *Journal of Cell Biology* 170.1, pp. 91–101. ISSN: 00219525. DOI: 10.1083/jcb.200501131.

Bernheim-Groswasser, Anne et al. (2002). "The dynamics of actin-based motility depend on surface parameters". In: *Nature* 417.6886, pp. 308–311. ISSN: 00280836. DOI: 10.1038/417308a.

Bernstein, Barbara W. and James R. Bamburg (2010). "ADF/Cofilin: a functional node in cell biology". In: *Trends in Cell Biology* 20.4, pp. 187–195. ISSN: 09628924. DOI: 10.1016/j.tcb.2010.01.001. arXiv: NIHMS150003. URL: https://www.ncbi.nlm.nih.gov/pmc/articles/PMC3624763/pdf/nihms412728.pdf%20https://linkinghub.elsevier.com/retrieve/pii/S0962892410000024.

Bi, Erfei and Hay Oak Park (2012). "Cell polarization and cytokinesis in budding yeast". In: *Genetics* 191.2, pp. 347–387. ISSN: 00166731. DOI: 10.1534/genetics.111.132886.

Bidone, Tamara C., Haosu Tang, and Dimitrios Vavylonis (2014). "Dynamic network morphology and tension buildup in a 3D model of cytokinetic ring assembly". In: *Biophysical Journal* 107.11, pp. 2618–2628. ISSN: 15420086. DOI: 10.1016/j.bpj.2014.10.034. URL: http://dx.doi.org/10.1016/j.bpj.2014.10.034.

Bidone, Tamara Carla, Wonyeong Jung, et al. (2017). "Morphological Transformation and Force Generation of Active Cytoskeletal Networks". In: *PLoS Computational Biology* 13.1, pp. 1–22. ISSN: 15537358. DOI: 10.1371/journal.pcbi.1005277.

Bieling, Peter et al. (2016). "Force Feedback Controls Motor Activity and Mechanical Properties of Self-Assembling Branched Actin Networks". In: *Cell* 164.1-2, pp. 115–127. ISSN: 10974172. DOI: 10.1016/j.cell.2015.11.057. URL: http://dx.doi.org/10.1016/j.cell.2015.11.057.

Bishop, Anne L. and Alan Hall (2000). "Rho GTPases and their effector proteins". In: *Biochemical Journal* 348.2, pp. 241–255. ISSN: 02646021. DOI: 10.1042/0264-6021:3480241.

Blanchoin, Laurent et al. (2014). "Actin dynamics, architecture, and mechanics in cell motility". In: *Physiological Reviews* 94.1, pp. 235–263. ISSN: 00319333. DOI: 10.1152/physrev.00018.2013.

Bogdan, Sven, Jörg Schultz, and Jörg Grosshans (2013). "Formin' cellular structures". In: *Communicative & Integrative Biology* 6.6, e27634. DOI: 10.4161/cib.27634.

Bolado-Carrancio, Alfonso et al. (2020). "Periodic propagating waves coordinate rhogtpase network dynamics at the leading and trailing edges during cell migration". In: *eLife* 9.i, pp. 1–34. ISSN: 2050084X. DOI: 10.7554/eLife.58165.

Boulter, Etienne et al. (2010). "Regulation of Rho GTPase crosstalk, degradation and activity by RhoGDI1". In: *Nature Cell Biology* 12.5, pp. 477–483. ISSN: 14657392. DOI: 10.1038/ncb2049.

Brandt, Dominique T. and Robert Grosse (2007). "Get to grips: Steering local actin dynamics with IQGAPs". In: *EMBO Reports* 8.11, pp. 1019–1023. ISSN: 1469221X. DOI: 10.1038/sj.embor.7401089.

Breitsprecher, Dennis and Bruce L. Goode (2013). "Formins at a glance". In: *Journal of Cell Science* 126.1, pp. 1–7. ISSN: 00219533. DOI: 10.1242/jcs.107250.

Breitsprecher, Dennis, Stefan A. Koestler, et al. (2011). "Cofilin cooperates with fascin to disassemble filopodial actin filaments". In: *Journal of Cell Science* 124.19, pp. 3305–3318. ISSN: 00219533. DOI: 10.1242/jcs.086934.

Brieher, William (2013). "Mechanisms of actin disassembly". In: *Molecular Biology of the Cell* 24.15, pp. 2299–2302. ISSN: 10591524. DOI: 10.1091/mbc.E12-09-0694.

Bubb, Michael R. et al. (2000). "Effects of jasplakinolide on the kinetics of actin polymerization. An explanation for certain in vivo observations". In: *Journal of Biological Chemistry* 275.7, pp. 5163–5170. ISSN: 00219258. DOI: 10.1074/jbc.275.7.5163.

Burnette, Dylan T. et al. (2011). "A role for actin arcs in the leading-edge advance of migrating cells". In: *Nature Cell Biology* 13.4, pp. 371–382. ISSN: 14657392. DOI: 10.1038/ncb2205. URL: http://dx.doi.org/10.1038/ncb2205.

Cameron, Lisa A. et al. (1999). "Motility of ActA protein-coated microspheres driven by actin polymerization". In: *Proceedings of the National Academy of Sciences of the United States of America* 96.9, pp. 4908–4913. ISSN: 00278424. DOI: 10.1073/pnas.96.9.4908.

Campellone, Kenneth G. and Matthew D. Welch (2010). "A nucleator arms race: cellular control of actin assembly". In: *Nature Reviews Molecular Cell Biology* 11.4, pp. 237–251. ISSN: 1471-0072. DOI: 10.1038/nrm2867. arXiv: NIHMS150003. URL: https://www.ncbi.nlm.nih.gov/pmc/articles/PMC3624763/pdf/nihms412728.pdf%20http://www.nature.com/articles/nrm2867.

Cao, Wenxiang, Jim P. Goodarzi, and Enrique M. De La Cruz (2006). "Energetics and Kinetics of Cooperative Cofilin-Actin Filament Interactions". In: *Journal of Molecular Biology* 361.2, pp. 257–267. ISSN: 00222836. DOI: 10.1016/j.jmb.2006.06.019.

Carlier, M. F. et al. (1993). "Modulation of the interaction between G-actin and thymosin β4 by the ATP/ADP ratio: Possible implication in the regulation of actin dynamics". In: *Proceedings of the National Academy of Sciences of the United States of America* 90.11, pp. 5034–5038. ISSN: 00278424. DOI: 10.1073/pnas.90.11.5034.

Carvalho, Ana, Arshad Desai, and Karen Oegema (2009). "Structural Memory in the Contractile Ring Makes the Duration of Cytokinesis Independent of Cell Size". In: *Cell* 137.5, pp. 926–937. ISSN: 00928674. DOI: 10.1016/j.cell.2009.03.021. URL: http://dx.doi.org/10.1016/j.cell.2009.03.021.

Castrillon, Diego H. and Steven A. Wasserman (1994). "diaphanous is required for cytokinesis in Drosophila and shares domains of similarity with the products of the limb deformity gene". In: *Development* 120.12, pp. 3367–3377. ISSN: 09501991.

Chan, Fung Yi et al. (2019). "The ARP2/3 complex prevents excessive formin activity during cytokinesis". In: *Molecular Biology of the Cell* 30.1, pp. 96–107. ISSN: 19394586. DOI: 10.1091/mbc.E18-07-0471.

Chang, Fred, Alison Woollard, and Paul Nurse (1996). "Isolation and characterization of fission yeast mutants defective in the assembly and placement of the contractile actin ring". In: *Journal of Cell Science* 109.1, pp. 131–142. ISSN: 00219533.

Chant, John and John R. Pringle (1995). "Patterns of bud-site selection in the yeast Saccharomyces cerevisiae". In: *Journal of Cell Biology* 129.3, pp. 751–765. ISSN: 00219525. DOI: 10.1083/jcb.129.3.751.

Chen, Qian, Shalini Nag, and Thomas D. Pollard (2012). "Formins filter modified actin subunits during processive elongation". In: *Journal of Structural Biology* 177.1, pp. 32–39. ISSN: 10478477. DOI: 10.1016/j.jsb.2011.10.005. URL: http://dx.doi.org/10.1016/j.jsb.2011.10.005.

Chen, Qian and Thomas D. Pollard (2011). "Actin filament severing by cofilin is more important for assembly than constriction of the cytokinetic contractile ring". In: *Journal of Cell Biology* 195.3, pp. 485–498. ISSN: 00219525. DOI: 10.1083/jcb.201103067.

Chernoff, Jonathan (1999). "Close encounters of the LIM-kinase". In: *Nature Cell Biology* 1.5, E115–E117. ISSN: 14764679. DOI: 10.1038/12942.

Chesarone, Melissa A., Amy Grace Dupage, and Bruce L. Goode (2010). "Unleashing formins to remodel the actin and microtubule cytoskeletons". In: *Nature Reviews Molecular Cell Biology* 11.1, pp. 62–74. ISSN: 14710072. DOI: 10.1038/nrm2816.

Chew, Ting Gang et al. (2017). "Actin turnover maintains actin filament homeostasis during cytokinetic ring contraction". In: *Journal of Cell Biology* 216.9, pp. 2657–2667. ISSN: 15408140. DOI: 10.1083/jcb.201701104.

Christensen, Jenna R., Glen M. Hocky, et al. (2017). "Competition between tropomyosin, fimbrin, and ADF/cofilin drives their sorting to distinct actin filament networks". In: *eLife* 6, pp. 1–31. ISSN: 2050084X. DOI: 10.7554/eLife.23152.

Christensen, Jenna R., Kaitlin E. Homa, et al. (2019). "Cooperation between tropomyosin and α-actinin inhibits fimbrin association with actin filament networks in fission yeast". In: *eLife* 8, pp. 1–18. ISSN: 2050084X. DOI: 10.7554/eLife.47279.

Chrzanowska-Wodnicka, Magdalena and Keith Burridge (1996). "Rho-stimulated contractility drives the formation of stress fibers and focal adhesions". In: *Journal of Cell Biology* 133.6, pp. 1403–1415. ISSN: 00219525. DOI: 10.1083/jcb.133.6.1403.

Chugh, Priyamvada and Ewa K. Paluch (2018). "The actin cortex at a glance". In: *Journal of Cell Science* 131.14, pp. 1–9. ISSN: 14779137. DOI: 10.1242/jcs.186254.

Clancy, James W et al. (2019). "Coordinated Regulation of Intracellular Fascin Distribution". In: *Molecular and Cellular Biology* 39.3, pp. 1–16.

Cooper, John A. et al. (1983). "Kinetic Evidence for a Monomer Activation Step in Actin Polymerization". In: *Biochemistry* 22.9, pp. 2193–2202. ISSN: 15204995. DOI: 10.1021/bi00278a021.

Costa, Carlotta et al. (2007). "Negative feedback regulation of Rac in leukocytes from mice expressing a constitutively active phosphatidylinositol 3-kinase γ". In: *Proceedings of the National Academy of Sciences of the United States of America* 104.36, pp. 14354–14359. ISSN: 00278424. DOI: 10.1073/pnas.0703175104.

Cotteret, Sophie and Jonathan Chernoff (2002). "The evolutionary history of effectors downstream of Cdc42 and Rac". In: *Genome Biology* 3.2, pp. 1–8. ISSN: 14656906. DOI: 10.1186/gb-2002-3-2-reviews0002.

Courson, David S. and Ronald S. Rock (2010). "Actin cross-link assembly and disassembly mechanics for α-actinin and fascin". In: *Journal of Biological Chemistry* 285.34, pp. 26350–26357. ISSN: 00219258. DOI: 10.1074/jbc.M110.123117.

Crocker, John C. and David G. Grier (1996). "Methods of digital video microscopy for colloidal studies". In: *Journal of Colloid and Interface Science* 179.1, pp. 298–310. ISSN: 00219797. DOI: 10.1006/jcis.1996.0217.

Dabiri, G. A. et al. (1990). "Listeria monocytogenes moves rapidly through the host-cell cytoplasm by inducing directional actin assembly". In: *Proceedings of the National Academy of Sciences of the United States of America* 87.16, pp. 6068–6072. ISSN: 00278424. DOI: 10.1073/pnas.87.16.6068.

Davies, Tim, Shawn N. Jordan, et al. (2014). "High-Resolution Temporal Analysis Reveals a Functional Timeline for the Molecular Regulation of Cytokinesis". In: *Developmental Cell* 30.2, pp. 209–223. ISSN: 18781551. DOI: 10.1016/j.devcel.2014.05.009. URL: http://dx.doi.org/10.1016/j.devcel.2014.05.009.

Davies, Tim, Han X. Kim, et al. (2018). "Cell-intrinsic and -extrinsic mechanisms promote cell-type-specific cytokinetic diversity". In: *eLife* 7, pp. 1–30. ISSN: 2050084X. DOI: 10.7554/eLife.36204.

Dayel, Mark J. et al. (2009). "In silico reconstitution of actin-based symmetry breaking and motility". In: *PLoS Biology* 7.9. ISSN: 15449173. DOI: 10.1371/journal.pbio.1000201.

De La Cruz, Enrique M. (2005). "Cofilin binding to muscle and non-muscle actin filaments: Isoform-dependent cooperative interactions". In: *Journal of Molecular Biology* 346.2, pp. 557–564. ISSN: 00222836. DOI: 10.1016/j.jmb.2004.11.065.

De La Cruz, Enrique M. and Margaret L. Gardel (2015). "Actin mechanics and fragmentation". In: *Journal of Biological Chemistry* 290.28, pp. 17137–17144. ISSN: 1083351X. DOI: 10.1074/jbc.R115.636472.

De La Cruz, Enrique M. and E. Michael Ostap (2004). "Relating biochemistry and function in the myosin superfamily". In: *Current Opinion in Cell Biology* 16.1, pp. 61–67. ISSN: 09550674. DOI: 10.1016/j.ceb.2003.11.011.

Descovich, Carlos Patino et al. (2018). "Cross-linkers both drive and brake cytoskeletal remodeling and furrowing in cytokinesis". In: *Molecular Biology of the Cell* 29.5, pp. 622–631. ISSN: 19394586. DOI: 10.1091/mbc.E17-06-0392.

Dickinson, Daniel J., Francoise Schwager, et al. (2017). "A Single-Cell Biochemistry Approach Reveals PAR Complex Dynamics during Cell Polarization". In: *Developmental Cell* 42.4, 416–434.e11. ISSN: 18781551. DOI: 10.1016/j.devcel.2017.07.024. URL: http://dx.doi.org/10.1016/j.devcel.2017.07.024.

Dickinson, Richard B., Luzelena Caro, and Daniel L. Purich (2004). "Force generation by cytoskeletal filament end-tracking proteins." In: *Biophysical journal* 87.4, pp. 2838–2854. ISSN: 00063495. DOI: 10.1529/biophysj.104.045211.

Ding, Wei Yung et al. (2017). "Plastin increases cortical connectivity to facilitate robust polarization and timely cytokinesis". In: *Journal of Cell Biology* 216.5, pp. 1371–1386. ISSN: 15408140. DOI: 10.1083/jcb.201603070.

Diogon, Marie et al. (2007). "The RhoGAP RGA-2 and LET-502/ROCK achieve a balance of actomyosin-dependent forces in C. elegans epidermis to control morphogenesis". In: *Development* 134.13, pp. 2469–2479. ISSN: 09501991. DOI: 10.1242/dev.005074.

Dix, Christina L. et al. (2018). "The Role of Mitotic Cell-Substrate Adhesion Re-modeling in Animal Cell Division". In: *Developmental Cell* 45.1, 132–145.e3. ISSN: 18781551. DOI: 10.1016/j.devcel.2018.03.009. URL: https://doi.org/10.1016/j.devcel.2018.03.009.

Dominguez, Roberto and Kenneth C. Holmes (2011). "Actin structure and function". In: *Annual Review of Biophysics* 40.1, pp. 169–186. ISSN: 1936122X. DOI: 10.1146/annurev-biophys-042910-155359.

Dorn, Jonas F. et al. (2016). "A theoretical model of cytokinesis implicates feedback between membrane curvature and cytoskeletal organization in asymmetric cytokinetic furrowing". In: *Molecular Biology of the Cell* 27.8, pp. 1286–1299. ISSN: 19394586. DOI: 10.1091/mbc.E15-06-0374.

Dos Remedios, C. G. et al. (2003). "Actin binding proteins: Regulation of cytoskeletal microfilaments". In: *Physiological Reviews* 83.2, pp. 433–473. ISSN: 00319333. DOI: 10.1152/physrev.00026.2002.

Edwards, Marc et al. (2014). "Capping protein regulators fine-tune actin assembly dynamics". In: *Nature Reviews Molecular Cell Biology* 15.10, pp. 677–689. ISSN: 14710080. DOI: 10.1038/nrm3869.

Egile, Coumaran et al. (1999). "Activation of the Cdc42 Effector N-Wasp by the Shigella flexneri Icsa Protein Promotes Actin Nucleation by Arp2/3 Complex and Bacterial Actin-Based Motility". In: *Journal of Cell Biology* 146.6, pp. 1319–1332. ISSN: 0021-9525. DOI: 10.1083/jcb.146.6.1319. URL: https://rupress.org/jcb/article/146/6/1319/31991/Activation-of-the-Cdc42-Effector-NWasp-by-the.

Ellis, Sara and Harry Mellor (2000). "The novel Rho-family GTPase Rif regulates coordinated actin-based membrane rearrangements". In: *Current Biology* 10.21, pp. 1387–1390. ISSN: 09609822. DOI: 10.1016/S0960-9822(00)00777-6.

Ennomani, Hajer et al. (2016). "Architecture and Connectivity Govern Actin Network Contractility". In: *Current Biology* 26.5, pp. 616–626. ISSN: 09609822. DOI: 10.1016/j.cub.2015.12.069.

Esue, Osigwe et al. (2008). "The Filamentous Actin Cross-Linking/Bundling Activity of Mammalian Formins". In: *Journal of Molecular Biology* 384.2, pp. 324–334. ISSN: 00222836. DOI: 10.1016/j.jmb.2008.09.043. URL: http://dx.doi.org/10.1016/j.jmb.2008.09.043.

Fededa, Juan Pablo and Daniel W. Gerlich (2012). "Molecular control of animal cell cytokinesis". In: *Nature Cell Biology* 14.5, pp. 440–447. ISSN: 14764679. DOI: 10.1038/ncb2482. URL: http://dx.doi.org/10.1038/ncb2482.

Fenix, Aidan M. et al. (2016). "Expansion and concatenation of nonmuscle myosin IIA filaments drive cellular contractile system formation during interphase and mitosis". In: *Molecular Biology of the Cell* 27.9, pp. 1465–1478. ISSN: 19394586. DOI: 10.1091/mbc.E15-10-0725.

Field, Christine M. and Bruce M. Alberts (1995). "Anillin, a contractile ring protein that cycles from the nucleus to the cell cortex". In: *Journal of Cell Biology* 131.1, pp. 165–178. ISSN: 00219525. DOI: 10.1083/jcb.131.1.165.

Fischer, Doris, Richard P. Tucker, et al. (1997). "Cell-adhesive responses to Tenascin-C splice variants involve formation of fascin microspikes". In: *Molecular Biology of the Cell* 8.10, pp. 2055–2075. ISSN: 10591524. DOI: 10.1091/mbc.8.10.2055.

Fischer, Robert S., Pui Ying Lam, et al. (2019). "Filopodia and focal adhesions: An integrated system driving branching morphogenesis in neuronal pathfinding and angiogenesis". In: *Developmental Biology* 451.1, pp. 86–95. ISSN: 1095564X. DOI: 10.1016/j.ydbio.2018.08.015. URL: http://dx.doi.org/10.1016/j.ydbio.2018.08.015.

Fishkind, Douglas J., John D. Silverman, and Yu Li Wang (1996). "Function of spindle microtubules in directing cortical movement and actin filament organization in dividing cultured cells". In: *Journal of Cell Science* 109.8, pp. 2041–2051. ISSN: 00219533.

Fletcher, Daniel A. and R. Dyche Mullins (2010). "Cell mechanics and the cytoskeleton". In: *Nature* 463.7280, pp. 485–492. ISSN: 00280836. DOI: 10.1038/nature08908.

Funk, Johanna et al. (2019). "Profilin and formin constitute a pacemaker system for robust actin filament growth". In: *eLife* 8, pp. 1–34. ISSN: 2050084X. DOI: 10.7554/eLife.50963.

Gallop, Jennifer L. et al. (2013). "Phosphoinositides and membrane curvature switch the mode of actin polymerization via selective recruitment of toca-1 and Snx9". In: *Proceedings of the National Academy of Sciences of the United States of America* 110.18, pp. 7193–7198. ISSN: 00278424. DOI: 10.1073/pnas.1305286110.

Glotzer, Michael (2017). "Cytokinesis in metazoa and fungi". In: *Cold Spring Harbor Perspectives in Biology* 9.10, pp. 1–18. ISSN: 19430264. DOI: 10.1101/cshperspect.a022343.

Goley, Erin D. and Matthew D. Welch (2006). "The ARP2/3 complex: An actin nucleator comes of age". In: *Nature Reviews Molecular Cell Biology* 7.10, pp. 713–726. ISSN: 14710072. DOI: 10.1038/nrm2026.

Goode, Bruce L. and Michael J. Eck (2007). "Mechanism and Function of Formins in the Control of Actin Assembly". In: *Annual Review of Biochemistry* 76.1, pp. 593–627. ISSN: 0066-4154. DOI: 10.1146/annurev.biochem.75.103004.142647.

Goodson, Holly V and Erin M Jonasson (2018). "Microtubules and Microtubule-Associated Proteins". In: *Cold Spring Harbor Perspectives in Biology* 10.6, a022608. ISSN: 1943-0264. DOI: 10.1101/cshperspect.a022608. URL: http://cshperspectives.cshlp.org/lookup/doi/10.1101/cshperspect.a022608.

Green, Rebecca A., Ewa Paluch, and Karen Oegema (2012). "Cytokinesis in Animal Cells". In: *Annual Review of Cell and Developmental Biology* 28.1, pp. 29–58. ISSN: 1081-0706. DOI: 10.1146/annurev-cellbio-101011-155718.

Grego, Sonia, Viviana Cantillana, and E. D. Salmon (2001). "Microtubule treadmilling in vitro investigated by fluorescence speckle and confocal microscopy". In: *Biophysical Journal* 81.1, pp. 66–78. ISSN: 00063495. DOI: 10.1016/S0006-3495(01)75680-9. URL: http://dx.doi.org/10.1016/S0006-3495(01)75680-9.

Großhans, Jörg et al. (2005). "RhoGEF2 and the formin Dia control the formation of the furrow canal by directed actin assembly during Drosophila cellularisation". In: *Development* 132.5, pp. 1009–1020. ISSN: 09501991. DOI: 10.1242/dev.01669.

Guilluy, Christophe, Rafael Garcia-Mata, and Keith Burridge (2011). "Rho protein crosstalk: Another social network?" In: *Trends in Cell Biology* 21.12, pp. 718–726. ISSN: 09628924. DOI: 10.1016/j.tcb.2011.08.002. URL: http://dx.doi.org/10.1016/j.tcb.2011.08.002.

Gulli, Marie Pierre et al. (2000). "Phosphorylation of the Cdc42 exchange factor Cdc24 by the PAK-like kinase Cla4 may regulate polarized growth in yeast". In: *Molecular Cell* 6.5, pp. 1155–1167. ISSN: 10972765. DOI: 10.1016/S1097-2765(00)00113-1.

Gustafsson, Nils et al. (2016). "Fast live-cell conventional fluorophore nanoscopy with ImageJ through super-resolution radial fluctuations". In: *Nature Communications* 7, pp. 1–9. ISSN: 20411723. DOI: 10.1038/ncomms12471.

Haglund, Kaisa, Ioannis P. Nezis, and Harald Stenmark (2011). "Structure and functions of stable intercellular bridges formed by incomplete cytokinesis during development". In: *Communicative and Integrative Biology* 4.1, pp. 1–9. ISSN: 19420889. DOI: 10.4161/cib.13550.

Hansen, Scott D. and R. Dyche Mullins (2010). "VASP is a processive actin polymerase that requires monomeric actin for barbed end association". In: *Journal of Cell Biology* 191.3, pp. 571–584. ISSN: 00219525. DOI: 10.1083/jcb.201003014.

Harker, Alyssa J. et al. (2019). "Ena/VASP processive elongation is modulated by avidity on actin filaments bundled by the filopodia cross-linker fascin". In: *Molecular Biology of the Cell* 30.7, pp. 851–862. ISSN: 19394586. DOI: 10.1091/mbc.E18-08-0500.

Harris, Elizabeth S. et al. (2006). "Mechanistic differences in actin bundling activity of two mammalian formins, FRL1 and mDia2". In: *Journal of Biological Chemistry* 281.20, pp. 14383–14392. ISSN: 00219258. DOI: 10.1074/jbc.M510923200.

Haviv, Lior et al. (2006). "Reconstitution of the transition from lamellipodium to filopodium in a membrane-free system". In: *Proceedings of the National Academy of Sciences of the United States of America* 103.13, pp. 4906–4911. ISSN: 00278424. DOI: 10.1073/pnas.0508269103.

Havrylenko, Svitlana et al. (2015). "WAVE binds Ena/VASP for enhanced Arp2/3 complex-based actin assembly". In: *Molecular Biology of the Cell* 26.1, pp. 55–65. ISSN: 19394586. DOI: 10.1091/mbc.E14-07-1200.

Hayakawa, Kimihide, Hitoshi Tatsumi, and Masahiro Sokabe (2011). "Actin filaments function as a tension sensor by tension-dependent binding of cofilin to the filament". In: *Journal of Cell Biology* 195.5, pp. 721–727. ISSN: 00219525. DOI: 10.1083/jcb.201102039.

Heald, Rebecca et al. (1996). "Self-organization of microtubules into bipolar spindles around artificial chromosomes in Xenopus egg extracts". In: *Nature* 382.6590, pp. 420–425. ISSN: 00280836. DOI: 10.1038/382420a0.

Henson, John H. et al. (2017). "The ultrastructural organization of actin and myosin II filaments in the contractile ring: New support for an old model of cytokinesis". In: *Molecular Biology of the Cell* 28.5, pp. 613–623. ISSN: 19394586. DOI: 10.1091/mbc.E16-06-0466.

Higashida, Chiharu (2004). "Actin Polymerization-Driven Molecular Movement of mDia1 in Living Cells". In: *Science* 303.5666, pp. 2007–2010. ISSN: 0036-8075. DOI: 10.1126/science.1093923. URL: https://www.sciencemag.org/lookup/doi/10.1126/science.1093923.

Higashida, Chiharu et al. (2008). "G-actin regulates rapid induction of actin nucleation by mDia1 to restore cellular actin polymers". In: *Journal of Cell Science* 121.20, pp. 3403–3412. ISSN: 00219533. DOI: 10.1242/jcs.030940.

Higgs, Henry N. (2005). "Formin proteins: A domain-based approach". In: *Trends in Biochemical Sciences* 30.6, pp. 342–353. ISSN: 09680004. DOI: 10.1016/j.tibs.2005.04.014.

Hodge, Richard G. and Anne J. Ridley (2016). "Regulating Rho GTPases and their regulators". In: *Nature Reviews Molecular Cell Biology* 17.8, pp. 496–510. ISSN: 14710080. DOI: 10.1038/nrm.2016.67.

Honer, B. et al. (1988). "Modulation of cellular morphology and locomotory activity by antibodies against myosin". In: *Journal of Cell Biology* 107.6 I, pp. 2181–2189. ISSN: 00219525. DOI: 10.1083/jcb.107.6.2181.

Hotulainen, Pirta and Pekka Lappalainen (2006). "Stress fibers are generated by two distinct actin assembly mechanisms in motile cells". In: *Journal of Cell Biology* 173.3, pp. 383–394. ISSN: 00219525. DOI: 10.1083/jcb.200511093.

Hueschen, Christina L. et al. (2017). "NuMA recruits dynein activity to microtubule minus-ends at mitosis". In: *eLife* 6, pp. 1–26. ISSN: 2050084X. DOI: 10.7554/eLife.29328.

Huxley, A. F. (1957). "Muscle structure and theories of contraction." In: *Progress in biophysics and biophysical chemistry* 7, pp. 255–318. ISSN: 00964174. DOI: 10.1016/s0096-4174(18)30128-8.

Huxley, Hugh E. (2004). "Fifty years of muscle and the sliding filament hypothesis". In: *European Journal of Biochemistry* 271.8, pp. 1403–1415. ISSN: 00142956. DOI: 10.1111/j.1432-1033.2004.04044.x.

Ichetovkin, Ilia, Wayne Grant, and John Condeelis (2002). "Cofilin produces newly polymerized actin filaments that are preferred for dendritic nucleation by the Arp2/3 complex". In: *Current Biology* 12.1, pp. 79–84. ISSN: 09609822. DOI: 10.1016/S0960-9822(01)00629-7.

Jacinto, Antonio and Lewis Wolpert (2001). "Quick guide Filopodia". In: *Current Biology* 11.16, R634.

Jacquemet, Guillaume, Hellyeh Hamidi, and Johanna Ivaska (2015). "Filopodia in cell adhesion, 3D migration and cancer cell invasion". In: *Current Opinion in Cell Biology* 36, pp. 23–31. ISSN: 18790410. DOI: 10.1016/j.ceb.2015.06.007. URL: http://dx.doi.org/10.1016/j.ceb.2015.06.007.

Jaiswal, Richa et al. (2013). "The formin daam1 and fascin directly collaborate to promote filopodia formation". In: *Current Biology* 23.14, pp. 1373–1379. ISSN: 09609822. DOI: 10.1016/j.cub.2013.06.013.

Jansen, Silvia et al. (2011). "Mechanism of actin filament bundling by fascin". In: *Journal of Biological Chemistry* 286.34, pp. 30087–30096. ISSN: 00219258. DOI: 10.1074/jbc.M111.251439.

Jaqaman, Khuloud et al. (2008). "Robust single-particle tracking in live-cell time-lapse sequences". In: *Nature Methods* 5.8, pp. 695–702. ISSN: 15487091. DOI: 10.1038/nmeth.1237.

Johnson, Douglas I. (1999). "Cdc42: An Essential Rho-Type GTPase Controlling Eukaryotic Cell Polarity". In: *Microbiology and Molecular Biology Reviews* 63.1, pp. 54–105. ISSN: 1092-2172. DOI: 10.1128/mmbr.63.1.54-105.1999.

Kamath, Ravi S. et al. (2003). "Systematic functional analysis of the Caenorhabditis elegans genome using RNAi". In: *Nature* 421.6920, pp. 231–237. ISSN: 00280836. DOI: 10.1038/nature01278.

Khaliullin, Renat N. et al. (2018). "A positive-feedback-based mechanism for constriction rate acceleration during cytokinesis in Caenorhabditis elegans". In: *eLife* 7, pp. 1–32. ISSN: 2050084X. DOI: 10.7554/eLife.36073.

Kinosian, H. J., L. A. Selden, et al. (2000). "Interdependence of profilin, cation, and nucleotide binding to vertebrate non-muscle actin". In: *Biochemistry* 39.43, pp. 13176–13188. ISSN: 00062960. DOI: 10.1021/bi001520+.

Kinosian, Henry J., Jay Newman, et al. (1998). "Ca2+ regulation of gelsolin activity: Binding and severing of F-actin". In: *Biophysical Journal* 75.6, pp. 3101–3109. ISSN: 00063495. DOI: 10.1016/S0006-3495(98)77751-3. URL: http://dx.doi.org/10.1016/S0006-3495(98)77751-3.

Kitayama, Chikako and Taro Q.P. Uyeda (2003). "ForC, a novel type of formin family protein lacking an FH1 domain, is involved in multicellular development in Dictyostelium discoideum". In: *Journal of Cell Science* 116.4, pp. 711–723. ISSN: 00219533. DOI: 10.1242/jcs.00265.

Kovar, David R., Elizabeth S. Harris, et al. (2006). "Control of the assembly of ATP- and ADP-actin by formins and profilin". In: *Cell* 124.2, pp. 423–435. ISSN: 00928674. DOI: 10.1016/j.cell.2005.11.038.

Kovar, David R. and Thomas D. Pollard (2004). "Insertional assembly of actin filament barbed ends in association with formins produces piconewton forces". In: *Proceedings of the National*

Academy of Sciences of the United States of America 101.41, pp. 14725–14730. ISSN: 00278424. DOI: 10.1073/pnas.0405902101.

Kovar, David R., Vladimir Sirotkin, and Matthew Lord (2011). "Three's company: The fission yeast actin cytoskeleton". In: *Trends in Cell Biology* 21.3, pp. 177–187. ISSN: 09628924. DOI: 10.1016/j.tcb.2010.11.001. URL: http://dx.doi.org/10.1016/j.tcb.2010.11.001.

Krause, Matthias and Alexis Gautreau (2014). "Steering cell migration: Lamellipodium dynamics and the regulation of directional persistence". In: *Nature Reviews Molecular Cell Biology* 15.9, pp. 577–590. ISSN: 14710080. DOI: 10.1038/nrm3861.

Krugmann, Sonja et al. (2001). "Cdc42 induces filopodia by promoting the formation of an IRSp53:Mena complex". In: *Current Biology* 11.21, pp. 1645–1655. ISSN: 09609822. DOI: 10.1016/S0960-9822(01)00506-1.

Kruse, K. and F. Jülicher (2000). "Actively contracting bundles of polar filaments". In: *Physical Review Letters* 85.8, pp. 1778–1781. ISSN: 00319007. DOI: 10.1103/PhysRevLett.85.1778. arXiv: 0007409 [cond-mat].

Kuhn, Thomas B. et al. (2000). "Regulating actin dynamics in neuronal growth cones by ADF/cofilin and Rho family GTPases". In: *Journal of Neurobiology* 44.2, pp. 126–144. ISSN: 00223034. DOI: 10.1002/1097-4695(200008)44:2<126::AID-NEU4>3.0.CO;2-Z.

Lardennois, Alicia et al. (2019). "An actin-based viscoplastic lock ensures progressive body-axis elongation". In: *Nature* 573.7773, pp. 266–270. ISSN: 14764687. DOI: 10.1038/s41586-019-1509-4.

Lawson, Campbell D. and Keith Burridge (2014). "The on-off relationship of Rho and Rac during integrin-mediated adhesion and cell migration". In: *Small GTPases* 5.MAR. ISSN: 21541256. DOI: 10.4161/sgtp.27958.

Lee, Kwonmoo et al. (2010). "Self-assembly of filopodia-like structures on supported lipid bilayers". In: *Science* 329.5997, pp. 1341–1345. ISSN: 00368075. DOI: 10.1126/science.1191710.

Leite, Joana et al. (2019). "Network contractility during cytokinesis—from molecular to global views". In: *Biomolecules* 9.5, pp. 1–28. ISSN: 2218273X. DOI: 10.3390/biom9050194.

Lenz, Martin (2020). "Reversal of contractility as a signature of self-organization in cytoskeletal bundles". In: *eLife* 9, pp. 1–17. ISSN: 2050084X. DOI: 10.7554/eLife.51751.

Lenz, Martin et al. (2012). "Contractile units in disordered actomyosin bundles arise from f-actin buckling". In: *Physical Review Letters* 108.23, pp. 1–5. ISSN: 00319007. DOI: 10.1103/PhysRevLett.108.238107.

Levayer, Romain and Thomas Lecuit (2012). "Biomechanical regulation of contractility: Spatial control and dynamics". In: *Trends in Cell Biology* 22.2, pp. 61–81. ISSN: 09628924. DOI: 10.1016/j.tcb.2011.10.001. URL: http://dx.doi.org/10.1016/j.tcb.2011.10.001.

Li, Jing et al. (2017). "Buckling-induced F-actin fragmentation modulates the contraction of active cytoskeletal networks". In: *Soft Matter* 13.17, pp. 3213–3220. ISSN: 17446848. DOI: 10.1039/c6sm02703b.

Lieleg, Oliver, Mireille M.A.E. Claessens, and Andreas R. Bausch (2010). "Structure and dynamics of cross-linked actin networks". In: *Soft Matter* 6.2, pp. 218–225. ISSN: 1744683X. DOI: 10.1039/b912163n.

Lisa, Timmons, L. Court Donald, and Fire Andrew (2001). "Ingestion of bacterially expressed dsRNAs can produce specific and potent genetic interference in Caenorhabditis elegans". In: *Gene* 263, pp. 103–112. URL: www.elsevier.com/locate/gene.

Lo, Chiu An et al. (2015). "Quantification of Protein Levels in Single Living Cells". In: *Cell Reports* 13.11, pp. 2634–2644. ISSN: 22111247. DOI: 10.1016/j.celrep.2015.11.048. URL: http://dx.doi.org/10.1016/j.celrep.2015.11.048.

Loisel, Thomas P. et al. (1999). "Reconstitution of actin-based motility of Listeria and Shigella using pure proteins". In: *Nature* 401.6753, pp. 613–616. ISSN: 00280836. DOI: 10.1038/44183.

Lord, Matthew, Ellen Laves, and Thomas D Pollard (2005). "Cytokinesis depends on the motor domains of myosin-II in fission yeast but not in budding yeast." In: *Molecular biology of the cell* 16.11, pp. 5346–55. ISSN: 1059-1524. DOI: 10.1091/mbc.e05-07-0601. URL: http://www.ncbi.nlm.nih.gov/pubmed/16148042%20http://www.pubmedcentral.nih.gov/articlerender.fcgi?artid=PMC1266431.

Ma, Xuefei et al. (2012). "Nonmuscle myosin II exerts tension but does not translocate actin in vertebrate cytokinesis". In: *Proceedings of the National Academy of Sciences of the United States of America* 109.12, pp. 4509–4514. ISSN: 00278424. DOI: 10.1073/pnas.1116268109.

Machaidze, Gia et al. (2010). "Actin Filament Bundling and Different Nucleating Effects of Mouse Diaphanous-Related Formin FH2 Domains on Actin/ADF and Actin/Cofilin Complexes". In: *Journal of Molecular Biology* 403.4, pp. 529–545. ISSN: 00222836. DOI: 10.1016/j.jmb.2010.09.017. URL: http://dx.doi.org/10.1016/j.jmb.2010.09.017.

Machesky, Laura M. et al. (1994). "Purification of a cortical complex containing two unconventional actins from Acanthamoeba by affinity chromatography on profilin-agarose". In: *Journal of Cell Biology* 127.1, pp. 107–115. ISSN: 00219525. DOI: 10.1083/jcb.127.1.107.

Maddox, Amy Shaub et al. (2007). "Anillin and the Septins Promote Asymmetric Ingression of the Cytokinetic Furrow". In: *Developmental Cell* 12.5, pp. 827–835. ISSN: 15345807. DOI: 10.1016/j.devcel.2007.02.018.

Maekawa, Midori et al. (1999). "Signaling from Rho to the actin cytoskeleton through protein kinases ROCK and LIM-kinase". In: *Science* 285.5429, pp. 895–898. ISSN: 00368075. DOI: 10.1126/science.285.5429.895.

Mallavarapu, Aneil and Tim Mitchison (1999). "Regulated actin cytoskeleton assembly at filopodium tips controls their extension and retraction". In: *Journal of Cell Biology* 146.5, pp. 1097–1106. ISSN: 00219525. DOI: 10.1083/jcb.146.5.1097.

Mandato, Craig A. and William M. Bement (2001). "Contraction and polymerization cooperate to assemble and close actomyosin rings around Xenopus oocyte wounds". In: *Journal of Cell Biology* 154.4, pp. 785–797. ISSN: 00219525. DOI: 10.1083/jcb.200103105.

Manhart, Angelika et al. (2019). "Quantitative regulation of the dynamic steady state of actin networks". In: *eLife* 8, pp. 1–37. ISSN: 2050084X. DOI: 10.7554/eLife.42413.

Matsumura, Fumio (2005). "Regulation of myosin II during cytokinesis in higher eukaryotes". In: *Trends in Cell Biology* 15.7, pp. 371–377. ISSN: 09628924. DOI: 10.1016/j.tcb.2005.05.004.

Mattila, Pieta K. and Pekka Lappalainen (2008). "Filopodia: Molecular architecture and cellular functions". In: *Nature Reviews Molecular Cell Biology* 9.6, pp. 446–454. ISSN: 14710072. DOI: 10.1038/nrm2406.

McCullough, Brannon R. et al. (2008). "Cofilin Increases the Bending Flexibility of Actin Filaments: Implications for Severing and Cell Mechanics". In: *Journal of Molecular Biology* 381.3, pp. 550–558. ISSN: 00222836. DOI: 10.1016/j.jmb.2008.05.055.

McFadden, William M. et al. (2017). "Filament turnover tunes both force generation and dissipation to control long-range flows in a model actomyosin cortex". In: *PLoS Computational Biology* 13.12, pp. 1–27. ISSN: 15537358. DOI: 10.1371/journal.pcbi.1005811.

Melli, Luca et al. (2018). "Bipolar filaments of human nonmuscle myosin 2-A and 2-B have distinct motile and mechanical properties". In: *eLife* 7, pp. 1–25. ISSN: 2050084X. DOI: 10.7554/eLife.32871.

Mendes Pinto, Inês et al. (2012). "Actin Depolymerization Drives Actomyosin Ring Contraction during Budding Yeast Cytokinesis". In: *Developmental Cell* 22.6, pp. 1247–1260. ISSN: 15345807. DOI: 10.1016/j.devcel.2012.04.015.

Meraldi, Patrick (2016). "Centrosomes in spindle organization and chromosome segregation: a mechanistic view". In: *Chromosome Research* 24.1, pp. 19–34. ISSN: 15736849. DOI: 10.1007/s10577-015-9508-2.

Merdes, Andreas et al. (2000). "Formation of spindle poles by dynein/dynactin-dependent transport of NuMA". In: *Journal of Cell Biology* 149.4, pp. 851–861. ISSN: 00219525. DOI: 10.1083/jcb.149.4.851.

Mi-Mi, Lei et al. (2012). "Z-line formins promote contractile lattice growth and maintenance in striated muscles of C. elegans". In: *Journal of Cell Biology* 198.1, pp. 87–102. ISSN: 00219525. DOI: 10.1083/jcb.201202053.

Michaux, Jonathan B. et al. (2018). "Excitable RhoA dynamics drive pulsed contractions in the early C. Elegans embryo". In: *Journal of Cell Biology* 217.12, pp. 4230–4252. ISSN: 15408140. DOI: 10.1083/JCB.201806161.

Michelot, Alphée et al. (2005). "The formin homology 1 domain modulates the actin nucleation and bundling activity of arabidopsis FORMIN1". In: *Plant Cell* 17.8, pp. 2296–2313. ISSN: 10404651. DOI: 10.1105/tpc.105.030908.

Michison, Tim (2011). "Self-organization of microtubule assemblies". In: *YouTube*. URL: https://www.youtube.com/watch?v=AsPYlJEWMdo.

Miller, Ann L. (2011). "The contractile ring". In: *Current Biology* 21.24, R976–R978. ISSN: 09609822. DOI: 10.1016/j.cub.2011.10.044. URL: http://dx.doi.org/10.1016/j.cub.2011.10.044.

Mishra, Mithilesh et al. (2013). "In vitro contraction of cytokinetic ring depends on myosin II but not on actin dynamics". In: *Nature Cell Biology* 15.7, pp. 853–859. ISSN: 14657392. DOI: 10.1038/ncb2781.

Mogilner, Alexander and George Oster (1996). "Cell motility driven by actin polymerization". In: *Biophysical Journal* 71.6, pp. 3030–3045. ISSN: 00063495. DOI: 10.1016/S0006-3495(96)79496-1. URL: http://dx.doi.org/10.1016/S0006-3495(96)79496-1.

Moseley, James B. and Bruce L. Goode (2005). "Differential activities and regulation of Saccharomyces cerevisiae formin proteins Bni1 and Bnr1 by Bud6". In: *Journal of Biological Chemistry* 280.30, pp. 28023–28033. ISSN: 00219258. DOI: 10.1074/jbc.M503094200.

Moussavi, Robabeh S., Christine A. Kelley, and Robert S. Adelstein (1993). "Phosphorylation of vertebrate nonmuscle and smooth muscle myosin heavy chains and light chains". In: *Molecular and Cellular Biochemistry* 127-128.1, pp. 219–227. ISSN: 03008177. DOI: 10.1007/BF01076773.

Mullins, R. Dyche, John A. Heuser, and Thomas D. Pollard (1998). "The interaction of Arp2/3 complex with actin: Nucleation, high affinity pointed end capping, and formation of branching networks of filaments". In: *Proceedings of the National Academy of Sciences of the United States of America* 95.11, pp. 6181–6186. ISSN: 00278424. DOI: 10.1073/pnas.95.11.6181.

Munjal, Akankshi and Thomas Lecuit (2014). "Actomyosin networks and tissue morphogenesis". In: *Development (Cambridge)* 141.9, pp. 1789–1793. ISSN: 14779129. DOI: 10.1242/dev.091645.

Murrell, Michael and Margaret L. Gardel (2014). "Actomyosin sliding is attenuated in contractile biomimetic cortices". In: *Molecular Biology of the Cell* 25.12, pp. 1845–1853. ISSN: 19394586. DOI: 10.1091/mbc.E13-08-0450.

Murrell, Michael, Patrick W. Oakes, et al. (2015). "Forcing cells into shape: The mechanics of actomyosin contractility". In: *Nature Reviews Molecular Cell Biology* 16.8, pp. 486–498. ISSN: 14710080. DOI: 10.1038/nrm4012.

Murthy, Kausalya and Patricia Wadsworth (2005). "Myosin-II-dependent localization and dynamics of F-actin during cytokinesis". In: *Current Biology* 15.8, pp. 724–731. ISSN: 09609822. DOI: 10.1016/j.cub.2005.02.055.

Murugesan, Sricharan et al. (2016). "Formin-generated actomyosin arcs propel t cell receptor microcluster movement at the immune synapse". In: *Journal of Cell Biology* 215.3, pp. 383–399. ISSN: 15408140. DOI: 10.1083/jcb.201603080.

Narumiya, Shuh and Dean Thumkeo (2018). "Rho signaling research: history, current status and future directions". In: *FEBS Letters* 592.11, pp. 1763–1776. ISSN: 18733468. DOI: 10.1002/1873-3468.13087.

Neidt, Erin M., Colleen T. Skau, and David R. Kovar (2008). "The cytokinesis formins from the nematode worm and fission yeast differentially mediate actin filament assembly". In: *Journal of Biological Chemistry* 283.35, pp. 23872–23883. ISSN: 00219258. DOI: 10.1074/jbc.M803734200.

Niederman, Richard and Thomas D. Pollard (1975). "Human platelet myosin: II. In vitro assembly and structure of myosin filaments". In: *Journal of Cell Biology* 67.1, pp. 72–92. ISSN: 15408140. DOI: 10.1083/jcb.67.1.72.

Nishimura, Yukako and Shigenobu Yonemura (2006). "Centralspindlin regulates ECT2 and RhoA accumulation at the equatorial cortex during cytokinesis". In: *Journal of Cell Science* 119.1, pp. 104–114. ISSN: 00219533. DOI: 10.1242/jcs.02737.

Nobes, C.D. and Alan Hall (1994). "Rho , rac and cdc42 GTPases : regulators of actin structures , cell adhesion and motility Rac stimulates actin polymerization to form lamellipodia Addition of other growth factors to serum-starved Rho induces the assembly of actin stress fibres and focal". In: *Biochemical socienty Transactions* 23.1986, pp. 456–459.

O'Connell, Christopher B., Anne K. Warner, and Yu li Wang (2001). "Distinct roles of the equatorial and polar cortices in the cleavage of adherent cells". In: *Current Biology* 11.9, pp. 702–707. ISSN: 09609822. DOI: 10.1016/S0960-9822(01)00181-6.

Oelz, Dietmar B., Boris Y. Rubinstein, and Alex Mogilner (2015). "A Combination of Actin Treadmilling and Cross-Linking Drives Contraction of Random Actomyosin Arrays". In: *Biophysical Journal* 109.9, pp. 1818–1829. ISSN: 15420086. DOI: 10.1016/j.bpj.2015.09.013. URL: http://dx.doi.org/10.1016/j.bpj.2015.09.013.

Olson, Michael F. (2003). "GTPase signalling: New functions for Diaphanous-related formins". In: *Current Biology* 13.9, pp. 360–362. ISSN: 09609822. DOI: 10.1016/S0960-9822(03)00277-X.

Ong, Katy et al. (2014). "Architecture and dynamic remodelling of the septin cytoskeleton during the cell cycle". In: *Nature Communications* 5.May, pp. 1–10. ISSN: 20411723. DOI: 10.1038/ncomms6698.

Osório, Daniel S. et al. (2019). "Crosslinking activity of non-muscle myosin II is not sufficient for embryonic cytokinesis in C. elegans". In: *Development (Cambridge, England)* 146.21. ISSN: 14779129. DOI: 10.1242/dev.179150.

Padmanabhan, Anup, Hui Ting Ong, and Ronen Zaidel-Bar (2017). "Non-junctional E-Cadherin Clusters Regulate the Actomyosin Cortex in the C. elegans Zygote". In: *Current Biology* 27.1, pp. 103–112. ISSN: 09609822. DOI: 10.1016/j.cub.2016.10.032. URL: http://dx.doi.org/10.1016/j.cub.2016.10.032.

Paoletti, A. and F. Chang (2000). "Analysis of mid1p, a protein required for placement of the cell division site, reveals a link between the nucleus and the cell surface in fission yeast". In: *Molecular Biology of the Cell* 11.8, pp. 2757–2773. ISSN: 10591524. DOI: 10.1091/mbc.11.8.2757.

Parsons, Maddy and Josephine C. Adams (2008). "Rac regulates the interaction of fascin with protein kinase C in cell migration". In: *Journal of Cell Science* 121.17, pp. 2805–2813. ISSN: 00219533. DOI: 10.1242/jcs.022509.

Paul, Aditya S. and Thomas D. Pollard (2009). "Review of the mechanism of processive actin filament elongation by formins". In: *Cell Motility and the Cytoskeleton* 66.8, pp. 606–617. ISSN: 08861544. DOI: 10.1002/cm.20379.

Pawlik, Agnieszka Hanna (2009). "The C.elegans cytokinesis formin CYK-1 is regulated by autoinhibition and GTP-RhoA activation". In: *The University of Chicago Master Thesis* I.

Pelletier, Vincent et al. (2009). "Microrheology of microtubule solutions and actin-microtubule composite networks". In: *Physical Review Letters* 102.18, pp. 100–103. ISSN: 00319007. DOI: 10.1103/PhysRevLett.102.188303.

Peskin, C. S., G. M. Odell, and G. F. Oster (1993). "Cellular motions and thermal fluctuations: the Brownian ratchet". In: *Biophysical Journal* 65.1, pp. 316–324. ISSN: 00063495. DOI:

10.1016/S0006-3495(93)81035-X. URL: http://dx.doi.org/10.1016/S0006-3495(93)81035-X.

Petry, Sabine (2016). "Mechanisms of Mitotic Spindle Assembly". In: *Annual Review of Biochemistry* 85.1, pp. 659–683. ISSN: 0066-4154. DOI: 10.1146/annurev-biochem-060815-014528.

Pollard, Thomas (2016). "Actin and Actin-Binding Proteins". In: *Cold Spring Harbor Perspectives in Biology* 8.8, a018226. ISSN: 1943-0264. DOI: 10.1101/cshperspect.a018226. URL: http://cshperspectives.cshlp.org/lookup/doi/10.1101/cshperspect.a018226.

Pollard, Thomas D. (2010). "Mechanics of cytokinesis in eukaryotes". In: *Current Opinion in Cell Biology* 22.1, pp. 50–56. ISSN: 09550674. DOI: 10.1016/j.ceb.2009.11.010. URL: http://dx.doi.org/10.1016/j.ceb.2009.11.010.

Pollard, Thomas D, Laurent Blanchoin, and R Dyche Mullins (2000). "Molecular Mechanisms Controlling Actin Filament Dynamics in Nonmuscle Cells". In: *Annual Review of Biophysics and Biomolecular Structure* 29.1, pp. 545–576. ISSN: 1056-8700. DOI: 10.1146/annurev.biophys.29.1.545. URL: https://doi.org/10.1146/annurev.biophys.29.1.545%20http://www.annualreviews.org/doi/10.1146/annurev.biophys.29.1.545.

Pollard, Thomas D and Gary G Borisy (2003). "Cellular Motility Driven by Assembly and Disassembly of Actin Filaments". In: *Cell* 112.4, pp. 453–465. ISSN: 00928674. DOI: 10.1016/S0092-8674(03)00120-X. URL: https://linkinghub.elsevier.com/retrieve/pii/S009286740300120X.

Pollard, Thomas D. and John A. Cooper (1984). "Quantitative Analysis of the Effect of Acanthamoeba Profilin on Actin Filament Nucleation and Elongation". In: *Biochemistry* 23.26, pp. 6631–6641. ISSN: 15204995. DOI: 10.1021/bi00321a054.

Pollard, Thomas D. and Ben O'Shaughnessy (2019). "Molecular Mechanism of Cytokinesis". In: *Annual Review of Biochemistry* 88.1, pp. 661–689. ISSN: 0066-4154. DOI: 10.1146/annurev-biochem-062917-012530.

Pollard, Thomas D. and Jian Qiu Wu (2010). "Understanding cytokinesis: Lessons from fission yeast". In: *Nature Reviews Molecular Cell Biology* 11.2, pp. 149–155. ISSN: 14710072. DOI: 10.1038/nrm2834.

Prévost, Coline et al. (2015). "IRSp53 senses negative membrane curvature and phase separates along membrane tubules". In: *Nature Communications* 6. ISSN: 20411723. DOI: 10.1038/ncomms9529.

Priess, James R. and David I. Hirsh (1986). "Caenorhabditis elegans morphogenesis: The role of the cytoskeleton in elongation of the embryo". In: *Developmental Biology* 117.1, pp. 156–173. ISSN: 00121606. DOI: 10.1016/0012-1606(86)90358-1.

Pring, Martin et al. (2003). "Mechanism of formin-induced nucleation of actin filaments". In: *Biochemistry* 42.2, pp. 486–496. ISSN: 00062960. DOI: 10.1021/bi026520j.

Prosser, Suzanna L. and Laurence Pelletier (2017). "Mitotic spindle assembly in animal cells: A fine balancing act". In: *Nature Reviews Molecular Cell Biology* 18.3, pp. 187–201. ISSN: 14710080. DOI: 10.1038/nrm.2016.162.

Reymann, A.-C., R. Boujemaa-Paterski, et al. (2012). "Actin Network Architecture Can Determine Myosin Motor Activity". In: *Science* 336.6086, pp. 1310–1314. ISSN: 0036-8075. DOI: 10.1126/science.1221708. URL: https://www.sciencemag.org/lookup/doi/10.1126/science.1221708.

Reymann, Anne Cecile, Fabio Staniscia, et al. (2016). "Cortical flow aligns actin filaments to form a furrow". In: *eLife* 5.OCTOBER2016, pp. 1–25. ISSN: 2050084X. DOI: 10.7554/eLife.17807.

Rincon, Sergio A. et al. (2014). "Pom1 regulates the assembly of Cdr2-Mid1 cortical nodes for robust spatial control of cytokinesis". In: *Journal of Cell Biology* 206.1, pp. 61–77. ISSN: 15408140. DOI: 10.1083/jcb.201311097.

Robin, François B. et al. (2014). "Single-molecule analysis of cell surface dynamics in Caenorhabditis elegans embryos". In: *Nature Methods* 11.6, pp. 677–682. ISSN: 15487105. DOI: 10.1038/nmeth.2928.

Robinson, Douglas N. (1996). "Stable intercellular bridges in development: The cytoskeleton lining the tunnel". In: *Trends in Cell Biology* 6.12, pp. 474–479. ISSN: 09628924. DOI: 10.1016/0962-8924(96)84945-2.

Rodionov, Vladimir I. and Gary G. Borisy (1997). "Microtubule treadmilling in vivo". In: *Science* 275.5297, pp. 215–220. ISSN: 00368075. DOI: 10.1126/science.275.5297.215.

Rottner, Klemens, Jan Faix, et al. (2017). "Actin assembly mechanisms at a glance". In: *Journal of Cell Science* 130.20, pp. 3427–3435. ISSN: 14779137. DOI: 10.1242/jcs.206433.

Rottner, Klemens and Matthias Schaks (2019). "Assembling actin filaments for protrusion". In: *Current Opinion in Cell Biology* 56, pp. 53–63. ISSN: 18790410. DOI: 10.1016/j.ceb.2018.09.004. URL: https://doi.org/10.1016/j.ceb.2018.09.004.

Sagot, Isabelle et al. (2002). "An actin nucleation mechanism mediated by Bni1 and profilin". In: *Nature Cell Biology* 4.8, pp. 626–631. ISSN: 14657392. DOI: 10.1038/ncb834.

Salbreux, G., J. Prost, and J. F. Joanny (2009). "Hydrodynamics of cellular cortical flows and the formation of contractile rings". In: *Physical Review Letters* 103.5, pp. 1–4. ISSN: 00319007. DOI: 10.1103/PhysRevLett.103.058102.

Salbreux, Guillaume, Guillaume Charras, and Ewa Paluch (2012). "Actin cortex mechanics and cellular morphogenesis". In: *Trends in Cell Biology* 22.10, pp. 536–545. ISSN: 09628924. DOI: 10.1016/j.tcb.2012.07.001. URL: http://dx.doi.org/10.1016/j.tcb.2012.07.001.

Schaks, Matthias, Grégory Giannone, and Klemens Rottner (2019). "Actin dynamics in cell migration". In: *Essays in Biochemistry* 63.5, pp. 483–495. ISSN: 00711365. DOI: 10.1042/EBC20190015.

Schuldt, Alison (2004). "Centrosome migration: Until myosin drags us apart". In: *Nature Cell Biology* 6.7, p. 581. ISSN: 14657392. DOI: 10.1038/ncb0704-581.

Sehring, Ivonne M. et al. (2014). "An Equatorial Contractile Mechanism Drives Cell Elongation but not Cell Division". In: *PLoS Biology* 12.2. ISSN: 15457885. DOI: 10.1371/journal.pbio.1001781.

Sellers, James R. (2000). "Myosins: A diverse superfamily". In: *Biochimica et Biophysica Acta - Molecular Cell Research* 1496.1, pp. 3–22. ISSN: 01674889. DOI: 10.1016/S0167-4889(00)00005-7.

Severson, Aaron F., David L. Baillie, and Bruce Bowerman (2002). "A Formin Homology protein and a profilin are required for cytokinesis and Arp2/3-independent assembly of cortical

microfilaments in C. elegans". In: *Current Biology* 12.24, pp. 2066–2075. ISSN: 09609822. DOI: 10.1016/S0960-9822(02)01355-6.

Shivas, Jessica M. and Ahna R. Skop (2012). "Arp2/3 mediates early endosome dynamics necessary for the maintenance of PAR asymmetry in Caenorhabditis elegans". In: *Molecular Biology of the Cell* 23.10, pp. 1917–1927. ISSN: 10591524. DOI: 10.1091/mbc.E12-01-0006.

Silva, Ana M. et al. (2016). "Robust gap repair in the contractile ring ensures timely completion of cytokinesis". In: *Journal of Cell Biology* 215.6, pp. 789–799. ISSN: 15408140. DOI: 10.1083/jcb.201605080.

Singh, Deepika et al. (2019). "Mechanical stress induces a scalable switch in cortical flow polarization during cytokinesis". In: *Journal of Cell Science* 132.19. ISSN: 14779137. DOI: 10.1242/jcs.231357.

Sit, Soon Tuck and Ed Manser (2011). "Rho GTPases and their role in organizing the actin cytoskeleton". In: *Journal of Cell Science* 124.5, pp. 679–683. ISSN: 00219533. DOI: 10.1242/jcs.064964.

Skau, Colleen T. et al. (2011). "Actin filament bundling by fimbrin is important for endocytosis, cytokinesis, and polarization in fission yeast". In: *Journal of Biological Chemistry* 286.30, pp. 26964–26977. ISSN: 00219258. DOI: 10.1074/jbc.M111.239004.

Smith, Mark A. et al. (2010). "A Zyxin-mediated mechanism for actin stress fiber maintenance and repair". In: *Developmental Cell* 19.3, pp. 365–376. ISSN: 15345807. DOI: 10.1016/j.devcel.2010.08.008. URL: http://dx.doi.org/10.1016/j.devcel.2010.08.008.

Spira, Felix et al. (2017). "Cytokinesis in vertebrate cells initiates by contraction of an equatorial actomyosin network composed of randomly oriented filaments". In: *eLife* 6, pp. 1–24. ISSN: 2050084X. DOI: 10.7554/eLife.30867.

Stachowiak, Matthew R., Caroline Laplante, et al. (2014). "Mechanism of cytokinetic contractile ring constriction in fission yeast". In: *Developmental Cell* 29.5, pp. 547–561. ISSN: 18781551. DOI: 10.1016/j.devcel.2014.04.021. URL: http://dx.doi.org/10.1016/j.devcel.2014.04.021.

Stachowiak, Matthew R., Patrick M. McCall, et al. (2012). "Self-organization of myosin II in reconstituted actomyosin bundles". In: *Biophysical Journal* 103.6, pp. 1265–1274. ISSN: 00063495. DOI: 10.1016/j.bpj.2012.08.028. URL: http://dx.doi.org/10.1016/j.bpj.2012.08.028.

Stachowiak, Matthew R., Mark A. Smith, et al. (2014). "A mechanical-biochemical feedback loop regulates remodeling in the actin cytoskeleton". In: *Proceedings of the National Academy of Sciences of the United States of America* 111.49, pp. 17528–17533. ISSN: 10916490. DOI: 10.1073/pnas.1417686111.

Steketee, Michael B. and Kathryn W. Tosney (2002). "Three functionally distinct adhesions in filopodia: Shaft adhesions control lamellar extension". In: *Journal of Neuroscience* 22.18, pp. 8071–8083. ISSN: 02706474. DOI: 10.1523/jneurosci.22-18-08071.2002.

Straight, Aaron F. et al. (2003). "Dissecting temporal and spatial control of cytokinesis with a myosin II inhibitor". In: *Science* 299.5613, pp. 1743–1747. ISSN: 00368075. DOI: 10.1126/science.1081412.

Sun, Hui Qiao, Masaya Yamamoto, et al. (1999). "Gelsolin, a Multifunctional Actin Regulatory Protein". In: *Journal of Biological Chemistry* 274.47, pp. 33179–33182. ISSN: 0021-9258. DOI: 10.1074/jbc.274.47.33179. URL: http://www.jbc.org/lookup/doi/10.1074/jbc.274.47.33179.

Sun, Sean X., Sam Walcott, and Charles W. Wolgemuth (2010). "Cytoskeletal cross-linking and bundling in motor-independent contraction". In: *Current Biology* 20.15, R649–R654. ISSN: 09609822. DOI: 10.1016/j.cub.2010.07.004. URL: http://dx.doi.org/10.1016/j.cub.2010.07.004.

Surrey, Thomas et al. (2001). "Physical properties determining self-organization of motors and microtubules". In: *Science* 292.5519, pp. 1167–1171. ISSN: 00368075. DOI: 10.1126/science.1059758.

Svitkina, Tatyana (2018a). "The actin cytoskeleton and actin-based motility". In: *Cold Spring Harbor Perspectives in Biology* 10.1, pp. 1–22. ISSN: 19430264. DOI: 10.1101/cshperspect.a018267.

Svitkina, Tatyana M. (2018b). "Ultrastructure of the actin cytoskeleton". In: *Current Opinion in Cell Biology* 54, pp. 1–8. ISSN: 18790410. DOI: 10.1016/j.ceb.2018.02.007. URL: https://doi.org/10.1016/j.ceb.2018.02.007.

Swan, Kathryn A. et al. (1998). "cyk-1: A C. elegans FH gene required for a late step in embryonic cytokinesis". In: *Journal of Cell Science* 111.14, pp. 2017–2027. ISSN: 00219533.

Tanenbaum, Marvin E. and René H. Medema (2010). "Mechanisms of Centrosome Separation and Bipolar Spindle Assembly". In: *Developmental Cell* 19.6, pp. 797–806. ISSN: 15345807. DOI: 10.1016/j.devcel.2010.11.011. URL: https://linkinghub.elsevier.com/retrieve/pii/S1534580710005381.

Theriot, Julie A. et al. (1994). "Involvement of profilin in the actin-based motility of L. monocytogenes in cells and in cell-free extracts". In: *Cell* 76.3, pp. 505–517. ISSN: 00928674. DOI: 10.1016/0092-8674(94)90114-7.

Ti, Shih Chieh et al. (2011). "Structural and biochemical characterization of two binding sites for nucleation-promoting factor WASp-VCA on arp2/3 complex". In: *Proceedings of the National Academy of Sciences of the United States of America* 108.33, pp. 463–471. ISSN: 00278424. DOI: 10.1073/pnas.1100125108.

Tian, Dong et al. (2015). "Anillin regulates neuronal migration and neurite growth by linking RhoG to the actin cytoskeleton". In: *Current Biology* 25.9, pp. 1135–1145. ISSN: 09609822. DOI: 10.1016/j.cub.2015.02.072. URL: http://dx.doi.org/10.1016/j.cub.2015.02.072.

Tojkander, Sari, Gergana Gateva, and Pekka Lappalainen (2012). "Actin stress fibers - Assembly, dynamics and biological roles". In: *Journal of Cell Science* 125.8, pp. 1855–1864. ISSN: 00219533. DOI: 10.1242/jcs.098087.

Tominaga, Tomoko et al. (2000). "Diaphanous-related formins bridge Rho GTPase and Src tyrosine kinase signaling". In: *Molecular Cell* 5.1, pp. 13–25. ISSN: 10972765. DOI: 10.1016/S1097-2765(00)80399-8.

Tse, Yu Chung et al. (2012). "RhoA activation during polarization and cytokinesis of the early Caenorhabditis elegans embryo is differentially dependent on NOP-1 and CYK-4". In: *Molecular Biology of the Cell* 23.20, pp. 4020–4031. ISSN: 10591524. DOI: 10.1091/mbc.E12-04-0268.

Vavylonis, Dimitrios, David R. Kovar, et al. (2006). "Model of formin-associated actin filament elongation". In: *Molecular Cell* 21.4, pp. 455–466. ISSN: 10972765. DOI: 10.1016/j.molcel.2006.01.016.

Vavylonis, Dimitrios, Jian Qiu Wu, et al. (2008). "Assembly mechanism of the contractile ring for cytokinesis by fission yeast". In: *Science* 319.5859, pp. 97–100. ISSN: 00368075. DOI: 10.1126/science.1151086.

Vicente-Manzanares, Miguel et al. (2009). "Non-muscle myosin II takes centre stage in cell adhesion and migration". In: *Nature Reviews Molecular Cell Biology* 10.11, pp. 778–790. ISSN: 1471-0072. DOI: 10.1038/nrm2786. URL: http://www.nature.com/articles/nrm2786.

Vignjevic, Danijela et al. (2003). "Formation of filopodia-like bundles in vitro from a dendritic network". In: *Journal of Cell Biology* 160.6, pp. 951–962. ISSN: 00219525. DOI: 10.1083/jcb.200208059.

Vuong-Brender, Thanh Thi Kim et al. (2017). "The interplay of stiffness and force anisotropies drives embryo elongation". In: *eLife* 6, pp. 1–49. ISSN: 2050084X. DOI: 10.7554/eLife.23866.

Walczak, Claire E. and Sidney L. Shaw (2010). "A MAP for bundling microtubules". In: *Cell* 142.3, pp. 364–367. ISSN: 00928674. DOI: 10.1016/j.cell.2010.07.023.

Walczak, Claire E., Isabelle Vernos, et al. (1998). "A model for the proposed roles of different microtubule-based motor proteins in establishing spindle bipolarity". In: *Current Biology* 8.16, pp. 903–913. ISSN: 09609822. DOI: 10.1016/S0960-9822(07)00370-3.

Wang, Yu Li (1985). "Exchange of actin subunits at the leading edge of living fibroblasts: Possible role of treadmilling". In: *Journal of Cell Biology* 101.2, pp. 597–602. ISSN: 15408140. DOI: 10.1083/jcb.101.2.597.

Watanabe, Naoki, Pascal Madaule, et al. (1997). "p140mDia, a mammalian homolog of Drosophila diaphanous, is a target protein for Rho small GTPase and is a ligand for profilin". In: *EMBO Journal* 16.11, pp. 3044–3056. ISSN: 02614189. DOI: 10.1093/emboj/16.11.3044.

Watanabe, Sadanori, Katsuya Okawa, et al. (2010). "Rho and Anillin-dependent Control of mDia2 Localization and Function in Cytokinesis". In: *Molecular Biology of the Cell* 21.18.

Ed. by Fred Chang, pp. 3193–3204. ISSN: 1059-1524. DOI: 10.1091/mbc.e10-04-0324. URL: https://www.molbiolcell.org/doi/10.1091/mbc.e10-04-0324.

Wegner, Albrecht (1976). "Head to tail polymerization of actin". In: *Journal of Molecular Biology* 108.1, pp. 139–150. ISSN: 00222836. DOI: 10.1016/S0022-2836(76)80100-3. URL: https://linkinghub.elsevier.com/retrieve/pii/S0022283676801003.

Weigert, Martin et al. (2018). "Content-aware image restoration: pushing the limits of fluorescence microscopy". In: *Nature Methods* 15.12, pp. 1090–1097. ISSN: 15487105. DOI: 10.1038/s41592-018-0216-7.

Weiner, Orion D., William A. Marganski, et al. (2007). "An actin-based wave generator organizes cell motility". In: *PLoS Biology* 5.9, pp. 2053–2063. ISSN: 15449173. DOI: 10.1371/journal.pbio.0050221.

Weiner, Orion D., Paul O. Neilsen, et al. (2002). "A PtdInsP3- and Rho GTPase-mediated positive feedback loop regulates neutrophil polarity". In: *Nature Cell Biology* 4.7, pp. 509–512. ISSN: 14657392. DOI: 10.1038/ncb811.

Welch, Matthew D, Akihiro Iwamatsu, and Timothy J Mitchison (1997). "Actin polymerization is induced by Arp 2/3 protein complex at the surface of Listeria monocytogenes". In: *Nature* 385.6613, pp. 265–269. ISSN: 0028-0836. DOI: 10.1038/385265a0. URL: http://dx.doi.org/10.1038/385265a0%20http://www.nature.com/articles/385265a0.

Welch, Matthew D., Jody Rosenblatt, et al. (1998). "Interaction of human Arp2/3 complex and the Listeria monocytognes ActA protein in actin filament nucleation". In: *Science* 281.5373, pp. 105–108. ISSN: 00368075. DOI: 10.1126/science.281.5373.105.

Werner, Michael, Ed Munro, and Michael Glotzer (2007). "Astral Signals Spatially Bias Cortical Myosin Recruitment to Break Symmetry and Promote Cytokinesis". In: *Current Biology* 17.15, pp. 1286–1297. ISSN: 09609822. DOI: 10.1016/j.cub.2007.06.070.

White, J. G. and G. G. Borisy (1983). "On the mechanisms of cytokinesis in animal cells". In: *Journal of Theoretical Biology* 101.2, pp. 289–316. ISSN: 10958541. DOI: 10.1016/0022-5193(83)90342-9.

Winkelman, Jonathan D., Colleen G. Bilancia, et al. (2014). "Ena/VASP Enabled is a highly processive actin polymerase tailored to self-assemble parallel-bundled F-actin networks with

Fascin". In: *Proceedings of the National Academy of Sciences of the United States of America* 111.11, pp. 4121–4126. ISSN: 10916490. DOI: 10.1073/pnas.1322093111.

Winkelman, Jonathan D., Cristian Suarez, et al. (2016). "Fascin- and α-Actinin-Bundled Networks Contain Intrinsic Structural Features that Drive Protein Sorting". In: *Current Biology* 26.20, pp. 2697–2706. ISSN: 09609822. DOI: 10.1016/j.cub.2016.07.080. URL: http://dx.doi.org/10.1016/j.cub.2016.07.080.

Wittmann, Torsten, Anthony Hyman, and Arshad Desai (2001). "The spindle: A dynamic assembly of microtubules and motors". In: *Nature Cell Biology* 3.1. ISSN: 14657392. DOI: 10.1038/35050669.

Woods, Benjamin and Daniel J. Lew (2019). "Polarity establishment by Cdc42: Key roles for positive feedback and differential mobility". In: *Small GTPases* 10.2, pp. 130–137. ISSN: 21541256. DOI: 10.1080/21541248.2016.1275370.

Wu, Jian Qiu, Jeffrey R. Kuhn, et al. (2003). "Spatial and temporal pathway for assembly and constriction of the contractile ring in fission yeast cytokinesis". In: *Developmental Cell* 5.5, pp. 723–734. ISSN: 15345807. DOI: 10.1016/S1534-5807(03)00324-1.

Wu, Jian Qiu and Thomas D. Pollard (2005). "Cell biology: Counting cytokinesis proteins globally and locally in fission yeast". In: *Science* 310.5746, pp. 310–314. ISSN: 00368075. DOI: 10.1126/science.1113230.

Wu, Jian Qiu, Vladimir Sirotkin, et al. (2006). "Assembly of the cytokinetic contractile ring from a broad band of nodes in fission yeast". In: *Journal of Cell Biology* 174.3, pp. 391–402. ISSN: 00219525. DOI: 10.1083/jcb.200602032.

Wu, Min, Xudong Wu, and Pietro De Camilli (2013). "Calcium oscillations-coupled conversion of actin travelling waves to standing oscillations". In: *Proceedings of the National Academy of Sciences of the United States of America* 110.4, pp. 1339–1344. ISSN: 00278424. DOI: 10.1073/pnas.1221538110.

Xu, Yingwu et al. (2004). "Crystal structures of a formin homology-2 domain reveal a tethered dimer architecture". In: *Cell* 116.5, pp. 711–723. ISSN: 00928674. DOI: 10.1016/S0092-8674(04)00210-7.

Xue, Bo et al. (2014). "Structural basis of thymosin-β4/profilin exchange leading to actin filament polymerization". In: *Proceedings of the National Academy of Sciences of the United States of America* 111.43, E4596–E4605. ISSN: 10916490. DOI: 10.1073/pnas.1412271111.

Yamashiro, Sawako et al. (2012). "Tropomodulins: Pointed-end capping proteins that regulate actin filament architecture in diverse cell types". In: *Cytoskeleton* 69.6, pp. 337–370. ISSN: 19493592. DOI: 10.1002/cm.21031.

Yang, Changsong and Tatyana Svitkina (2011). "Filopodia initiation: Focus on the Arp2/3 complex and formins". In: *Cell Adhesion and Migration* 5.5, pp. 402–408. ISSN: 19336926. DOI: 10.4161/cam.5.5.16971.

Yarmola, Elena G, Thayumanasamy Somasundaram, and Todd A Boring (2000). "Actin-latrunculin A structure and function : differential modulation of actin-binding protein function by latrunculin A Department of Medicine , University of Florida , Gainesville , FL 32610 , 1 Institute of Molecular Biophysics , Florida State Universit". In: *The Journal Of Biological Chemistry* 275.36, pp. 28120–7.

Young, Kevin G. and John W. Copeland (2010). "Formins in cell signaling". In: *Biochimica et Biophysica Acta - Molecular Cell Research* 1803.2, pp. 183–190. ISSN: 01674889. DOI: 10.1016/j.bbamcr.2008.09.017. URL: http://dx.doi.org/10.1016/j.bbamcr.2008.09.017.

Young, Lorna E., Ernest G. Heimsath, and Henry N. Higgs (2015). "Cell type-dependent mechanisms for formin-mediated assembly of filopodia". In: *Molecular Biology of the Cell* 26.25, pp. 4646–4659. ISSN: 19394586. DOI: 10.1091/mbc.E15-09-0626.

Yu, F. X. et al. (1993). "Thymosin β10 and thymosin β4 are both actin monomer sequestering proteins". In: *Journal of Biological Chemistry* 268.1, pp. 502–509. ISSN: 00219258.

Yüce, Özlem, Alisa Piekny, and Michael Glotzer (2005). "An ECT2-centralspindlin complex regulates the localization and function of RhoA". In: *Journal of Cell Biology* 170.4, pp. 571–582. ISSN: 00219525. DOI: 10.1083/jcb.200501097.

Zhang, J. et al. (2009). "Rab35 Controls Actin Bundling by Recruiting Fascin as an Effector Protein". In: *Science* 325.5945, pp. 1250–1254. ISSN: 0036-8075. DOI: 10.1126/science.1174921. URL: https://www.sciencemag.org/lookup/doi/10.1126/science.1174921.

Zhao, Wei Meng and Guowei Fang (2005). "MgcRacGAP controls the assembly of the contractile ring and the initiation of cytokinesis". In: *Proceedings of the National Academy of Sciences of the United States of America* 102.37, pp. 13158–13163. ISSN: 00278424. DOI: 10.1073/pnas.0504145102.

Zhou, Mian and Yu-Li Wang (2008). "Distinct pathways for the early recruitment of myosin II and actin to the cytokinetic furrow." In: *Molecular biology of the cell* 19.1, pp. 318–26. ISSN: 1939-4586. DOI: 10.1091/mbc.e07-08-0783. URL: http://www.ncbi.nlm.nih.gov/pubmed/17959823%20http://www.pubmedcentral.nih.gov/articlerender.fcgi?artid=PMC2174197.

Zumdieck, Alexander et al. (2007). "Stress generation and filamnet turnover during actin ring constriction". In: *PLoS ONE* 2.8. ISSN: 19326203. DOI: 10.1371/journal.pone.0000696.

APPENDIX A

DYNAMIC OPPOSITION OF CLUSTERED PROTEINS STABILIZES CORTICAL POLARITY IN THE *C. ELEGANS* ZYGOTE

Statement of contribution: I carried out all of the experiments and data analysis in Figure 6 studying the dynamics of Chin-1 clusters.

Sailer, Anne et al. (2015). "Dynamic Opposition of Clustered Proteins Stabilizess Cortical Polarity in the *C.elegans* Zyote". In: *Developmental Cell* 35.1, pp. 131-142. ISSN: 18781551. DOI: 10.1016/j.devcel.2015.09.006.

APPENDIX B

RAPID DIFFUSION-STATE SWITCHING UNDERLIES STABLE CYTOPLASMIC GRADIENTS IN THE *CAENORHABDITIS* ELEGANS ZYGOTE

Statement of contribution: I trained Youjun Wu single molecule imaging and the corresponding data analysis.

Wu, Youjun et al. (2018). "Rapid diffusion-state switching underlies stable cytoplasmic gradients in the *Caenorhabditis elegans* zygote". In: *PNAS* 115(36), pp. E8440-E8449. DOI: 10.1073/pnas.1722162115.